Optimization and Energy Management of Battery Energy Storage Systems in Residential and Industrial Applications

by

Rodrigo Castro Martins

A thesis submitted in partial fulfillment of the requirements for the degree of

Doctor of Philosophy

in

Energy Systems

Department of Electrical and Computer Engineering

University of Alberta

Abstract

Battery Energy Storage System (BESS) provides a fast and high power capability, making them an ideal solution for residential and industrial application. However, given today's high investment costs of BESS, a well-matched design and adequate sizing of the storage systems are prerequisites to allow profitability for the end-user. The economic viability of a BESS depends also on the battery operation, storage technology, and aging of the system. For instance, BESS coupled with residential photovoltaic (PV) generation, designed as PV-BESS, can reduce the energy dependency of individual households while mitigating the impact of the intermittent renewable energy sources on the electric power grid. However, to maximize the benefits, efficient operational strategies must be defined to manage flows of energy in such systems.

In this thesis, a general method for comprehensive PV-BESS techno-economic analysis and optimization is presented and applied to the state-of-art PV-BESS to determine its optimal parameters. Then, it shows two cases of how the optimal power flows can be used to develop advanced energy management systems. In the first case, the time series of the optimal flows, determined using linear programming, are used to set the parameters of the controller for the next time window. In the second case, an energy management system is designed in the form of a fuzzy rule based system, and the time series of the optimal power flows are used to set the parameters of a Takagi-Sugeno fuzzy controller through differential evolution.

Similarly to the desire to apply BESS in residential areas, the interest in BESSs for industrial peak shaving application has drastically increased. There have been several reports examining the optimal sizing of storage systems. Because most

such works make significant assumptions about the key factors that affect battery degradation, this thesis proposes a linear aging model that considers a state of charge dependent calendric aging, and verifies that the depth of discharge cycling aging dependency is not relevant to peak shaving application. The linear model reveals that considering a SOC-aware charge control strategy for peak shaving applications the battery storage system lifetime could be significantly prolonged. To verify the applicability of the linear aging model, this work proposes a general framework for cost-optimal sizing of the battery and power electronics in peak shaving application. A case study conducted with real-world industrial profiles shows the applicability of the approach and reveals the best storage operation patterns when considering the trade-offs between energy purchase, peak-power tariff, and battery aging. However, the deployment of BESS for industrial peak shaving applications can substantially reduce the peak power, it is noticed that the storage system is underused, staying idle most of the time. Motivated by that, this thesis proposes a new business model where battery energy storage is offered as a service by a new stakeholder. This new model allows sharing a single battery storage system among multiple clients. The results show that sharing batteries in peak shaving applications for multiple clients shortens the payback period.

The results show that the best economic performances require specific storage technology and component sizing which change depending on the scenario of load demand and PV generation. At the same time, it confirms the operational and economic benefits of using the proposed energy management systems. The results also show that while batteries used in peak shaving applications are sensitive to calendric aging, the depth of discharge cycling is much less relevant. This is an important observation that will simplify relevant optimization studies and thus contribute to more widespread application of industrial peak shaving systems.

Each of these topics is justified with experimental case studies, using real-world data sets, demonstrating the feasibility of the proposed models as compared to existing methodologies.

Preface

The research presented in this thesis was performed under the supervision of Dr Petr Musilek and was supported by funding from the Science Without Borders PhD grant (BEX 13301/13-6), Future Energy Systems under the Canada First Research Excellence Fund (CFREF), and the National Sciences and Engineering Research Council (NSERC) of Canada.

Chapter 3 of this thesis has been published as "Economic optimization of component sizing for residential battery storage systems" [42]. Holger Hesse established the mathematical framework for the techno-economic analysis of energy storage systems. Rodrigo Martins developed the optimization model and executed the simulation experiments. Maik Naumann and Cong Nam Truong contributed to the result analysis and sensitivity study. Petr Musilek and Andreas Jossen provided overall guidance for the study and contributed with many fruitful discussions on the methodology.

Chapter 4 of this thesis has been published as "LP-based predictive energy management system for residential PV/BESS" [68]. Rodrigo Martins conceived and designed the optimization model of energy storage system, the implementation of experimental code, and manuscript composition. Pavel Krömer contributed to the analysis of the results. Petr Musilek took on this study in a supervisory role, aiding in the initial formation of the research topic, and having meaningful contributions to the manuscript composition and refinement process.

Chapter 5 of this thesis has been published as "Optimal Energy Management of Residential PV/HESS Using Evolutionary Fuzzy Control" [85]. Rodrigo Martins conceived and designed the optimization model of energy storage system, and the fuzzy rule base. Pavel Krömer designed and implemented the controller and described the controller interpretation. Petr Musilek took on this study in a supervisory role, aiding in the initial formation of the research topic and manuscript composition.

Chapter 6 of this thesis has been published as "Linear Battery Aging Model for Industrial Peak Shaving Applications" [70]. Rodrigo Martins conceived and designed the optimization model of energy storage system, the implementation of experimental code and manuscript composition. Holger Hesse and Johanna Jungbauer contributed to the result analysis. Thomas Vorbuchner developed the linearization of the aging model. Petr Musilek took on this study in a supervisory role, aiding in the initial formation of the research topic and having meaningful contributions to the manuscript composition and refinement process.

Chapter 7 of this thesis has been published as "Optimal component sizing for peak shaving in battery energy storage system for industrial applications" [71]. Rodrigo Martins conceived and designed the optimization model of energy storage system, and executed the simulation experiments. Holger Hesse contributed to the result analysis. Johanna Jungbauer contributed to the regulatory framework. Thomas Vorbuchner developed the linearization of the aging model. Petr Musilek provided overall guidance for the study and contributed with many fruitful discussions on the methodology. Rodrigo Martins and Petr Musilek wrote the paper with contributions of all co-authors.

Chapter 8 of this thesis has been submitted to Applied Energy Journal as "Battery Energy Storage as a Service for Peak Shaving in Multiple Industrial Clients". Rodrigo Martins conceived and designed the optimization model of energy storage system, the implementation of experimental code and manuscript composition. Alexandre Nassif contributed to the regulatory framework and the analysis of the intermediate results. Petr Musilek took on this study in a supervisory role, aiding in the initial formation of the research topic, and having meaningful contributions to the manuscript composition and refinement process.

Once you stop learning, you start dying.

– Albert Einstein.

Acknowledgements

I want to thank my supervisor, Prof. Petr Musilek, for the patient guidance, encouragement, and advice he has provided throughout my time as his student. I want to thank you for encouraging my research and for allowing me to grow as a researcher. Your advice on both research as well as on my career, have been invaluable. I would also like to thank my committee members for letting my defense be an enjoyable moment, and for your brilliant comments and suggestions, thanks to you. I would also like to thank all the members of Prof. Musilek's research group. In particular, I would like to thank Tomas Barton for all the fruitful discussions.

I must express my gratitude to Tallitha, my wife, for her support. I was continually amazed by her willingness to proofread countless pages, and by her patience for experienced all of the ups and downs of my research. I am also extremely grateful for all the continued encouragement I received from my family in Brazil. Your motivation was what sustained me thus far.

Finally, I would like to thank the Science Without Border project from CAPES, for providing the funding which allowed me to undertake this research.

Contents

List of Tables

List of Figures

Chapter 1

Introduction

Smart grid technologies aim to improve the efficiency, reliability, economics, and sustainability of the production and distribution of electricity [25]. The smart grid is capable of effectively responding to changes in demand which helps balance the consumption and supply of electricity, supporting the integration of renewable energy sources in the power grid. Hassan et al. [40] review the basic concepts of smart grid and corresponding technologies. Rohjans et al. [114] discuss in their paper related standardization issues, while Fang et al. [24] have surveyed the protection, management and infrastructure aspects of the smart grid technology

Further improvements of renewable energy integration can be attained through the deployment of sustainable power sources. An important example of fast-growing renewable technologies is Photo-Voltaic (PV) generation systems. Such PV systems installed locally at individual households can provide significant cost savings by avoiding purchasing energy from the grid. However, studies have shown that high PV penetration may cause voltage level issues in the distribution grid, especially at light load [110], [116]. The main concern is the over-voltage due to reverse power flow in distribution networks [133]. A simple way used by the utilities to avoid this problem is to limit the amount of power injected from the clients back to the grid. However, this approach causes significant underutilization of potentially available PV power generation that might be otherwise beneficial for the system. In addition, this approach may not be sustainable in the long term given the growing interest of consumers in PV installations.

An important alternative to maximize the local generation can be obtained by coupling the PV sources with the use of Energy Storage (ES) systems. These technologies also increase grid reliability and economy compared to single source gener-

ation without storage. In addition, such systems may contribute to better balancing of the entire power grid by smoothing out peaks in power demand. They generate power when the solar radiation is higher than demand and store it for later usage when the demand increases.

ES systems are not limited to only augmenting the local generation. For instance, battery energy storage systems (BESS) are considered for a variety of applications in modern power grids [59]. As the cost of these systems declines, commercial and residential consumer interest for this type of storage grows. Integrating BESS in the power system offers many benefits. For instance, BESS can support Distribution System Operators (DSO) to diminish the challenges created when increasing complex distribution network. At the same time, storage system can integrate and manage the fluctuating and uncertain generation from Renewable Energy Sources (RESs) such as PV generation [45]. In addition, BESS is well suited as a solution for improving power quality, voltage regulation, renewable penetration, and peak load shaving [62], [74], [108], [146].

This thesis examines the role of BESS in residential applications and for industrial customers. However, renewable generation can also be used in other sectors, e.g. in agricultural or commercial applications [54]. Although the principles outlined in this work can be extended outside the residential sector and industry, feasibility of using BESS must be analyzed for each application individually. For example, standalone photovoltaic generation is well suited to rural and natural areas, where the costs and environmental impacts of power lines are relatively high [16]. However, BESS is usually not applied in these scenarios because the variability of production and demand would require significant oversizing of the system to guarantee supply. As a result, the cost of the long-term storage may exceed the savings.

1.1 Research Objectives

The key objectives of the presented research can be organized in the following three groups:

Optimal component sizing for battery system and power electronics:

- To define a power flow optimization[1] model and use it to identify the best storage operation patterns considering a trade-off between energy purchase,

[1]The reader must note that power flow in the context of this research is related to the flows within a residential or industrial facility, not as usually considering "power flow" in power engineering.

feed-in remuneration, and battery aging.

- To conduct a comprehensive power flow analysis and to present a highly reproducible and easily adaptable linear optimization approach to assess both the cost and the maximum profit attainable for a residential BESS.
- To evaluate the linear optimization model using up to date technology-specific aging information and the investment cost of battery and inverter systems of diverse mature battery chemistries.
- To design a general framework for sizing of BESS in peak shaving applications.
- To propose a new business model where battery energy storage is offered as a peak shaving service; this model should allow sharing a single battery storage system among multiple industrial clients.

Energy management system:

- To design an advanced energy management system in the form of a rule-based controller where the time series of the optimal flows, determined using linear programming, are used to set the parameters of the controller.
- To use the optimal power flows to develop an advanced energy management system in the form of a fuzzy control system.

The impact of battery degradation:

- To propose a model of BESS aging processes that can be reductively applied to obtain a linearized degradation function.
- To propose a linear aging model that considers state of charge-dependent calendric aging; verify whether the depth of discharge cycling aging dependency is relevant for peak shaving applications.
- To show the applicability of the developed approaches using case studies with real-world generation and demand profiles. At the same time, to demonstrate the return on investment and battery aging dependencies.

1.2 Research Originality

All topics covered in this thesis show notable novelty in their particular areas of research and indicate new opportunities for study. They make use of existing work and well-known methodologies, but with essential aspects of originality. The proposed cost model that considers storage degradation instead of storage purchasing cost is of the most significant novelty, with no other work having been developed in this field to our knowledge. No other study addresses the use of the optimal power flow to determine the parameters of the energy management controller. The critical factors impacting the aging model for industrial clients have not been previously investigated. The application of a BESS as a service is, to our knowledge, unique and demonstrates a significant improvement in peak shaving applications. Additionally, this work raises further questions, providing opportunities for expanding the presented topics in future studies.

Chapter 3 conducts a comprehensive power flow analysis, implements technology-specific battery degradation algorithm, and presents a highly reproducible and easily adaptable linear optimization approach to assess both the cost and the maximum profit attainable for residential BESS. This approach allows the most suitable storage type and power electronics size to be selected for households with rooftop-mounted PV generators.

Responding to the necessity of having an energy management system, Chapter 4 proposes an advanced energy management system in form of a rule-based controller. The model developed in Chapter 3 is used to iteratively generate the optimal power flows among the components of the PV/HESS and the grid, for a selected time window. The optimal power flows are then used by the rule-based system to direct power through the system in an optimal way. This forms a general predictive energy management strategy that can be implemented to control power flows in other PV-BESS or similar hybrid energy systems. The performance of the proposed controller is thoroughly tested using simulations and compared with three different strategies: greedy strategy, schedule mode, and feed-in damping.

Similarly, Chapter 5 builds on the optimal power flows to develop an advanced energy management system in the form of a fuzzy controller. The model in the previous study is used to determine the parameters of a Takagi-Sugeno fuzzy controller using an evolutionary computing approach.

The necessity of proper BESS sizing has been highlighted in several studies. Most reports also recognize that aging of BESS cannot be neglected and point out battery deterioration as a major cost driver during the storage operation. To gain a better understanding of peak-shaving battery aging, Chapter 6 proposes a linear aging model that considers state of charge (SoC) dependent calendric aging suitable for BESS sizing for peak shaving applications in industrial settings. It also reveals the potential of an SOC-aware charge control strategy for peak shaving applications.

Therefore, Chapter 8 proposes a new business model where battery energy storage is offered as a service by a new stakeholder. This model allows sharing a single battery storage system among multiple clients. This chapter also presents a case study conducted with industrial load profiles, a techno-economic analysis evaluating the ROI of the system and battery degradation, and a linear programming(LP) approach allowing an exact solution determination for BESS sizing and operation strategy. In addition, break even point, to which a balance between the BESS charges and clients expenses, is discussed.

1.3 Thesis Organization

The chapters of this document are structured as follows:

Chapter 2: State of the Art and Theoretical Background

This chapter offers a focused literature review and background knowledge on the relevant topics to the research presented in this thesis. It also provides details of established algorithms and processes which are used in the construction of the models presented in later sections. The topics covered include fuzzy rule-based control systems, differential evolution, linear programming, energy storage system, aging models, component sizing for PV-BESS, and energy management system.

Chapter 3: Economic Optimization of Component Sizing for Residential Battery Storage Systems

Battery energy storage systems (BESSs) coupled with rooftop-mounted residential Photo-Voltaic (PV) generation, designated as PV-BESS, have been drawing increasing attention and market penetration as more and more of such systems become available. The manifold BESS deployed to date rely on a variety of different battery technologies, showing a significant variation of battery size, and power elec-

tronics dimensioning. However, given today's high investment costs of BESS, a well-matched design and adequate sizing of the storage systems are prerequisites to allow profitability for the end-user. The economic viability of a PV-BESS depends also on the battery operation, storage technology, and aging of the system. In this chapter, a general method for comprehensive PV-BESS techno-economic analysis and optimization is presented and applied to the state-of-art PV-BESS to determine its optimal parameters. Using a linear optimization method, a cost-optimal sizing of the battery and power electronics is derived based on solar energy availability and local demand. At the same time, the power flow optimization reveals the best storage operation patterns considering a trade-off between energy purchase, feed-in remuneration, and battery aging. Using up to date technology-specific aging information and the investment cost of battery and inverter systems, three mature battery chemistries are compared; one lead-acid (PbA) system and two lithium-ion systems; of the two lithium-ion systems, one uses lithium-iron-phosphate (LFP) and the other uses lithium-nickel-manganese-cobalt (NMC) for the cathode respectively. The results show that different storage technology and component sizing can provide the best economic performances depending on the scenario of load demand and PV generation.

Chapter 4: LP-based Predictive Energy Management System for Residential PV-BESS

The deployment of solar energy generation combined with energy storage systems can reduce the energy dependency of individual households while mitigating the impact of the intermittent renewable energy sources on the electric power grid. However, to maximize the benefits, efficient operational strategies must be defined to manage flows of energy in such systems. The first step towards the development of such energy management system, described in previous work, is the determination of the optimal power flows that reflects the current and future solar energy availability and household load, as well as the state of the energy storage system. This chapter builds on the optimal power flows to develop an advanced energy management system. The time series of the optimal flows, determined using Linear Programming (LP), are used to set the parameters of the controller for the next time window. The results confirm the operational and economic benefits of using the proposed LP-based predictive energy management. It also compares favorably

with other commonly used strategies.

Chapter 5: Optimal Energy Management of Residential PV-BESS Using Evolutionary Fuzzy Control

The adoption of residential Photo-Voltaic (PV) power generators combined with energy storage system can reduce the energy dependency of individual households while alleviating the impact of intermittent solar energy on the electric power grid; however, to maximize the benefits, energy in such systems must be carefully managed. This chapter builds on the optimal power flows to develop an advanced energy management system in form of a fuzzy rule-based system. The time series of the optimal flows, determined using LP, are used to determine the parameters of a Takagi-Sugeno fuzzy controller through differential evolution. The resulting system can be implemented to control power flows in other systems composed of PV generation and energy storage. The results confirm the operational and economic benefits of using the optimal operational strategy, while allowing its in-depth analysis through the evolved fuzzy rule base.

Chapter 6: Linear Battery Aging Model for Industrial Peak Shaving Applications

Recent attention to industrial peak shaving applications sparked an increased interest in BESSs. Among other studies, there have been several reports examining optimal sizing of such storage systems. Most such works make significant assumptions about the key factors that affect battery degradation. This work examines these assumptions using a linear aging model that considers a state of charge (SOC) dependent calendric aging. The linear model reveals the potential of an SOC-aware charge control strategy for peak shaving applications: with adequate forecasting, the battery storage system lifetime could be significantly prolonged. The results also show that while batteries used in peak shaving applications are sensitive to calendric aging, the depth of discharge cycling is much less relevant. This is an important observation that will simplify relevant optimization studies and thus contribute to more widespread application of industrial peak shaving systems.

Chapter 7: Optimal Component Sizing for Peak Shaving in Battery Energy Storage Systems for Industrial Applications

Batteries provide a fast and high power capability, making them an ideal solution for industrial peak shaving application. This work proposes a general framework for sizing of BESS in peak shaving applications. A cost-optimal sizing of the battery and power electronics is derived using LP based on a local demand and billing scheme. A case study conducted with real-world industrial profiles shows the applicability of the approach as well as the return on investment dependence on the load profile. At the same time, the power flow optimization reveals the best storage operation patterns considering a trade-off between energy purchase, peak-power tariff, and battery aging. This underlines the need for a general mathematical optimization approach to efficiently tackle the challenge of peak shaving using an energy storage system. The case study also compares the applicability of yearly and monthly billing schemes, where the highest load of the year/month is the base for the price per kW. The results demonstrate that batteries in peak shaving applications can shorten the payback period when used for large industrial loads. They also show the impacts of peak shaving variation on the return of investment and battery aging of the system.

Chapter 8: Battery Energy Storage as a Service for Peak Shaving Applications With Multiple Industrial Clients

The usage of battery energy storage system in industrial peak shaving application has increased in recent years. Among other studies, there have been several reports examining optimal sizing of these storage systems for individual clients. However such individual applications result in the battery energy storage system standing idle most of the time. Concerning the under-utilization of BESS in such cases, this chapter proposes a new business model where battery energy storage is offered as a service by a new stakeholder. This new model allows sharing a single battery storage system among multiple clients. The results show that sharing batteries in peak shaving applications for multiple clients shortens the payback period. Herein, a general framework for the sizing of BESS in peak shaving application is presented. A case study shows the effectiveness of the approach, the strong dependence of the battery energy storage system dispatch, and resulting return on investment on the industry load profile. At the same time, the results show a sensitivity analysis of the profit margin variance in the studied scenarios.

Chapter 9: Conclusion and Future Studies

The work presented in this thesis is summarized in Chapter 9 The limitation of the current work is identified. In addition to that, this chapter shows possible directions for future research on the topics presented in this thesis.

Chapter 2

State of the Art and Theoretical Background

This chapter provides the complete necessary background knowledge for the research topics presented in Chapters 3 through 8. It also offers a focused literature review on those topics fully relevant to the research presented in this thesis.

2.1 Economic Value of Residential Battery Storage Systems

While most existing studies assess the economic value of residential battery storage using sensitivity analysis, there is lack of system size optimization studies considering technology specific parameters and aging information [46]. Nevertheless, numerous significant contributions in the literature describe the usage of optimization routines for storage dispatch and size optimization in a distinct, but related context. Their overview is presented in Table 2.1.

Complex optimization approaches can be applied to storage dispatch optimization in various use cases. Although this helps to reveal possible operation modes of a system, such approaches often require extensive computational resources and may fail to find a globally optimal solution.

Geth et al. [32] show an optimization method for the best positioning and sizing of energy storage in distribution grids. Using a multi-objective optimization method, the authors find an optimized dispatch operation strategy for multiple households with respect to BESS profit generation via energy market trading. They also provide a detailed discussion of concerns of distribution system operators related to security of the energy service, *e.g.* using voltage control.

Table 2.1: Non-comprehensive overview of literature in the field of battery energy storage system (BESS) analysis and optimization.

Application	Type/Focus of Research	References
Vehicle	Economic analysis	[97]
Residential	Market analysis	[30], [51]
	Techno-economic analysis	[31], [46], [87], [134]
	Online economic estimation tools	[9], [35], [103], [106]
	Size optimization (genetic algorithm)	[64]
	Optimization of power flow (dynamic programming)	[82]
	Inverter size (sensitivity analysis)	[140]
	Co-optimization of electricity and thermal energy flow	[56]
Commercial	Techno-economic analysis	[77]
Other/grid level	BESS for distribution grid support	[32], [129]
	BESS microgrid support	[76]
Various/comparison of applications	Technical review	[60]
	Economic value assessment	[27]

In a subsequent work, Tant et al. [129] demonstrated how complex optimization methods can be applied to find the best-suited battery storage system for PV integration in a given distribution grid. The authors analyze in detail the storage dispatch optimization using PbA and lithium-ion batteries. However, this work focuses on multi-objective optimization for peak shaving and voltage regulation, rather than on aspects relevant to a single household cost optimization.

Recent work by Merei et al. [77] concentrates on commercial applications of BESS. The authors use sensitivity analysis to study the maximization of energy self-consumption via storage integration. The techno-economic analysis reveals that, for most commercial applications, BESS is not favored economically when battery degradation is taken into account.

Interestingly, currently available and announced PV-BESS rely on different battery technologies. At a first glance, there appears to be a market trend towards lithium-ion based systems with storage capacity above 5 kWh coupled with inverter sizes of Nominal Power, often exceeding 3 kW [52]. Nevertheless, lead-acid (PbA) systems still hold an appreciable market share of over 10% for new system installations, and there is a strong competition within the category of lithium-ion batteries to which the various cell chemistries have significantly different performance, cost, and aging [52].

Despite the market availability of these various systems, there is still an obvious lack of accurate quantitative assessment tools to determine Return On Investment (ROI)-optimal storage solutions for individual households with particular PV gen-

eration and load demand. While most existing studies assess the economic value of residential battery storage using sensitivity analysis, there is lack of system size optimization studies considering technology specific parameters and aging information [47]. For instance, Geth et al. show an optimization method for the best positioning and sizing of energy storage in distribution grids [33]. Using a multi-objective optimization method, the authors found an optimized dispatch operation strategy for multiple households with respect to BESS profit generation via energy market trading. In a subsequent work, Tant et al. demonstrate how complex optimization methods can be applied to find the best-suited battery storage system, focusing on multi-objective optimization for peak shaving and voltage regulation, rather than on aspects relevant to a single household cost optimization [131]. Other previous work by Magnor and Sauer, and Merei et al. analyzed the optimal sizing of storage in the context of island grids and home storage systems [65], [78]. The solver considers a genetic algorithm-based method. Therefore, it may not find a globally optimal solution to the described problem, and the studies do not provide design rules for future storage systems.

2.2 Battery Energy Storage System (BESS)

In response to the need to properly size BESS, several studies aiming to find the optimal sizing of BESS have been conducted. Previous work by Magnor and Sauer [64] and Merei et al. [76] analyzed the optimal sizing of storage in the context of island grids and home storage systems. A genetic algorithm-based method allows the modeling of a non-linear set of equations including battery-aging models. However, the solver results may not find a globally optimal solution to the described problem, and the studies do not provide design rules for future storage systems.

A sophisticated optimization method applied to find the best-suited battery storage system located in a residential suburban area has been described by Tant et al. [130]. A multi-objective function is used to find the balance between voltage regulation, peak power reduction, and annual cost. A grid operator can use this method to support the decision of temporarily installing a BESS in problematic feeders to postpone grid upgrades in the short term due to work planning issues. By comparing the cost of grid upgrades, the grid operator may conclude that the BESS is also a valuable alternative in the long term. Recent work by Rahmann et al. [108] proposed an approach to determine the break-even points for different

BESS considering a wide range of life cycles, efficiency, energy price, and power price. The results presented in this work show that depending on the values of round trip efficiency, life cycles, and power price, there are BESS technologies that are already profitable when considering only peak shaving applications. Although the authors model an optimization algorithm used for the sizing of the storage system, only the distribution company perspective is considered.

Storage deterioration is a significant cost driver during storage operation. As a result, the aging of storage devices must be taken into consideration when simulating BESS operations. Lithium-ion batteries [41] suffer from continuous aging. For most batteries of this type, it is possible to separate the degradation into a pure time-dependent irreversible loss of battery capacity called *calendric aging*, and an energy throughput dependent *cyclic aging* [128].

The battery cyclic and calendric lifetime define the remaining State of Health (SoH) until a certain capacity fade for a battery cell becomes evident. In this work, we assume that the BESS must be replaced when SoH drops to 80% of the nominal capacity. The overall aging can be estimated using the superposition principle [120]:

$$\text{aging}_{\text{tot}} \approx \text{aging}_{\text{cyc}} + \text{aging}_{\text{cal}}. \tag{2.1}$$

Value $\text{aging}_{\text{tot}} = 0$ represents a new, unused battery, while $\text{aging}_{\text{tot}} = 1$ corresponds to a situation when the remaining capacity of the battery is 80% of its original capacity. However, it is important to note that additional use of the storage system with $\text{aging}_{\text{tot}} > 1$ may be allowed if the replacement of storage is set to below 80% of the SoH. A detailed analysis and validation of battery performance and aging models is provided in [37].

Calendric aging

The analytical term for the calendar capacity fade $\text{C}_{\text{fade,cal}}$ as a function of battery SoC (%), temperature T (°C), and time Δ_t, takes the following form:

$$\text{C}_{\text{fade,cal}}(SOC, T, \Delta_t). \tag{2.2}$$

Cycling aging

The stress factors that influence the cycling lifetime are the C-rate, depth of discharge (DoD) and charge throughput Q. Cycling aging can be calculated as:

$$C_{\text{fade,cyc}} = f(\text{C-rate}) \cdot f(\text{DoD}) \cdot Q^{0.5562} \tag{2.3}$$

For a better understanding of the cyclic aging model, the functions for the stress factors C-rate and DoD are shown in Figure 2.1. It can be seen that variation of the C-rate between $-0.5C$ and $0.5C$ does not affect cyclic capacity fade. Battery discharging corresponds to the negative values of the C-rate factor, limited to $-2C$ according to manufacturer specifications. For charging, there is a steeper impact of cell degradation compared to discharging, limited to $1C$.

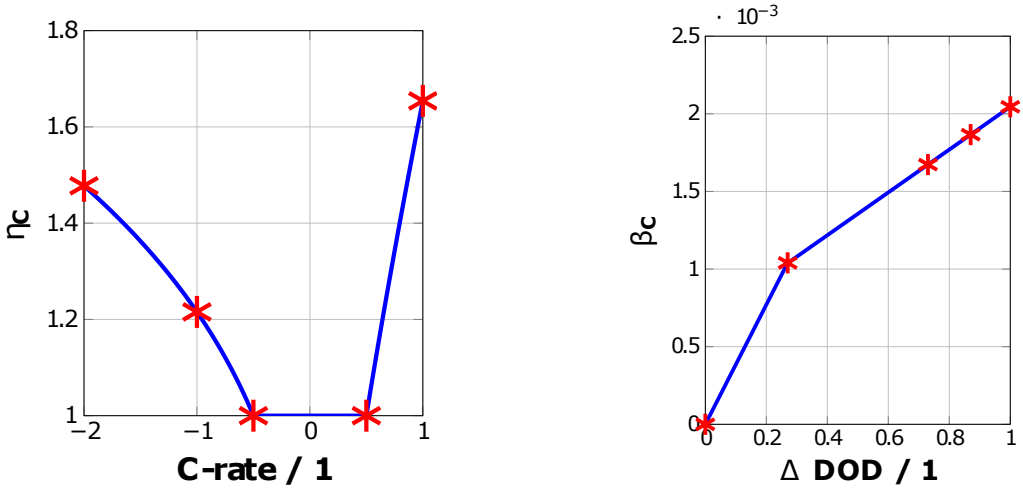

Figure 2.1: Gain factor in the current rate range of -2 C-rate in discharge direction to 1 C-rate in charge direction (left), and pure cyclic aging stress factor in the Δ *DoD* range from 0% to 100% (right) [13]

2.3 Energy Management System for Residential PV-BESS

Integration of intermittent, renewable energy sources into existing electric power grids is a difficult task. The most important approaches include demand control and energy storage [61]. Demand control requires shifting significant energy loads in time to coincide with periods of large energy production. Energy storage systems maximize local self-consumption of energy and smooth out the amount of energy supplied to and drawn from the grid.

The combination of Active Demand-Side Management (ADSM) and BESS is described by Castillo-Cagigal et al. [17]. The proposed system maximizes the use of the local PV generation by displacing deferrable loads. The experiments show

that the proposed energy management strategy improves the self-consumption and reduces the electricity transport and overall costs.

Senjyu et al. [123] present an approach to define the optimal configuration of residential renewable generation systems using GA as the optimization method. The goal of their approach is to minimize the initial costs with the annual operation and maintenance costs. The model considers different power sources such as PV systems and wind turbines. The developed algorithm finds the optimum energy system configuration for each household, minimizing the total cost and maximizing the overall self-consumption.

Taking advantage of historical data on energy production and consumption, Martins et al. [69] determined that optimal power flows in a residential PV-BESS can be used to minimize the overall energy costs. Using linear programming, the authors obtained optimal distribution of PV energy production and optimal composition of sources to satisfy energy demand. Considering data for a period of one year, the resulting time series represent ideal distribution of power flows taking into account not only solar energy harvestable at the current time, but also energy available in all future time steps. However, this approach cannot be used to manage energy in real time, as the future energy availability is not available with sufficient confidence. In addition, the optimal power flows obtained for a particular PV-BESS cannot be effectively analyzed or formalized for use in other, albeit similar systems.

Musilek et al. [85] proposed an advanced energy management system in the form of a fuzzy control system. The optimal power flows were scheduled using linear programming and used to determine the parameters of a Takagi-Sugeno fuzzy controller through evolutionary computing approach. The controller performance is comparable to the optimized system and can be effectively implemented to control power flows in other systems composed of PV and BESS.

2.4 Fuzzy Rule-Based Control Systems

Fuzzy rule-based control is an approach to deal with nonlinear relationships, and to analyse and control complex systems by capturing human knowledge in form of rules [23], [53], [83]. A fuzzy rule represents knowledge in continuous space, between 0 and 1, as a grouping of membership functions. It can be represented as a conditional statement in the following form

IF x is A THEN y is B,

where x and y are linguistics variables; and A and B are linguistics values determined by fuzzy sets in the universes of discourse X and Y, respectively [89]. A fuzzy control system specifies the input parameters in natural language and uses the fuzzy rules to define the relationships among different inputs with the output. The steps performed by a fuzzy control system during inference are: fuzzification of input variables, rule evaluation, aggregation of the rule outputs, and defuzzification [63], [95], [101].

2.5 Differential Evolution

Differential Evolution (DE) is an evolutionary optimization algorithm [105]. It is a real–valued optimizer that evolves a population of candidate solutions (vectors of floating point values) by iterative modification of the candidates through differential mutation and crossover. In each iteration, differential mutation is applied to the current population to form so called trial vectors. These vectors are further modified by various crossover operators. At the end of each iteration, the trial vectors compete with existing candidate solutions for survival in the population.

The basic operation of the traditional DE can be summarized as follows [105]. The i-th vector of N parameters is randomly initialized by:

$$\vec{x}_i[j] = rand(b_j^L, b_j^U), \quad j \in \{0, \ldots, N-1\}, \tag{2.4}$$

where b_j^L and b_j^U are, respectively, the lower and upper bound of the j-th parameter, and $rand(a, b)$ is a function generating a random number from the interval $[a, b]$. A fundamental differential mutation, *DE/rand/1*, can be described as:

$$\vec{v}_i = \vec{v}_{r1} + F(\vec{v}_{r2} - \vec{v}_{r3}), \tag{2.5}$$

where F is a scaling factor, and $\vec{v}_{r1}$, $\vec{v}_{r2}$ and $\vec{v}_{r3}$ are three vectors ($i \neq r1 \neq r2 \neq r3$) randomly selected from the population. Vector $\vec{v}_{r1}$ is the base vector, $\vec{v}_{r2}$ and $\vec{v}_{r3}$ are the difference vectors, and $\vec{v}_i$ is the target vector.

The target vector is combined with the trial vector using a uniform crossover operator:

$$l = rand(0, N-1), \tag{2.6}$$

$$\vec{v}_i[m] = \begin{cases} \vec{v}_i[m] & \text{if } (rand(0,1) < C) \text{ or } m = l \\ \vec{x}_i[m] \end{cases} \tag{2.7}$$

for each $m \in \{1, \ldots, N\}$. The operator replaces the parameters of $\vec{v}_i$ by the parameters from the target vector $\vec{x}_i$, with probability $1 - C$.

2.6 Linear Programming

Linear Programming (LP), also called linear optimization, is a method to determine the best outcome in a mathematical model whose requirements are represented by linear relationships. It aims to optimize an objective function subjected to linear equality and inequality constraints [144]. Its general form can be express as follows:

$$\min_x (c^T x) \tag{2.8}$$

$$\text{subject to:} \quad Ax \leq b \quad \text{(inequality constraints)}, \tag{2.9}$$

$$A_{eq}x = b_{eq} \quad \text{(equality constraints)}, \tag{2.10}$$

$$lb \leq x \leq ub \quad \text{(bound constraints)}, \tag{2.11}$$

where x represents the vector of decision variables; c, b, and b_{eq} are vectors of known coefficients; A and A_{eq} are matrices of known coefficients; and lb and ub are the lower and upper bound, respectively. The objective function $(c^T x)$ is the expression to be minimized or maximized. The inequalities $Ax \leq b$, $lb \leq x \leq ub$ and equalities $A_{eq}x = b_{eq}$ are the constraints over which the objective function is to be optimized.

Linear programming can be applied to industries as transportation, energy, telecommunications, and manufacturing. Also, it has proven useful in modeling diverse types of problems in planning, routing, scheduling, assignment, and design.

Chapter 3

Economic Optimization of Component Sizing for Residential Battery Storage Systems

Battery energy storage systems (BESS) are considered for a variety of applications in modern power grids [60]. As these systems decline drastically in cost, commercial and customer interest for this type of storage grows. As a result, the combination of residential Photo-Voltaic (PV) systems with battery storage (PV-Battery Energy Storage Systems; PV-BESS) and grid connection (grid-connected PV-BESS) have attained significant growth rates [27], [51], [97].

Such systems enable customers to avoid the retail electricity tariff for all energy fostered by surplus PV generation via buffering in the BESS as an alternative to selling surplus power at the feed-in tariff. This is a potentially profitable scenario in locations such as Australia, Canada, regions in the USA, and a number of countries in Europe where the electricity retail tariff exceeds PV feed-in tariffs. Academia has analyzed the economic value of PV-BESS for various individual systems [31], [87] for which small but positive business cases seem to be in reach for specific usage scenarios. In addition, several online tools are available, free of charge, and capable of analyzing the benefit for specific BESS with respect to load and PV size variation [9], [35], [103], [106]. Each of these approaches provide a sensitivity analysis for given BESS systems, but are unable to guide residential customers to find the economically best-suited storage and inverter combination for their specific needs.

Despite the fact that PV-BESS is still a niche market at present, various automotive companies have started to enter the market and have announced products with

drastically lower price tags, *e.g.* Tesla, Mercedes-Benz, and Nissan [75], [81], [93], making PV-BESS potentially economic in multiple regions around the world [27].

Interestingly, currently available and announced PV-BESS rely on different battery technologies and show a strong variation of storage size [30]. At a first glance, there appears to be a market trend towards lithium-ion based systems with storage capacity above 5 kWh coupled with inverter sizes of nominal power (P_N) often exceeding $P_N = 3$ kW [51]. Nevertheless, lead-acid (PbA) systems still hold an appreciable market share of over 10% for new system installations, and there is a strong competition within the category of lithium-ion batteries within which different cell chemistries differ significantly in performance, cost, and aging [51].

In contrast, others have used sensitivity studies to reveal the optimal size of storage system components. For example, Weniger et al. [140] provide a detailed analysis of power conversion efficiency of state-of-the-art battery home storage inverters. However, this work does not consider the economic impact of component sizing. Muenzel et al. [82] investigate the economics of residential storage systems with a dynamic programming derived operation strategy and screen payback periods achievable for several storage system sizes in Australia. Using generalized parameters for the inverter, cost, and degradation of an unspecified lithium-ion battery type, they anticipate a positive return on investment in the near future. In general, such sensitivity analyses commonly fail if various parameters are to be screened and optimized at the same time.

This issue can be effectively resolved using linear optimization approaches, which have been successfully applied to energy storage optimization. For example, Lauingera et al. provide a framework for electrical and thermal storage integration in households [56]. Based on linear programming, the energy dispatch of a residential building is optimized. However, this work does not consider the sizing optimization of storage and peripheral components, and battery storage aging is not part of the model.

In contrast to the aforementioned publications, this chapter conducts a comprehensive power flow analysis, implements technology-specific battery degradation, and presents a highly reproducible and easily adaptable linear optimization approach to assess both the cost and the maximum profit attainable for residential BESS. Parameterized with conditions matching the German regulatory framework as well as detailed cost and aging information for three commonly deployed battery

technologies (one PbA and two lithium-ion systems), this approach allows the best storage type and power electronics size to be selected for households with rooftop-mounted PV generators. The presented results also provide design rules applicable to residential PV-BESS around the world.

3.1 PV-BESS's Layout, Storage Model and Parametrization

This section summarizes all parameters relevant for BESS optimization. It describes the system layout, overviews technical parameters of the storage systems under investigation, and specifies the economic framework considered in this study.

3.1.1 System Layout

The schematic diagram of Figure 3.1 shows the system configuration as well as electrical connections and power flows for the PV-BESS system under study. All variables necessary for subsequent modeling are explained in more detail later, along with the definition of the optimization problem. The arrows in Figure 3.1 indicate the directions of power flow permitted for all component links. For this work, the optimization approach is confined to an Alternating Current (AC) coupling of battery storage, which offers the broadest flexibility in system design and is also suitable for the retrofitting of existent PV installations [134]. It is worth mentioning that a variety of different direct current (DC) system coupling topologies (*e.g.* generator coupled or converter link topology) have also been proposed for PV-BESS. Although such differing topologies have their individual strengths and weaknesses, an overall consistent trend in the choice of best technology and storage system sizing is expected [134].

3.1.2 Storage System Technical Parameters, Cost Assumptions, and Battery Aging Model

This study analyzes the economic potential and technical capabilities of three commonly used battery technologies for PV-BESS; a typical vented PbA system and two lithium-ion systems with lithium-iron-phosphate (LFP) and lithium-nickel-manganese-cobalt (NMC) cathodes respectively.

Table 3.1 provides an overview of the characteristic parameters for the individual technologies under investigation. Appendix A provides a more detailed survey

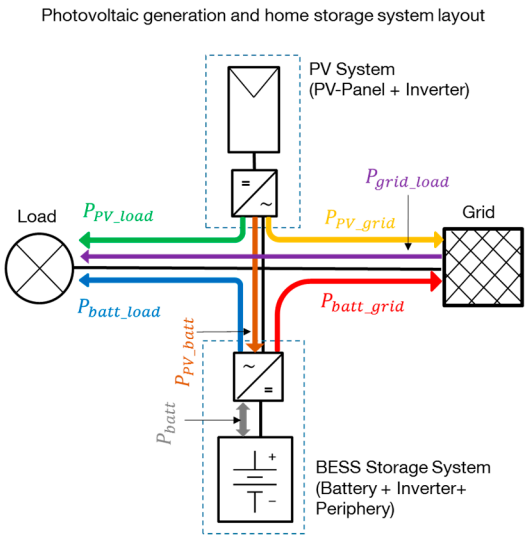

Figure 3.1: Schematic illustration of the investigated alternate current (AC) topology photovoltaic-battery energy storage systems coupling. Arrows indicate the direction of possible power flows between the individual components.

of common performance data and citations to literature references for all battery technologies under consideration. It is worth mentioning here that data on aging and lifetime predictions are highly sensitive to various influencing factors (*e.g.* cell construction type, sealing quality, and electrolyte additives) and test conditions. Furthermore, the values are likely to vary between batteries of individual manufacturers. However, questioning the correctness of the available lifetime data is not the focus of this work. The trends are well in accordance with the literature, and lifetime estimations derived in this work match well with the expert knowledge of BESS manufacturers.

The battery efficiency (η_{batt}) is given as an averaged number of round trip Watt-hour retention using typical low charge and discharge rates of 0.1 C (capacity-rate) and ambient temperature (approximately 25 °C). These conditions correspond well to the scenarios commonly present for a typical home storage system. Self-discharge (SD_{batt}) values considered in the optimization model are also listed in Table 2.1 and taken into account during simulations. However, having relatively small values, self-discharge plays a minor role, especially for the lithium-ion based battery chemistries.

In contrast, the aging of storage devices cannot be neglected. In fact, the deterioration of storage is a major cost driver during storage operation. It is common to differentiate between cyclic and calendric aging processes for battery degradation,

Table 3.1: Performance parameters of BESS using three different battery technologies. The data was derived from a literature survey (see Appendix A). Terms state of charge (SoC) and full equivalent cycles (FEC) are further explained in the text.

Parameter	**Unit**	**Battery Technology**		
		PbA	**LFP**	**NMC**
η_{batt} : Battery round-trip efficiency	%	85	98	95
SD_{batt}: Self-discharge per day	%	0.17	0.02	0.02
($\mathrm{SoC}_{min} - \mathrm{SoC}max$): Usable SoC	%	50–100%	5–95%	5–95%
$Life_{Cal}^{80\%}$: Calendric life indicator in years	(years)	10	15	13
$Life_{Cyc}^{80\%}$: Cycle life indicator in FEC	(FEC)	1500	10,000	4500
$C_{var,bat}$: Variable battery price	€/kWh	271	752	982
C_{fix} : Fixed price for storage (price for housing, cooling, and periphery)	€	1182	1723	580

as described in detail for PbA [117] and lithium-ion batteries [137]. The battery cyclic and calendric lifetime indicators ($Life_{Cyc}^{80\%}; Life_{Cal}^{80\%}$) specify a battery usage scenario, until a certain capacity fade for a battery cell becomes evident. As obvious from the nomenclature, values provided in the table are linked to the remaining state of health (SoH) of 80% nominal capacity, matching a typical replacement criterion for automotive applications. In this paper, we use a simple estimate solely for time-dependent calendric aging processes as well as a charge throughput-dependent cyclic aging model. The values of calendric lifetime ($Life_{Cal}^{80\%}$) provide a reference value for storage degradation to 80% SoH at 20 °C temperature, when no charge throughput is applied. To describe the cyclic aging ($Life_{Cyc}^{80\%}$) caused by energy throughput in the battery storage, a correlation with Full Equivalent Cycles (FEC), based on the definition by Fuchs et al. [28], is used:

$$\mathrm{FEC} = 0.5 \times \frac{1}{t} \int \mathrm{SoC}\,(t)\,dt \approx\ 0.5 \times \frac{\int |P_{batt}|\,dt}{E_{batt}^{nom}}. \tag{3.1}$$

The factor of 0.5 results from the conversion of charge throughput to full cycle counting consisting of one charging and one discharging process. SoC denotes the state of charge, P_{batt} is the power flow via the battery, and E_{batt}^{nom} is the nominal energy capacity of the battery. A theoretical maximum charge throughput is defined via $Life_{Cyc}^{80\%}$, *i.e.* the number of FEC until 80% capacity is reached if there is no calendric aging. To formulate battery aging for subsequent modeling, the following equations are derived:

$$aging_{cal} = \frac{\Delta t}{Life_{Cal}^{80\%}}. \tag{3.2}$$

$$aging_{cyc} = \frac{0.5 \times \int |P_{batt}|\,dt}{Life_{Cyc}^{80\%} \times E_{batt}^{nom}}. \tag{3.3}$$

In accordance with Schmalstieg et al. [119], a superposition principle is used to estimate the overall aging:

$$aging_{tot} = aging_{cal} + aging_{cyc}. \tag{3.4}$$

As such, a parameter value of $aging_{tot} = 0$ corresponds to a fresh, unused battery, whereas at $aging_{tot} = 1$, the remaining capacity of the battery is 80% of its original value as a result of calendric time and battery use. Further use of the storage system with $aging_{tot} > 1$ might be allowed if the replacement of storage is set to a remaining capacity below 80%, as further described below. A detailed analysis and validation of battery performance and aging models in the context of such techno-economic applications is given by Goebel et al. [36].

Table 3.1 also summarizes the economic parameters of the storage system. In this study, the investment costs of different battery types for BESS and the inverter coupling are analyzed independently. The values listed in the table are derived from a recent detailed market survey with $n = 445$ storage systems [30]. These values are discussed in more detail in a separate publication [44]. We attribute the lower fixed price for NMC storage, compared to the price offset determined for LFP and PbA systems, mainly to synergy effects attainable with storage systems that have been developed for the electric vehicle automotive market (relying mostly on NMC-based battery chemistry).

For the sole battery storage investment without an inverter, the following price structure is considered:

$$C_{Batt}\left(E_{batt}^{nom}\right) = C_{fix} + C_{var,Bat} \times E_{batt}^{nom}. \tag{3.5}$$

where C_{Batt} represents the price of the battery, C_{fix} is the fixed price including all peripheries and housing of the storage system, and $C_{var,Bat}$ is the energy specific price of a storage system. The storage maintenance cost within the battery lifetime is negligible and not considered herein. Furthermore, the separate installation cost of the storage system is not taken into account; such costs are strongly linked to the PV installation cost and may vary strongly for individual households. For the inverter systems, the following assumptions are made: one way conversion efficiency $\eta_{inv} =$ 97.5%, calendric life of 20 years, and a variable cost of approximately $C_{var,inv} =$ 155 $/kW$ (see also Table 3.2). Data used was derived from an internet market survey on standalone DC/AC inverters and expert interviews with leading brand inverter

manufacturers [30], [102]. As most PV-BESS package batteries and inverters are in one casing, no separate fixed costs for inverters are assumed but are given as part of the overall storage fixed cost C_{fix}.

Table 3.2: Inverter performance and price information derived from literature survey [30], [102].

Inverter Data	**Unit**	**Value**
η_{inv}: Average one way inverter efficiency	%	97.5
T_{inv}: Assumed inverter lifetime in years	(years)	20
$C_{var,inv}$: Cost of inverter per nominal power	€/kW	155

As such, the overall cost $C_{storage}$ for the energy storage system including battery storage with energy content E_{batt}^{nom}, inverter with nominal power P_{inv}^{nom}, and all peripherals cost C_{fix} totals to:

$$\begin{aligned} &C_{storage}\left(E_{batt}^{nom}, P_{inv}^{nom}\right) = C_{battery}\left(E_{batt}^{nom}\right) + C_{inverter}\left(P_{inv}^{nom}\right) \\ &= C_{fix} + C_{var,batt} \times E_{batt}^{nom} + C_{var,inv} \times P_{inv}^{nom}. \end{aligned} \tag{3.6}$$

3.1.3 Economic and Legal Framework for BESSs

For the economic framework refer to Table 3.3. A retail energy price of 28.69 ct€/kWh and feed-in tariff of 12.31 ct€/kWh are assumed, in accordance with a retail price analysis and EEG ("Erneuerbare Energien Gesetz"—German renewable energies act), which granted feed-in tariffs for PV installations in Germany for 2016 [6], [12]. Furthermore, in accordance with German regulations, a feed-in limit of $f^{noEES} = 70\%$ has to be taken into account for all residential PV installations. This means that power exceeding the feed-in limit $P_{feed,max} = f^{noEES} \times P_{peak,PV}$ may not be injected from the household back to the grid. Instead, this additional power can be either stored in a battery or an unfavorable curtailment becomes effective (*i.e.* regulatory forced dissipative energy loss at the PV generator/inverter). It is worth mentioning that, for storage installations taking advantage of a government funded subsidy program on home storage systems, the PV grid feed-in regulation is enforced with a more strict curtailment rate of 50% [3]. For such partially subsidized systems, a discount of storage system investment may be obtained. As such, for subsidized systems with discount rate $r_{subsidy}$, the storage investment cost is given as:

$$C_{storage}^{subsidy} = C_{\text{storage}} \times \left(1 - r_{subsidy}\right). \tag{3.7}$$

Table 3.3: Remuneration and retail energy prices for households in Germany (2016), and legal framework for PV-grid feed-in.

Economic and Legal Framework	Variable	Value
Retail energy price	c_{buy}	28.69 ct€/kWh
Feed-in energy reimbursement tariff	c_{sell}	12.31 ct€/kWh
Maximum feed-in ratio (without BESS subsidy)	f^{noEES}	0.7
Maximum feed-in ratio (with BESS subsidy)	f^{EES}	0.5
Government subsidy rate for storage systems	$r_{subsidy}$	0.22

3.2 Linear Optimization of PV-BESSs

The structure of the optimization problem addressed in this study can be represented by a mathematical model. The objective function and the constraints have linear relationships, meaning that the effect of changing a decision variable is proportional to its magnitude. This makes Linear Programming (LP) well suited to solve the optimization problem considered here due to the linearity of the decision variable on electricity price, feed-in tariff, and other parameters. While some aspects of battery system operation are not linear, they can be linearized to fit the requirements of LP. *e.g.* models of Battery Energy Storage System (BESS) aging processes can be reductively applied to obtain a linearized degradation function. In addition, linear optimization provides unambiguous, repeatable results with modes and controllable computational effort as compared to other optimization methods which are typically based on heuristics or meta-heuristics.

The economically optimal battery storage component sizing for a household equipped with PV and an energy storage system is obtained using LP. The load demand and PV-generation profiles considered in this study cover one full year so as to capture all seasons with their characteristic patterns of PV-generation, storage, and grid energy transfers. As the intent is to minimize electricity cost and maximize the revenue generation on the profit side, two types of profits are considered: the profit attainable by feeding energy into the grid, and the *avoided cost* stemming from the reduced need to purchase energy when a storage system is installed. On the annual cost side, a fraction of the total cost of the energy storage system C_{tot} is considered. This fraction is determined based on a battery storage technology-specific aging analysis as further described below. The presented cost flow analysis takes into account the discounted storage cost caused by degradation.

The data used for simulations was averaged with a resolution of $\Delta t_{res} = 15$ min,

which is a value that provides a reasonable compromise between the accuracy of the obtained results and computational speed [7]. As such, the one-year simulation time frame covers a total of 35,040 time intervals, indexed with variable i.

All variables and parameters considered in this study are described in Table 3.4. The locally generated PV power (P_{pv_i}) is first used to satisfy the local demand. When the local power production is greater than the demand, the surplus power is preferably transferred to the battery ($P_{pv-batt_i}$) and stored for later use. If there is still additional energy available, the surplus power is injected into the grid ($P_{pv-grid_i}$) or curtailed via a a feed-in limitation ($P_{curtail_i}$). The following equation considers all power flows from the PV generator:

$$P_{pv_i} = P_{pv-load_i} + P_{pv-batt_i} + P_{pv-grid_i} + P_{curtail_i}. \tag{3.8}$$

Table 3.4: Variables and parameters used for the battery modeling and optimization routines.

Battery Modelling Parameter	**Variable**	**Unit**	**Constraints/Comments**
Load demand (historical data)	P_{load_i}	kW	$\geq$0; input data
PV power generated (historical data)	P_{pv_i}	kW	$\geq$0; input data
Nominal power of the battery inverter	P_{inv}^{nom}	kW	subject to optimization
Nominal battery capacity	E_{batt}^{nom}	kWh	subject to optimization
Bidirectional power flow from/to the battery	P_{batt_i}	kW	result of optimization
PV power fed to the load	$P_{pv-load_i}$	kW	$\geq$0; see Equations 3.8 and 3.10
PV power stored in the battery	$P_{pv-batt_i}$	kW	$\geq$0; see Equation 3.8
PV power exported to the grid	$P_{pv-grid_i}$	kW	$\geq$0; see Equation 3.8
Power transferred from the battery to the load	$P_{batt-load_i}$	kW	see Equation 3.10
Power exported from the battery to the grid	$P_{batt-grid_i}$	kW	$\geq$0; see Equation 3.13
Power imported from the grid to the load	$P_{grid-load_i}$	kW	$\geq$0; see Equation 3.10
Surplus power-curtailed according to regulations	$P_{curtail_i}$	kW	$\geq$0; see Equation 3.9
State of health	SoH_i	p.u.	see Equations 3.18 and 3.19
Battery energy content at time i	E_{batt_i}	kWh	see Equations 3.14 and 3.15
State of charge	SoC_i	p.u.	$[\text{SoC}_{min}; \text{SoC}_{max}]$

To avoid back-feeding of power injected into the grid from PV system owners, a a feed-in limitation is enforced. Any power above the limitation threshold value must be discarded as a curtailment loss, *i.e.*:

$$P_{pv-grid_i} + P_{curtail_i} \leq P_{feed,max}. \tag{3.9}$$

To meet the electrical demand (P_{load_i}) the system first attempts to use power from local generation ($P_{pv-load_i}$). If this is not sufficient, power is drained from the battery ($P_{batt-load_i}$). As the last resource, the system draws power from the grid ($P_{grid-load_i}$). Consequently, demand is comprised of the following three components:

$$P_{load_i} = P_{pv-load_i} + P_{batt-load_i} + P_{grid-load_i}. \tag{3.10}$$

The bidirectional power flow from the storage inverter to the battery is stored in an auxiliary variable (P_{batt_i}) and correlated with the inverter efficiency η_{inv}:

$$P_{batt_i} = (\eta_{inv} \times P_{pv-batt_i}) - \frac{1}{\eta_{inv}} \times (P_{batt-load_i} + P_{batt-grid_i}). \tag{3.11}$$

where η_{inv} is the average one-way efficiency of the inverter. The reciprocal efficiencies are the battery charge power $P_{pv-batt_i}$ and the discharge power $P_{batt-load_i} + P_{batt-grid_i}$, both being limited by the nominal power flow from the inverter to the battery:

$$0 \leq P_{pv-batt_i} \leq P_{inv}^{nom}. \tag{3.12}$$

$$0 \leq P_{batt-load_i} + P_{batt-grid} \leq P_{inv}^{nom}. \tag{3.13}$$

where P_{inv}^{nom} corresponds to the inverter nominal size. The battery energy content at time step i (E_{batt_i}) satisfies the recurrence relation:

$$E_{batt_i} = \left(E_{batt_{i-1}} \times \frac{SD_{batt}}{d}\right) + \left(\eta_{batt} \times P_{batt_i} \times \frac{1h}{\Delta t_{res}}\right). \tag{3.14}$$

where SD_{batt} represents the self-discharge factor of the battery and $d = 96$ is a conversion factor of the number of time steps per day. The energy content of the storage system is further confined by an upper boundary that decreases upon usage and aging according to the State of Health (SoH):

$$E_{batt_i} \leq E_{batt}^{useable} \times \mathrm{SoH}_i. \tag{3.15}$$

The SoH is defined as the irreversible capacity fade over time, related to the nominal battery capacity, and $E_{batt}^{useable}$ is a fraction of the total energy content of the battery installed:

$$E_{batt}^{useable} = \mathrm{E}_{\mathrm{batt}}^{\mathrm{nom}} \times (\mathrm{SoC}_{max} - \mathrm{SoC}_{min}). \tag{3.16}$$

For battery usage in stationary and automotive applications, it is useful to define an End of Life (EOL) criterion, which is often linked to the SoH with a certain percentage value $\alpha_{Replace}$ [143]. This percentage value also defines the time of battery replacement:

$$\mathrm{EOL} \rightarrow \mathrm{SoH}_{t=EOL} \leq \alpha_{Replace}. \tag{3.17}$$

In many cases, $\alpha_{\mathrm{Replace}}$ varies between 80% and 70% for automotive applications. However, lower values are often stated for less demanding residential storage applications [5]. In this study, $\alpha_{\mathrm{Replace}} = 60\%$ is used as the replacement parameter,

matching *e.g.* the warranty conditions of the Tesla® Powerwall product. Using the definition of $aging_{tot} = 1$ at SoH = 80%, the SoH condition reads:

$$\mathrm{SoH} = 1 - aging_{tot} \times 0.2. \tag{3.18}$$

The time evolution of SoH also satisfies the recurrence relation:

$$\mathrm{SoH}_i = \mathrm{SoH}_{i-1} - (aging_{cal_i} + aging_{cyc_i}) \times 0.2. \tag{3.19}$$

Using Equations 3.1 and 3.2, the calendric and cyclic aging can be estimated as:

$$aging_{cal_i} = \frac{\mathrm{i} \times \Delta \mathrm{t_{res}}}{Life_{Cal}^{80\%}}. \tag{3.20}$$

$$aging_{cyc_i} = aging_{cyc_{i-1}} + 0.5 \times \frac{|P_{batt_i} \times \Delta t_{res}|}{E_{batt_i}} \times \frac{1}{Life_{Cyc}^{80\%}}. \tag{3.21}$$

As such, the additional cyclic aging degradation of time step i is estimated by the energy throughput in that time step ($P_{batt_j} \times \Delta t_{res}$) divided by the energy content of the system E_{batt_i}. Additionally, it is normalized with the factor 0.5 and the technology specific cycle life indicator $Life_{Cyc}^{80\%}$. Similarly, the SoC can be expressed as:

$$\mathrm{SoC}_i = \frac{E_{batt_i}}{E_{batt}^{useable} \times \mathrm{SoH}_i}. \tag{3.22}$$

The optimal solution must satisfy all constraints described above. The optimization process aims to reduce the overall cost by minimizing the expenses for energy purchase and the implicit cost caused by battery degradation. This cost model is divided into three components, *i.e.*:

$$\text{minimize } C_{tot} = C_{buy\_energy} - R_{sell\_energy} + C_{storage\_deg}^{subsidy}\ . \tag{3.23}$$

subject to constraints in equations 3.8– 3.22.

The first component C_{buy_energy} comprises the cost of energy purchased from the grid, while the second component R_{sell_energy} is the revenue from PV energy generation exported to the grid. These two components are evaluated as follows:

$$C_{buy\_energy} = \sum_i C_{buy} \times P_{grid-load_i}. \tag{3.24}$$

$$R_{sell\_energy} = \sum_i C_{sell} \times (P_{pv-grid_i} + P_{batt-grid}). \tag{3.25}$$

where C_{buy} and C_{sell} are the retail electricity price and feed-in tariff, respectively. The third component estimates the home storage system degradation cost that can be represented as:

$$C^{subsidy}_{storage\_deg} = \Delta\text{SoH}/(1-\alpha_{Replace}) \times C^{subsidy}_{battery}\left(E^{nom}_{batt}\right) + C^{subsidy}_{inverter}\left(P^{nom}_{inv}\right) \times \Delta t/T_{inv} \tag{3.26}$$

where Δt denotes the timespan covered with the simulation (one year for this work) and ΔSoH is the total battery aging. The full battery related cost is then calculated in consideration of the initial installation investment cost and the 22% subsidy scheme available in the German market.

For economic assessment, the cash flow for a household with the best-sized PV-BESS installed is compared against the cash flow for a household with the same PV-generation but no storage system. This is done because, the energy expenses, feed-in remuneration, and storage degradation cost for a PV-BESS household is related to the energy expenses and feed-in remuneration for a household with no storage:

$$R^{BESS}_{savings} = \left(-C^{BESS}_{buy_{energy}} + R^{BESS}_{sell_{energy}} - C^{subsidy}_{storage\_deg}\right) - \left(-C^{noStorage}_{buy_{Energy}} + R^{noStorage}_{sell_{energy}}\right). \tag{3.27}$$

For profitability analysis, the yearly Return on Investment (ROI) can be calculated considering the battery's savings in each year of operation, the initial investment cost, and the storage system life:

$$ROI = \frac{R^{BESS}_{savings} - C^{subsidy}_{storage}}{C^{subsidy}_{storage}}. \tag{3.28}$$

3.3 Results and Discussion

Optimization was performed for the three battery technologies (PbA, LFP, and NMC) with the parameters listed in Table 3.1. The load profiles were based on a reference smart meter-recorded dataset obtained from HTW Berlin and averaged to 15 min intervals [107]. The PV-generation data was acquired for one full year (2014) using a rooftop-mounted solar generator in downtown Munich, Germany (the profile data is shown in Figure 3.2). The one second resolution PV-generator output power data was normalized to the peak power of the system and preprocessed by averaging over the time frames of 15 min. To obtain a variation of load demand and PV-generation profiles, both time series were linearly scaled to the desired values.

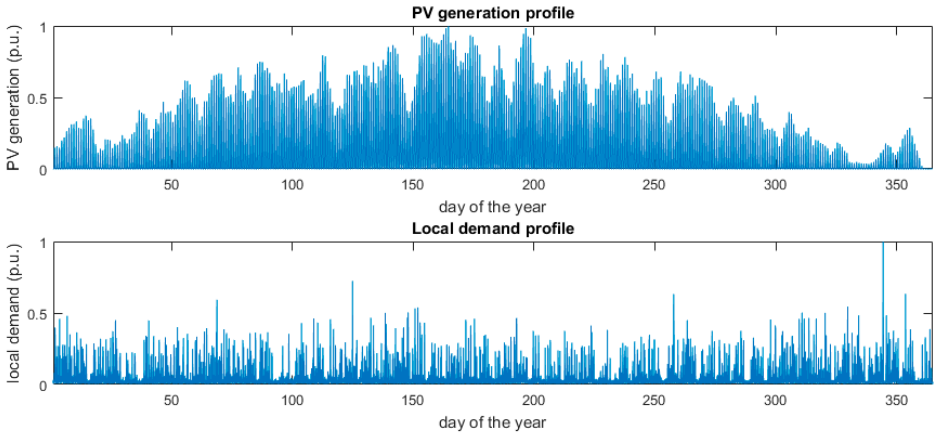

Figure 3.2: PV generation and load profile used for this simulation study. Both profiles are scaled according to the scenarios described in the paper. The load profile was taken from [107].

The linear optimization was implemented in MATLAB® (MathWorks, Natick, MA, USA) code using a dual-simplex algorithm, which is based on a conventional simplex algorithm on the dual problem [94]. Each one year system simulation (with co-optimization of storage and inverter size, and a 15-min time resolution for all power flows in the system) took approximately 300–800 s on a Dell® (Dell Inc, Round Rock, TX, USA) XPS 15 system with Intel i7, depending on the number of iterations necessary for the linear optimization.

A detailed analysis is conducted for an exemplary PV-BESS system using LFP battery chemistry for a typical four-person household (annual load of 6 MWh) and a small size PV-generator (PV size of 4 kWp). For this case, the one-year optimization calculates the optimal storage size of $E_{batt}^{nom} = 7.5$ kWh and inverter nominal power of $P_{inv}^{nom} = 1.6$ kW. Figure 3.3 shows the power flows for an exemplary three-day period during summer (first week of June) within the system using these optimally sized components. The top panel shows the local household consumption (grey area below zero), the PV generated power (yellow area above zero), as well as power flow covered by the storage system (green area). The second and third panels show the evolution of SoC and SoH during the same time span, clearly showing the periodically changing charge level of the storage system and its gradual degradation.

It can be seen that the optimization process maximizes profit using the full capacity of the storage system: it charges the battery up to the maximum allowed SoC during daytime and fully drains it over night. For almost all tested scenarios,

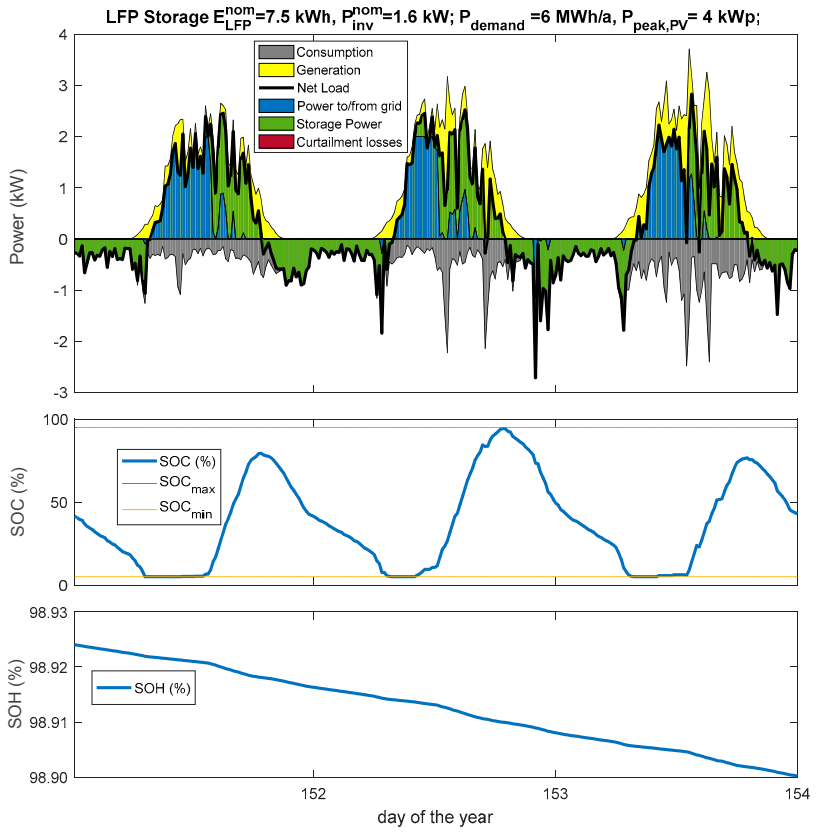

Figure 3.3: Power flow analysis for a three-day period using lithium-iron-phosphate (LFP) battery chemistry: load and power flows within the system (**top**); time correlated evolution of battery state of charge (**middle**); and resulting state of health (SoH) decline (**bottom**).

linear programming using a complete load and generation data set successfully avoids curtailment losses. To achieve this optimal operation of BESS, the generated power is sometimes split. This can be observed during the second day shown in Figure 3.3; power is partly fed to the grid ($p_{PV-grid} \leq 2$ kW) and partly used to charge the battery at a rate limited by the inverter size ($p_{batt_{in-out}} \leq 1.6$ kW). At all times, the resulting storage charging strategy favors the lowest cost, *i.e.* it prefers battery usage over curtailment of energy or power exchange with the grid, whenever possible. Furthermore, self-discharge losses are kept at a minimum by charging the battery in the later period of the day (except when a feed-in limitations would induce curtailment). A closer look at the spiky loads for the second day shown in the figure reveals that there are short time periods when power is drawn from the grid despite the fact that the battery is still above its minimal SoC. This can be explained by the limited size of the inverter (here $P_{inv}^{nom} = 1.6$ kW) that does not allow full load

saturation from the battery. In fact, a more powerful inverter would allow further reduction of the amount of energy drawn from the grid, but these small savings would not justify the additional cost of a larger inverter.

The third plot in Figure 3.3 shows the evolution of battery degradation during the three-day timespan; a continuous degradation progress (calendric aging) superimposed to additional charge throughput dependent degradation (cyclic aging) is apparent, albeit at a very slow rate.

Over the course of one year, the investigated storage system executes 202 FEC and provides electricity cost savings of about 238 €, when compared to a household with no storage system installed. It should be noted that the storage system does not execute a full cycle each day, a fact that is common to all storage systems and that can be mainly attributed to seasonal patterns.

Using Equation 3.7 for this optimally sized system, the cost of the subsidized storage system can be estimated as:

$$\begin{aligned} &C_{storage}^{subsidy}\,(\text{LFP},\ 7.5\ \text{kWh},\ 1.6\ \text{kW}) \\ &\quad = (\mathrm{C_{fix,LFP}} + \mathrm{C_{var,LFP}} \times 7.5\ \text{kWh}) \times (1 - r_{subsidy}) \\ &\qquad\qquad + (\mathrm{C_{var,inv}} \times 1.6\ \text{kW}) \times (1 - r_{subsidy}) \\ &\quad \approx 5743€\ + 193€\ = 5936€\ . \end{aligned} \tag{3.29}$$

At the same time, due to the continuous calendric aging and daily cycling of the battery system, the SoH is reduced by 1.79% over the course of one year. When considering this degradation, the value of the storage system is reduced according to Equation 3.26:

$$\begin{aligned} C_{storage\_deg}^{subsidy} &= \frac{\Delta\text{SoH}}{(1 - \alpha_{Replace})} \times C_{battery}^{subsidy}\,(\mathrm{E_{batt}^{nom}}) \\ &\qquad + \frac{\Delta t}{T_{inv}} \times C_{inverter}^{subsidy}\,(P_{inv}^{nom}) \\ &= \frac{1.79\%}{40\%} \times 5743€ + 193€ \times \frac{1}{20} \approx 267€. \end{aligned} \tag{3.30}$$

As a result, the overall ROI of the system is:

$$ROI = \frac{R_{savings}^{BESS}}{C_{storage\_deg}^{subsidy}} = \frac{238€ - 267€}{267€} = -10.86\%. \tag{3.31}$$

This calculation reveals that, for the example parameter setting chosen here (4 kWp PV and 6 MWh annual load demand), even the optimally sized LFP storage

system does not provide positive ROI. A closer look at the literature on the economics of PV-BESS systems confirms that such negative ROI is well in line with other studies based on similar parameters [87], [134]. It should be noted that, in contrast to this work, most other studies discuss the scenario of future rising electricity retail prices resulting in positive ROI numbers. To achieve positive ROI for this specific storage system, the price for the 7.5 kWh battery would need to drop by about 12% at below 5100 € (instead of the 5743 €assumed here).

For a more systematic comparison of the three examined battery technologies, consider the group of contour plots shown in Figure 3.4. Optimization runs were performed for a variety of load demand and PV-generation values using all three battery systems (PbA on the left, LFP in the middle, and NMC on the right). The upper row of plots show the optimal size of the respective battery, whereas the three plots in the middle row reveal the optimal inverter size for each storage system. The bottom row depicts the resulting maximum attainable ROI for the three systems. They compare the profit attainable for a household with a PV-BESS against the cost and revenue for a household with a PV system only.

As an overall trend, homes with large load and PV size require BESS with increased storage and inverter size. For the PbA technology, significantly larger systems are economically favored in comparison to lithium-ion based systems. This can be attributed to a lower average price per kWh of PbA batteries compared to the alternatives. However, it should be noted that only 50% of the installed battery capacity is usable for PbA systems due to a smaller usable SoC range for this technology (see also Table 3.1).

Interestingly, the optimal nominal power of the inverter systems remains low. With the cost assumed in this work, the ratio between storage capacity and nominal inverter size should be chosen at values as low as 0.25 kW/kWh for optimal ROI results. Currently, ratios of 1 kW/kWh are often used in commercial systems. Thus, this finding can be used as a guideline for cost reduction of future residential BESS.

A general trend of better ROI for large PV and high load demand can also be observed. This can be explained when analyzing the cost structure of storage with a fixed offset price for the battery housing and periphery. As such, larger installations reduce the overall cost per installed kWh of storage.

In direct comparison, and using the battery parameters chosen herein, the LFP storage systems appear to be economically superior to both NMC and PbA systems

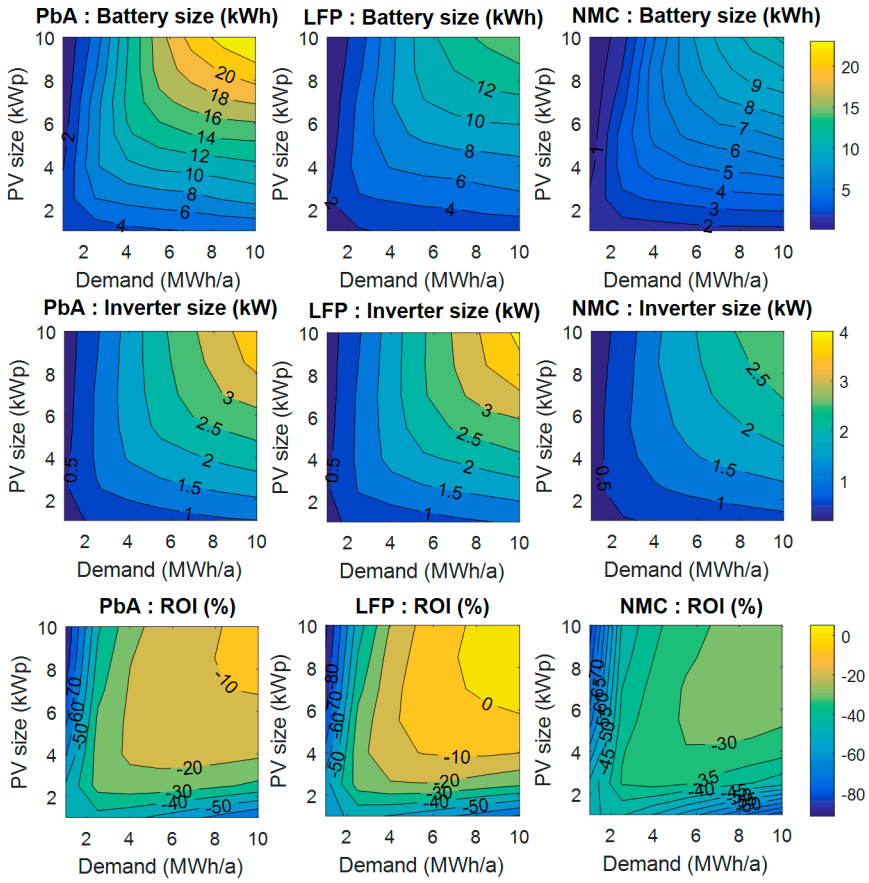

Figure 3.4: Graphical representation of the optimization results using contour plots: from top to bottom, the panels show optimum battery size, inverter size, and corresponding maximum attainable return on investment (ROI) for a variation of yearly load demand and local PV generation. From left to right, three battery technologies (lead-acid (PbA), LFP, and lithium-nickel-manganese-cobalt (NMC)) are depicted.

for most tested scenarios. In fact, there is a small area, for PV systems larger than 6 kWp and a yearly load greater than 6 MWh, where slightly positive ROI values can be achieved with today's costs. This shows that there is a good chance of BESS becoming economically viable with PV systems in the near future. Potentially, an increase in retail electricity tariffs may further improve the ROI of a residential storage system installed in 2016. A more important fact is that the prices of storage systems are rapidly declining. A recent report listed 20% annual reduction in 2015 [51], and this cost decline is expected to continue in the following years, likely making future BESS more economically feasible. As a result, the ROI values shown here will likely turn positive within the next few years.

Refer to Figure 3.5 and Table 3.5 for a detailed comparison among the examined

battery storage technologies. The three graphs depict the economically most favored settings in example cases with 1, 2.5, and 4 MWh annual load demand. The inset numbers in the right panel indicate the optimum sizing of battery and inverter for each simulation scenario (the first number indicates the optimum size of the storage system in kWh and the second number is the nominal size of the inverter in kW). The overall shape of the ROI curves reveals the existence of scenario specific peaks. When a small PV generator is used, most generated power is used directly by local consumption. As the amounts of grid feed-in are small, storage cannot add much value to the system, and aging related costs clearly dominate the overall price of the storage systems. On the other hand, for very large PV installations, a significant portion of the local demand can be covered from PV-generation without storage. As self-supply levels are high, storage provides only small additional benefits. Interestingly, for different combinations of PV size and household power demand, PbA and NMC storage might be favored over a LFP storage solution. While, for very small households, the NMC system operates at the lowest cost, LFP surpasses PbA and NMC for households at 4 MWh annual load demand. For loads of 2.5 MWh, LFP or PbA storage can be economically most viable, depending on the PV system size.

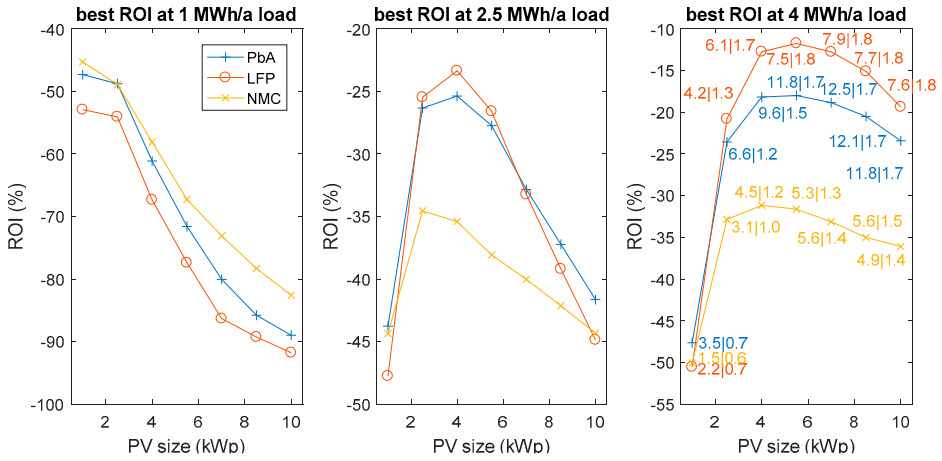

Figure 3.5: ROI comparison of optimally sized battery energy storage systems at varying PV size for three battery technologies (NMC, PbA, and LFP). Depending on the annual household load demand (**left**: 1 MWh/a, **center**: 2.5 MWh/a, **right**: 4 MWh/a) different technologies are favored. The inset numbers in the right panel indicate the optimum sizing of battery and inverter for each simulation scenario.

The fact that NMC performs best for small load demands and PV-generation can be attributed to the significantly lower fixed battery cost of NMC-based BESS

Table 3.5: Return on investment (ROI) optimal sizing of battery and inverter for an average four person household (load demand of 4 MWh/a).

PV Size (kWp)	**1**	**2.5**	**4**	**5.5**	**7**	**8.5**	**10**
PbA battery (kWh)	3.51	6.61	9.57	11.76	12.46	12.10	11.82
Inverter for PbA system (kW)	0.67	1.18	1.55	1.69	1.73	1.72	1.69
LFP battery (kWh)	2.23	4.18	6.12	7.50	7.94	7.68	7.56
Inverter for LFP system (kW)	0.69	1.26	1.66	1.75	1.80	1.78	1.76
NMC battery (kWh)	1.52	3.10	4.51	5.27	5.60	5.63	4.89
Inverter for NMC system (kW)	0.56	0.95	1.19	1.32	1.38	1.46	1.41

systems. This advantage is most prominent for small storage system sizes ($\leq$2 kWh). Despite the more than 2.5-fold higher specific cost of the LFP system compared to PbA (752 €/kWh vs. 271 €/kWh), its better aging performance, higher conversion efficiency, and the increased usable SoC range makes it superior in most cases, especially if the battery has to withstand an increased number of FEC. Only for cases where the optimally sized PbA systems undergo less than or equal to 100 FEC per year, PbA may out perform LFP. Such a scenario is found where ratios of PV-generation to local demand are 2 kWp/MWh or higher.

To validate the optimization results presented in this study, we conducted 1-s resolved time series analyses of power flows using an in house developed storage assessment tool *SimSES* [87]. All performed comparisons matched well, confirming the validity of results and analysis presented in this paper. For example, for LFP cell chemistry, the results of one year simulations for all tested load and PV generation cases differ by less than 0.5% for SoH and less than 3% for ROI. Such small deviations can be attributed to coarser discretization of validation points within the tool (0.5 kW inverter size and 0.5 kWh storage size) and to slight differences in the storage operational strategy, which was not optimized when using the validation tool.

3.4 Final Remarks

This chapter describes a linear optimization approach to find the most cost-effective BESS dimensioning, matching a variety of residential load demand and local PV generation profiles. To allow a direct comparison of one PbA and two lithium-ion batteries, the optimization problem formulated in this work maximizes the electricity cost savings while minimizing the storage specific degradation costs.

The optimization provides unambiguous, repeatable results with controllable computational effort and reveals the best suited sizing of the battery storage and

inverter based on present retail price information. Within the tested scenarios, the best economical results have been attained using LFP storage systems at high load demand (>6 MWh annual demand) and local generation (>6 kWp PV generation). However, it must be clearly stated that, considering the storage degradation and price information as presented in this work, the profit attainable remains very small and peaks at $ROI = 5\%$ per anum. In fact, the ROI values remain negative for most considered scenarios. Nevertheless, a comparison of the three storage systems reveals that different storage technologies perform best for specific combinations of PV generation and local demand. Optimally sized NMC storage systems appear most economical for households with very small local demand (2 MWh/a), whereas PbA-based systems show some advantages for a mid-scale demand (2.5 MWh) and high PV generation (>7.5 kWp). At a higher local electricity demand (≥4 MWh) coincident with higher PV generation (≥ 3 kWp), LFP batteries provide better results than PbA and NMC.

The obtained results can be used also to determine the optimal ratio of power electronics sizing (rated power of the inverter) to the installed battery capacity. An example would be that, for a typical residential scenario of 4 kWp PV and annual local demand of 6 MWh, about 0.25 kW rated power per 1 kWh installed battery capacity shows optimal performance. This detailed analysis of optimal power-to-energy ratio could also be taken as a guideline for designing new, more cost-effective BESS products. In many actual cases, power electronic components appear to be over-sized and do not properly match the needs of typical residential customers. This aspect will be of significant importance in other BESS applications, *e.g.* the provision of primary control reserves, industrial peak-shaving, and storage integration to micro grids.

As a general remark, it is important to note that, considering the current typical cost of a storage system and the retail energy tariff valid in Germany for 2016, most scenarios do not favor storage system installation over a sole PV system. Nevertheless, future electricity price evolution is likely to reverse this trend. The increased customer independence achieved using BESS may be profitable only in the long run under the assumption of rising retail electricity tariffs. In general, storage may provide additional value by stacking other applications, *e.g.* provision of uninterrupted power supply or energy market trading via cloud based pooling of battery storage systems.

Chapter 4

LP-based Predictive Energy Management System for Residential PV-BESS

The share of energy provided from renewable sources, such as Photo-Voltaic (PV) systems, has been increasing in the residential sector [57]. Renewable energy integration can be further improved through the deployment and integration of energy storage systems [84]. The goal of a PV generation system combined with Battery Energy Storage Systems (BESS) is to improve the efficiency and sustainability of the power grid [2], [39]. These technologies also increase grid reliability and economic efficiency, compared to single-source generation without storage.

Such PV-BESS installed locally at individual households can provide significant cost savings by consuming self-produced energy and reducing the need to purchase energy from the grid [141]. In addition, such systems contribute to better balancing of the entire power grid by smoothing out peaks in power demand and production. They produce extra power when the solar radiation is higher than local demand, and store the energy for later usage when solar radiation weakens or demand increases.

The operation of PV-BESS requires the use of sophisticated control strategies. Weniger et al. [142] analyzed forecast-based operation strategies for residential PV-BESS, and showed that such systems can improve self-sufficiency and provide feed-in peak shaving. A look-ahead energy management system for a grid-connected residential PV-BESS, based on Kalman Filtering, was proposed by Yoo et al. [145]. Other studies took into account the lifetime costs of hybrid renewable energy systems and optimized their operation using genetic algorithms [22].

This chapter proposes an advanced energy management system in the form of

a rule-based controller. A previously developed model [69] is used to iteratively generate the optimal power flows among the components of the PV-BESS and the grid, for a selected time window. The optimal power flows are then used by the rule-based system to direct power through the system in an optimal way. This forms a general predictive energy management strategy that can be implemented to control power flows in other PV-BESS or similar hybrid energy systems. The performance of the proposed controller is thoroughly tested using simulations and compared with three different strategies: greedy, schedule mode, and feed-in damping.

4.1 System Description and Power Flow Optimization

This section summarizes all parameters relevant for the PV-BESS optimization. It describes the system layout, introduces the evaluation criteria for measure the performance of a PV-BESS, specifies the cost model and constraints of the linear model, and presents the three operational strategies considered for comparison.

4.1.1 System Description

The energy management system proposed in this study is derived from measured and simulated data for an exemplar PV-BESS. The modeled system consists of a solar panel with nominal power of 10 kWp, LFP battery-based BESS with capacity of 10 kWh, 3 kW inverter, and annual demand of 6MWh. The simulations involve a grid-connected system shown in a block diagram in Figure 4.1, along with all considered power flows.

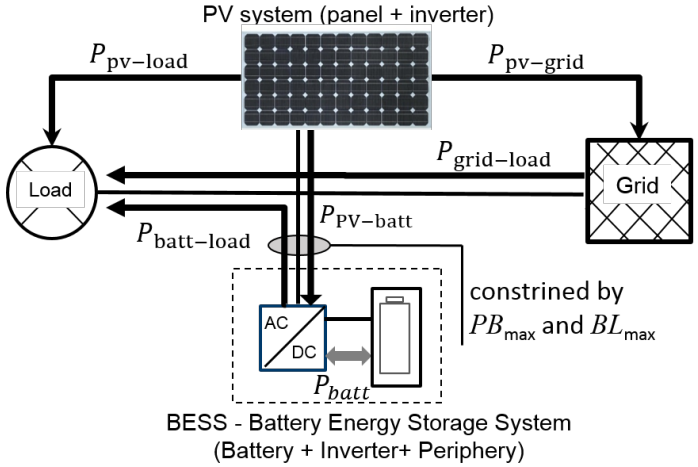

Figure 4.1: System configuration and power flows considered

Data used for simulations was averaged with a resolution of $\Delta t_{res} = 15$ min, a value that provides a reasonable compromise between accuracy of the obtained results and computational speed [8]. Thus, the one-year simulation period covers an overall of 35,040 time intervals, indexed with variable i. The analysis presented here takes into account the discounted storage cost caused by cyclic and calendric aging. As such, it allows realistic assessment of BESS operation, including battery degradation [85]. The operation of the entire PV-BESS system is governed by the following principles.

Any locally generated PV power, P_{pv_i}, is first used to satisfy the local demand, $P_{\mathrm{pv-load}_i}$. When the local power production is greater than the demand, the surplus power is preferably transferred and stored in the battery for later use, $P_{\mathrm{pv-batt}_i}$. If there is still additional surplus, it is injected into the grid, $P_{\mathrm{pv-grid}_i}$, or curtailed via a a feed-in limitation. Thus, the actual flows of power from the PV-generator must satisfy the following inequality:

$$P_{\mathrm{pv}_i} \geq P_{\mathrm{pv-load}_i} + P_{\mathrm{pv-batt}_i} + P_{\mathrm{pv-grid}_i}, \tag{4.1}$$

and any power above the feed-in limit, $P^{\max}_{\mathrm{pv-grid}}$, must be discarded as a curtailment loss, P_{curtail_i}.

To meet the electrical demand, P_{load_i}, the system first attempts to use power from local generation. If this is not sufficient, power is drained from the battery, $P_{\mathrm{batt-load}_i}$. As the last resource, the system draws power from the grid, $P_{\mathrm{grid-load}_i}$. Thus, demand is comprised of the following three components:

$$P_{\mathrm{load}_i} = P_{\mathrm{pv-load}_i} + P_{\mathrm{batt-load}_i} + P_{\mathrm{grid-load}_i} \tag{4.2}$$

The battery energy content at the i-th time step, E_{batt_i}, satisfies the following recurrent relation:

$$E_{\mathrm{batt}_i} = \left(E_{\mathrm{batt}_{i-1}} \cdot \frac{\mathrm{SD}_{batt}}{d} \right) + \left(\eta_{batt} \cdot P_{\mathrm{batt}_i} \cdot \frac{1\mathrm{h}}{\Delta t_{\mathrm{res}}} \right), \tag{4.3}$$

where P_{batt_i} represents the bidirectional power flow between the BESS inverter and the battery, SD_{batt} is the self-discharge factor of the battery, $d = 96$ is the conversion factor of time steps per day, and η_{batt} is the averaged number of round trip Watt-hour retentions for the battery. Auxiliary variable P_{batt_i} reflects the inverter efficiency:

$$\begin{aligned} P_{\mathrm{batt}_i} =& \eta_{inv} \cdot P_{\mathrm{pv-batt}_i} \\ & - \frac{1}{\eta_{inv}} \cdot (P_{\mathrm{batt-load}_i} + P_{\mathrm{batt-grid}_i}), \end{aligned} \tag{4.4}$$

where η_{inv} is the average one-way efficiency of the inverter. The reciprocal efficiencies are the battery charge power $P_{\mathrm{pv-batt_i}}$ and the discharge power $P_{\mathrm{batt-load_i}} + P_{\mathrm{batt-grid_i}}$, both limited by the maximal power flow from the inverter to the battery, $P_{\mathrm{inv}}^{\mathrm{max}}$, corresponding to the inverter size.

The remaining parameters used for the simulations are self-discharge $SD_{\mathrm{batt}} = 0.02\%/\mathrm{day}$, usable state of charge between 5% and 95%, and battery life cycle indicators $Life_{\mathrm{calendric}}^{80\%} = 15$ per year and $Life_{\mathrm{cyclic}}^{80\%} = 10000$ full equivalent cycles. The average one-way inverter efficiency is considered $\eta = 0.975$, and the battery round trip efficiency is $\eta_{\mathrm{batt}} = 0.98$. The reference cost scenario, based on the current situation in Germany, considers $C_{\mathrm{buy}} = 28.96¢/\mathrm{kWh}$, feed-in energy reimbursement tariff $C_{\mathrm{buy}} = 12.31¢/\mathrm{kWh}$, and maximum feed-in ratio $f_{\mathrm{pv-grid}}^{\mathrm{max}} = 0.5$.

4.1.2 Evaluation criteria

The performance of a PV-BESS operation strategy can be evaluated through several metrics related to the and operation of the system. In this contribution, the economic activity is gauged by the total cost of energy purchased from and sold to the grid. From the annual operational perspective, three energy-related factors are defined [111], [142]. Self-sufficiency factor, ξ, describes how much of the total load can be attended by the PV-BESS:

$$\xi = \frac{E_{pv-load} + E_{batt-load}}{E_{load}}, \tag{4.5}$$

i.e. $\xi = 0$ represents a household with no local generation or storage, and $\xi = 1$ correspond to a situation when the PV-BESS system supplies the total local demand. Self-consumption factor, ν, specifies how much of the total PV production is directly used or stored in the battery:

$$\nu = \frac{E_{pv-load} + E_{pv-batt}}{E_{pv}}. \tag{4.6}$$

Restriction in the feed-in power can lead to curtailment of PV power and thus result in energy losses. The curtailment loss factor, κ, indicates how much loss is due to curtailment:

$$\kappa = \frac{E_{curtail}}{E_{pv}}. \tag{4.7}$$

These metrics indicate the operational strategy performance [10]. The objectives of the strategies compared in this chapter are to maximize ξ and ν and minimize κ.

4.1.3 Determination of Optimal Power Flows

The optimal solution aims to reduce the overall cost by minimizing the expenses for energy purchase and the implicit cost caused by the battery degradation [42]. The optimal solution must also satisfy all constraints described in Section 4.1.1. The cost model can be divided into three components, *i.e.*:

$$\text{minimize} \quad C_{\text{tot}} = C_{\text{buy\_E}} + R_{\text{sell\_E}} + C^{\text{discount}}_{\text{storage\_deg}} \tag{4.8}$$

The first component $C_{\text{buy\_E}}$ comprises the cost of energy purchased from the grid, while the second component $R_{\text{sell\_E}}$ is the revenue from PV energy generation exported to the grid. These two components are evaluated as follows:

$$C_{\text{buy\_E}} = \sum_i C_{\text{buy}} \cdot P_{\text{grid}-\text{load}_\text{i}}, \tag{4.9}$$

$$R_{\text{sell\_E}} = \sum_i C_{\text{sell}} \cdot (P_{\text{pv}-\text{grid}_\text{i}} + P_{\text{batt}-\text{grid}_\text{i}}), \tag{4.10}$$

where C_{buy} and C_{sell} are the retail electricity price and feed-in tariff, respectively. The third component, $C^{\text{discount}}_{\text{storage\_deg}}$, is the discounted storage cost caused by cyclic and calendric aging that can be represented as:

$$C^{\text{discount}}_{\text{storage\_deg}} = \frac{\Delta\text{SoH}}{(1-\alpha_{\text{SoH}})} \cdot (E^{\text{nom}}_{\text{batt}}) + (P^{\text{nom}}_{\text{inv}}) \cdot \frac{\Delta t}{T_{\text{inv}}}, \tag{4.11}$$

where Δt denotes the time span covered with the simulation (here one year), T_{inv} represent the initial investment, $P^{\text{nom}}_{\text{inv}}$ and $E^{\text{nom}}_{\text{batt}}$ are respectively the nominal power of the battery inverter and the nominal battery capacity, and ΔSoH the total battery aging.

4.1.4 Operational Strategies

PV-BESS can be managed using different algorithms that focus on distinct objectives and result in distinct power flows. These algorithms, or *operational strategies*, have the objective of maximizing the self-sufficiency of a household equipped with a PV-BESS. This is achieved by storing the surplus PV energy produced during the day, and using it later when the residual load is positive. For comparison purposes, three strategies are considered: greedy strategy, schedule mode, and feed-in damping.

The greedy strategy only focuses to maximize the self-consumption. The locally generated PV power is first used to satisfy the local demand. When local power

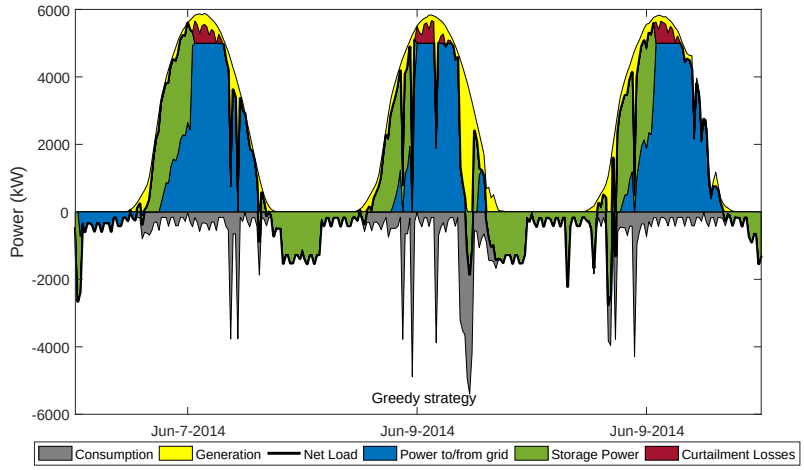

Figure 4.2: Power flows in the examined PV-BESS for June 2014 with high availability of solar energy, and greedy controller strategy

production is greater than the demand, the surplus energy is stored in the battery for later use. In the case of additional energy surplus, the extra power is injected into the grid. Unfortunately, this strategy usually charges the battery and reaches the SoC limit before the peak of production in the middle of the day. Figure 4.2 illustrates this for a day with high PV production: the battery charging is high in the first few hours of the PV production, and the storage system achieves its maximum SoC before noon. As a result, the curtailment losses increase because the surplus power cannot be exported to the grid given the a feed-in limitation.

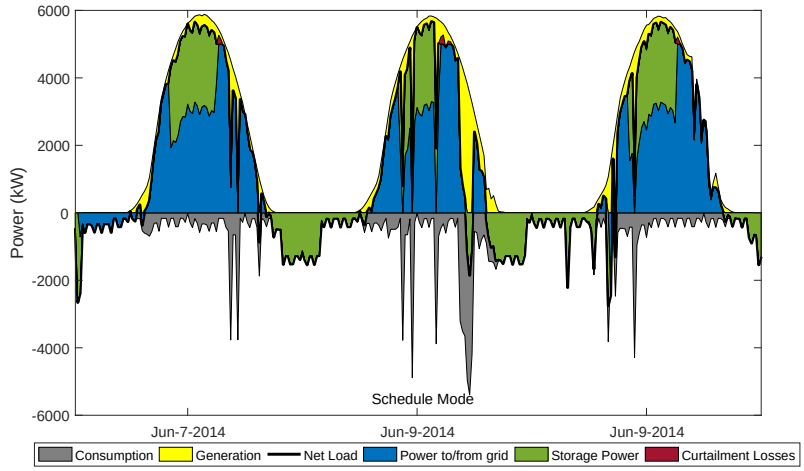

Figure 4.3: Power flows in the examined PV-BESS for June 2014 with high availability of solar energy, and schedule mode controller strategy

In contrast to the greedy strategy, the schedule mode strategy focuses on minimizing the curtailment losses [127], [135]. In this strategy, the battery is typically

charged at a predefined time, typically when there is high solar radiation. The residual PV production is exported to the grid until the activation of the charging mode instead of directly charging the battery with the surplus energy. Although this strategy avoids curtailment losses, the battery may not be totally charged at the sunset during days with low solar irradiation. The principle operation of this strategy is shown in Figure 4.3. In this example, the charging occurs between 10:00 a.m. and 3:00 p.m. This results in decreasing the curtailment losses when compared to the greedy strategy.

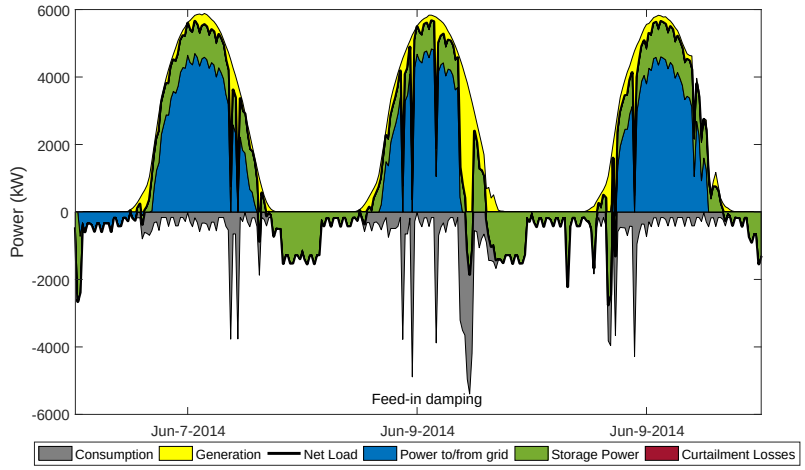

Figure 4.4: Power flows in the examined PV-BESS for June 2014 with high availability of solar energy, and feed damping controller strategy

A modification in the schedule mode strategy allowing constant charging power leads to the feed-in damping strategy [111]. This strategy uses a rough prediction of the PV production to define the charging time and decreases the curtailment losses in days with high solar radiation. Figure 4.4 depicts the feed-in damping strategy. It relies on the predicted duration of the residual power. It is possible that the actual residual power is not the same as the predicted value. For this reason, the battery may not be at the desired SoC at the end of the day.

4.2 Linear Programming Controller

To manage power flows in the PV-BESS system, a linear programming–based predictive energy manager (LP-PEMS) has been developed. Its operation, whose high-level description is shown in Figure 4.5, is based on the results of the LP simulations. At the beginning, the LP-PEMS is provided with the PV-BESS parameters (described

in Section 4.1.1), including the size-of optimization window. This window represents the time interval to run the optimization. The optimal power flows are determined using LP and then used at the time of control intervention.

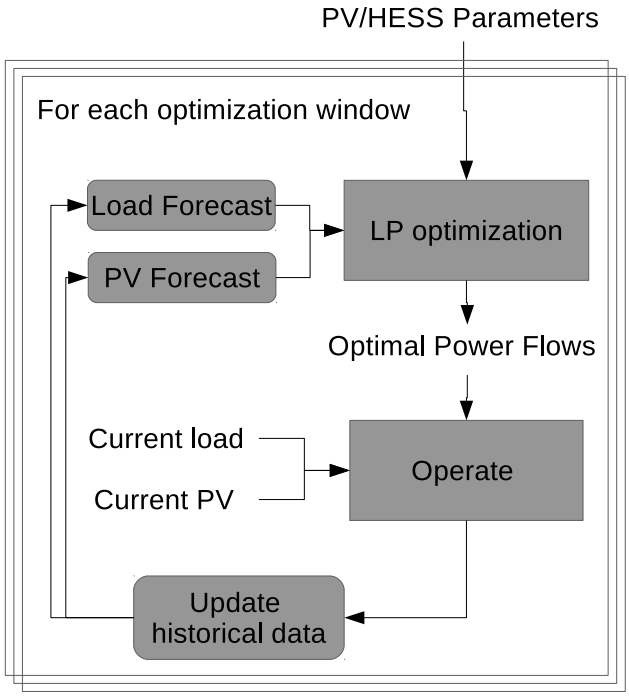

Figure 4.5: Linear programming controller schematic in high level

To facilitate the understanding, Figure 4.6 shows the steps executed in each iteration for three subsequent time windows. This example uses the electrical demand signal and a 10 days operation window. The historical signal (in blue) is known before the optimization starts, and it is used to generate the forecast signal (in red) that must be at least as long as the optimization window. The optimal power flows are then used to operate with the real signal (in black) that has in this example length of one day. After executing all determined operations on the PV-BESS, the controller updates the historical signal and shifts the optimization window before starting the next iteration.

The input variables, used by the controller to devise an efficient PV-BESS operation, reflect the state of the system and environmental conditions at the time of control intervention i. The first group of inputs, the optimal power flows, is defined during the LP run executed w.r.t. the optimization window. The second group of inputs is the electrical demand and the PV production at the same time step i.

In order to manage the PV-BESS power flows, the control strategy implemented

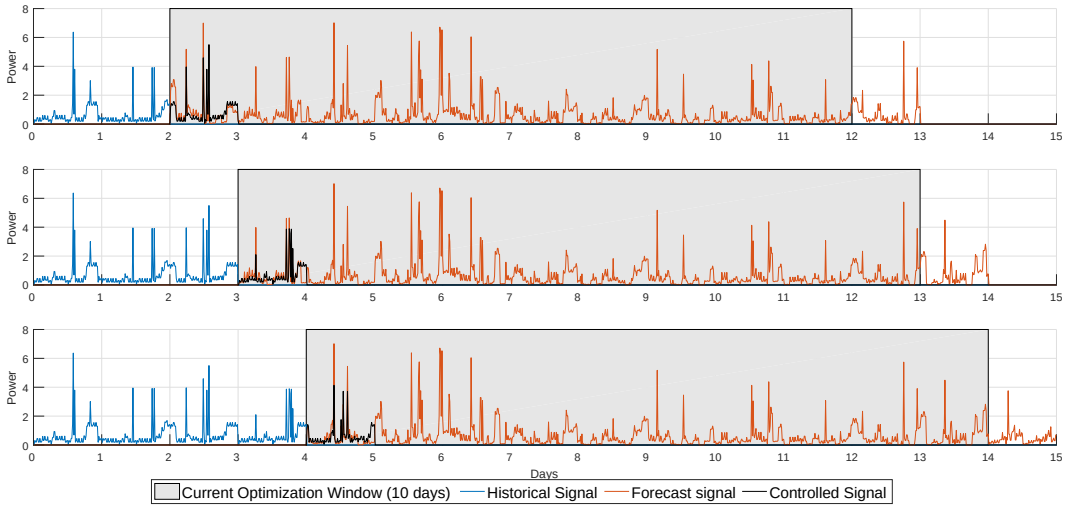

Figure 4.6: 3 iterations with a 10 days operation window iteration

by LP-PEMS makes the following assumptions:

i) all available PV energy is used to satisfy the electrical demand;

ii) extra PV energy is either stored into the battery or sent to the grid;

iii) outstanding electrical demand is satisfied either from the battery or the grid; and

iv) no power is transferred between the power grid and the battery (*i.e.* $P_{\text{grid}-\text{batt}} = 0$).

These assumptions correspond to the LP–based solution of the optimal power flow problem.

Table 4.1: Comparison of system performance

–	**Greedy**	**Schedule mode**	**Feed-in damping**	**Optimal**	**LP-PEMS with perfect forecast**	**LP-PEMS with flat load (mean)**
Self sufficiency(%)	65.99	58.56	62.93	68.40	68.39	54.50
Self consumption(%)	64.34	56.42	60.97	61.90	61.90	48.98
Curtailment Loss (%)	1.04	0.27	0.26	0.01	0.01	0.73
Energy purchased - Energy sold	334.36	407.38	364.39	219.06	219.06	354.20
Total Cost (equation (4.8))	482.25	548.27	509.45	366.23	366.22	489.26

The operation of the proposed linear programming controller can be formally

described as follows:

$$\begin{aligned}
&\text{IF } P_{\text{pv}} \geq P_{\text{load}} \text{ THEN} \qquad (4.12)\\
&\quad P_{\text{batt-load}} = 0,\\
&\quad P_{\text{pv-load}} = P_{\text{load}},\\
&\quad P_{\text{pv-batt}_{\text{factor}}} = \frac{P_{\text{pv-batt}_{\text{opt}}}}{P_{\text{pv}_{\text{opt}}} - P_{\text{load}_{\text{opt}}}},\\
&\quad P_{\text{pv-batt}} = \min\{P_{\text{pv-batt}_{\text{factor}}} \cdot (P_{\text{pv}} - P_{\text{load}}), PB_{\max}\},\\
&\quad P_{\text{pv-grid}} = \min\{P_{\text{pv}} - P_{\text{load}} - P_{\text{pv-batt}}, P_{\text{feed}}^{\max}\},\\
&\quad P_{\text{grid-load}} = 0,\\
&\text{IF } P_{\text{pv}} < P_{\text{load}} \text{ THEN} \qquad (4.13)\\
&\quad P_{\text{pv-load}} = P_{\text{pv}},\\
&\quad P_{\text{batt-load}} = \min\{P_{\text{pv}} - P_{\text{pv-load}}, P_{\text{batt-load}_{\text{opt}}}, BL_{\max}\},\\
&\quad P_{\text{pv-batt}} = 0,\\
&\quad P_{\text{pv-grid}} = 0,\\
&\quad P_{\text{grid-load}} = \max\{P_{\text{load}} - P_{\text{pv}} - P_{\text{batt-load}}, 0\},
\end{aligned}$$

$$P_{\text{batt-grid}} = P_{\text{batt-grid}_{\text{opt}}}, \qquad (4.14)$$

where $P_{\text{pv-batt}_{\text{factor}}}$ describes the fraction of the PV production stored in the battery during the LP optimization; $BL_{\max}$ and $PB_{\max}$ are coefficients representing the maximum possible power flow between the battery and load, and between the PV generation systems and battery respectively. Subscript $_{\text{opt}}$ represents the optimal power flow results defined during the LP execution (*i.e.* $P_{\text{pv-batt}_{\text{opt}}}$, $P_{\text{load}_{\text{opt}}}$, $P_{\text{pv}_{\text{opt}}}$).

4.3 Results and Discussion

As described in section 4.2, the goal of the proposed LP-PEMS is to develop an operational strategy that is based on the solution of the optimal power flow problem. In addition, the designed strategy should be effective to implement and easy to understand. At the same time, a significant performance improvement is expected w.r.t. to the alternative operational strategies (greedy, schedule mode, and feed-in damping).

The main advantage of the proposed LP-PEMS is the use of sort-term energy production and consumption forecasts. However, it is important to note that the

development of the (load and generation) forecasting is outside the scope of this work. Two default forecast signals are used instead: perfect forecast (known historical values of generation and load) and flat signal (means of the historical load data).

Operational strategies aim to improve the operational efficiency of the entire PV-BESS, and their success or failure can be gauged by examining the values of the previously introduced technical and economical metrics reported in Table 4.1. In the following analysis, the proposed LP-PEMS is compared to the three alternative strategies and to the optimal results reported earlier [69]. The values in the last column of the table correspond to the case of flat load that will be compared separately at the end of this section.

The increase of the self-sufficiency factor indicates that LP-PEMS provides more energy to the load compared to the other three strategies. On the other hand, in terms of self-consumption factor, LP-PEMS is surpassed by the greedy strategy. This strategy charges the battery as fast as possible, achieving full charge during the days with high solar radiation sometimes starting the next charging cycle before fully discharging the battery. In contrast, LP-PEMS only charges the battery so that the amount of stored energy can supply demand during the next few hours before PV production starts again. This way, LP-PEMS can increase the revenue from the PV generation exported directly to the grid. This desirable behavior is captured by the remaining three metrics that attain their optimal values for the proposed LP-PEMS. The fact that all metrics evaluate very close to the optimal results [69] indicates that the selected time window of 10 days is fully sufficient, providing the same results as when the entire year of data is considered.

To show the value of forecasts in predictive energy management, the load forecast was replaced by a flat signal representing the average historical load for a given household. As shown in the last column of Table 4.1, this simplification causes significant deterioration of system performance.

A more detailed look at the operation of LP-PEMS is provided in Figure 4.7 showing the time series of all involved power flows. Figure 4.8 offers a comparison of the distribution of PV energy in the systems among the load, battery, grid (left), and composition of the sources of energy used to satisfy demand(right), over the one year simulation period.

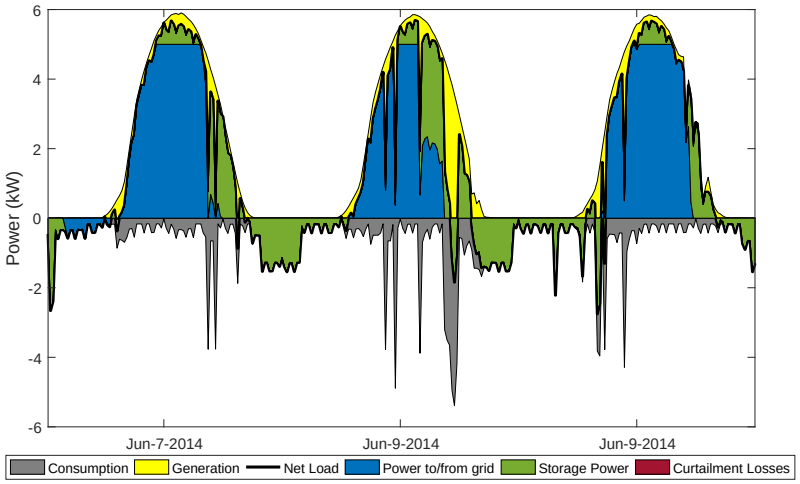

Figure 4.7: Operation of LP-PEMS (three days in 2014)

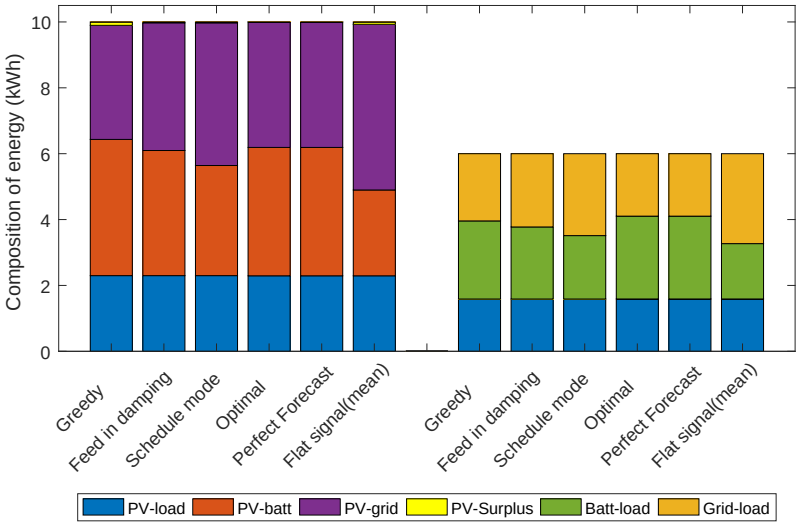

Figure 4.8: Composition of energy [kWh] generated by the PV system (left) and served to the load (right) over the one year period, comparing all the operational strategies

4.4 Final Remarks

This chapter introduces a linear programming-based predictive energy management system (LP-PEMS) for hybrid residential PV-BESS. Its operation is rooted in linear optimization of power flows within the system, based on forecast values of load and PV energy production. The resulting controller provides superior technical and economical performance compared to other common operational strategies.

Chapter 5

Optimal Energy Management of Residential PV-BESS Using Evolutionary Fuzzy Controller

The goal of *smart grid* is to improve the efficiency, economics, sustainability and reliability of the production and delivery of electricity [2]. It can effectively respond to changes in demand, help balancing electricity consumption and supply, and support integration of renewable energy sources in the power grid [39]. Renewable energy integration can be further improved through the deployment of hybrid energy sources [84] and the use of energy storage systems. These technologies also increase grid reliability and economic efficiency, compared to single-source generation without storage.

An important example of hybrid technologies with rapid uptake in the residential market are Photo-Voltaic (PV) generation systems combined with home Battery Energy Storage Systems (BESSs). Such PV-BESS installed locally at individual households can provide significant cost savings by reducing the need to purchase energy from the grid. In addition, such systems contribute to better balancing of the entire power grid by smoothing out peaks in power demand and production. They produce extra power when the solar radiation is higher than local demand, and store the energy for later usage when the solar radiation weakens or the demand increases.

Operation of PV-BESS hybrids requires use of sophisticated control strategies. Weniger et al. [142] analyzed forecast-based operation strategies for residential PV-BESS. They showed that such systems can improve self-sufficiency and provide feed-in peak shaving. A look-ahead energy management system for a grid-connected

residential PV-BESS, based on Kalman Filtering, was proposed by Yoo et al. [145]. Other studies took into account the lifetime costs of hybrid renewable energy systems and optimized their operation using genetic algorithms [22].

This chapter builds on the optimal power flows to develop an advanced energy management system in the form of a fuzzy control system. The model in the previous study [69] is used to determine the parameters of a Takagi-Sugeno fuzzy controller using an evolutionary computing approach. The resulting system is general and can be implemented to control power flows in other PV-BESS. In addition, owing to the transparent nature of fuzzy rules, it allows an in-depth analysis of the optimal operation strategies that would be impossible by direct examination of the power flows obtained using conventional optimization methods.

5.1 System Description and Power Flow Optimization

This section summarizes the system description, describe the constraints of the linear model, and the cost model that must be minimized to determinate the optimal power flows.

5.1.1 System Description

The energy management system proposed in this study is derived from measured and simulated data for an exemplar PV-BESS. The modeled system consisted of a solar panel with nominal power of 10 kWp, LFP battery-based BESS with capacity of 12 kWh, inverter size of 3.4 kW, and annual demand of 7MWh. The measurements include time series of load and PV generation collected at sites in Germany between January 1 and December 31, 2014. The simulations involve a grid-connected system shown in a block diagram in Figure 4.1. The diagram also depicts all power flows considered in the simulation and optimization studies described below.

Data used for simulations was averaged with a resolution of $\Delta t_{res} = 15$ min, a value that provides a reasonable compromise between accuracy of the obtained results and computational speed [8]. Thus, the one-year simulation period covers an overall of 35,040 time intervals, indexed with variable i. The operation of the entire PV-BESS system is governed by the following principles.

Any locally generated PV power, P_{pv_i}, is first used to satisfy the local demand, $P_{\mathrm{pv-load}_i}$. When the local power production is greater than the demand, the surplus power is preferably transferred to the battery, $P_{\mathrm{pv-batt}_i}$, and stored for later use. If

there is still additional surplus, it is injected into the grid, $P_{\mathrm{pv-grid}_i}$, or curtailed via a feed-in limitation. Thus, the actual flows of power from the PV-generator must satisfy the following inequality:

$$P_{\mathrm{pv}_i} \geq P_{\mathrm{pv-load}_i} + P_{\mathrm{pv-batt}_i} + P_{\mathrm{pv-grid}_i}, \tag{5.1}$$

and any power above the feed-in limit, $P^{\max}_{\mathrm{pv-grid}}$, must be discarded as a curtailment loss, P_{curtail_i}.

To meet the electrical demand, P_{load_i}, the system first attempts to use power from local generation. If this is not sufficient, power is drained from the battery, $P_{\mathrm{batt-load}_i}$. As the last resource, the system draws power from the grid, $P_{\mathrm{grid-load}_i}$. Thus, demand is comprised of the following three components:

$$P_{\mathrm{load}_i} = P_{\mathrm{pv-load}_i} + P_{\mathrm{batt-load}_i} + P_{\mathrm{grid-load}_i} \tag{5.2}$$

The battery energy content at the i-th time step, E_{batt_i}, satisfies the following recurrent relation:

$$E_{\mathrm{batt}_i} = (E_{\mathrm{batt}_{i-1}} \cdot \frac{\mathrm{SD}_{batt}}{d}) + (\eta_{batt} \cdot P_{\mathrm{batt}_i} \cdot \frac{1\mathrm{h}}{\Delta t_{\mathrm{res}}}) \tag{5.3}$$

where P_{batt_i} represents the bidirectional power flow between the BESS inverter to the battery, SD_{batt} is the self-discharge factor of the battery, and $d = 96$ is the conversion factor of time steps per day.

P_{batt_i} is an auxiliary variable that reflects the inverter efficiency:

$$\begin{aligned} P_{\mathrm{batt}_i} =& \eta_{inv} \cdot P_{\mathrm{pv-batt}_i} \\ & - \frac{1}{\eta_{inv}} \cdot (P_{\mathrm{batt-load}_i} + P_{\mathrm{batt-grid}_i}), \end{aligned} \tag{5.4}$$

where η_{inv} is the average one-way efficiency of the inverter. The reciprocal efficiencies are the battery charge power $P_{\mathrm{pv-batt_i}}$ and the discharge power $P_{\mathrm{batt-load_i}} + P_{\mathrm{batt-grid_i}}$, both limited by the maximal power flow from the inverter to the battery, $P^{\max}_{\mathrm{inv}}$, corresponding to the inverter size.

The remaining parameters used for the simulations were battery round trip efficiency $\eta_{\mathrm{batt}} = 0.98$, self-discharge $SD_{\mathrm{batt}} = 0.02\%/day$, usable state of charge between 5% and 95%, and battery life cycle indicators $Life^{80\%}_{\mathrm{calendric}} = 15$ per year and $Life^{80\%}_{\mathrm{cyclic}} = 10000$ full equivalent cycles. The average one-way inverter efficiency was considered $\eta = 0.975$. The economic and legal framework was based on the

current situation in Germany, *i.e.* retail energy price $C_{\text{buy}} = 28.96¢/\text{kWh}$, feed-in energy reimbursement tariff $C_{\text{buy}} = 12.31¢/\text{kWh}$, and maximum feed-in ratio $f_{\text{pv-grid}}^{\max} = 0.5$.

The performance of a PV-BESS operation strategy can be evaluated through a number of metrics related to the economic feasibility and self-sufficiency of the system. In this contribution, economic applicability is gauged by the total cost of energy purchases from and sold to the grid, while the self-sufficiency of the household by the self-consumption factor, ξ, calculated as follows:

$$\xi = \frac{P_{pv-load} + P_{bat-load}}{P_{load}}, \tag{5.5}$$

i.e. $\xi = 0$ represents a household with no local generation or storage, and $\xi = 1$ correspond to a situation when the PV-BESS system supplies the total local demand.

5.1.2 Determination of Optimal Power Flows

The optimal solution must satisfy all constraints described above. It aims to reduce the overall cost by minimizing the expenses for energy purchase and implicit cost caused by the battery degradation. This cost model is divided into three components, *i.e.*:

$$\text{minimize} \quad C_{\text{tot}} = C_{\text{buy\_E}} + R_{\text{sell\_E}}. \tag{5.6}$$

The first component $C_{\text{buy\_E}}$ comprises the cost of energy purchased from the grid, while the second component, $R_{\text{sell\_E}}$, is the revenue from PV energy generation exported to the grid. These two components are evaluated as follows:

$$C_{\text{buy\_E}} = \sum_i C_{\text{buy}} \cdot P_{\text{grid-load}_i} \tag{5.7}$$

and

$$R_{\text{sell\_E}} = \sum_i C_{\text{sell}} \cdot (P_{\text{pv-grid}_i} + P_{\text{batt-grid}_i}). \tag{5.8}$$

5.2 Fuzzy Logic Controller

To manage power flows in the PV-BESS system, a fuzzy logic controller has been developed based on the results of the Linear Programming (LP) optimization. This allows to transfer the optimization results based on available data to other time periods and possibly other locations with similar PV-BESS systems. In addition,

and more importantly, formalizing the optimal operation of such a system in the form of a rule-based system allows its in-depth analysis and understanding.

To facilitate the understanding, the goal of the study presented here was to simplify the structure of the fuzzy rule base. In addition to parsimony of the resulting model, a simplified rule base mitigates the curse of dimensionality problem. The current fuzzy logic controller uses two input variables, one output variable, and a rule base of 15 fuzzy rules.

5.2.1 Input and Output Variables

The input variables, used by the controller to devise efficient PV-BESS system operations, reflect the state of the system and environmental conditions at the time of control intervention i. The first input variable, residual load, is defined as the difference between electrical demand and locally generated PV power,

$$\mathit{rLoad}_i = \mathrm{norm}(P_{\mathrm{load}_i} - P_{\mathrm{pv}_i}), \tag{5.9}$$

normalized to the range $[-1, 1]$. Its domain is partitioned into five triangular fuzzy sets named Negative Large (NL), Negative Small (NS), Zero (Z), Positive Small (PS), and Positive Large (PL). The shape of the fuzzy sets was defined according to the distribution of actual *rLoad* values during the observed period (1 year) so that each set covers 20% of the values. The second input variable is the state of charge of the BESS normalized to the interval $[0, 1]$, *i.e.*:

$$\mathit{soc} = \frac{\mathrm{SoC}_i + \mathrm{SoC}_{min}}{\mathrm{SoC}_{max} - \mathrm{SoC}_{min}}. \tag{5.10}$$

It is covered by three fuzzy sets, Low (L), Medium (M), and High (H) that were again spread across the input domain with respect to the actual distribution of *soc* values. The partitioning of both input universes is illustrated in fig. 5.1.

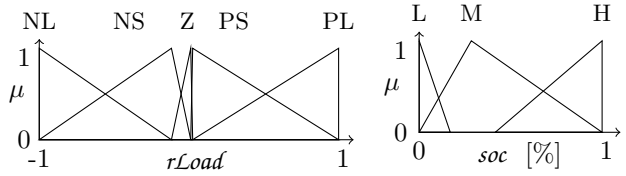

Figure 5.1: Fuzzy partition of *rLoad* and *soc*.

The controller has a single output, *flow*, that determines the volume of power flow between the PV generator, BESS, load, and power grid. The output variable is composed of 15 fuzzy singletons $\{F_1\}, \ldots, \{F_{15}\}$.

In order to manage the PV-BESS power flows with just a single output variable, the control strategy implemented by the controller makes the following assumptions:

i) all available PV energy is used to satisfy the electrical demand;

ii) extra PV energy is either stored into the battery or sent to the grid;

iii) outstanding electrical demand is satisfied either from the battery or the grid; and

iv) no power is transferred between the power grid and the battery.

These assumptions correspond to the LP–based solution of the power flow optimization problem. They neglect the power flows that represented only a small fraction of the overall power exchange in the PV-BESS system (*i.e.* $P_{\text{batt}-\text{grid}}$) and allow splitting of power between the battery and grid when there is extra PV energy production. When the PV production is scarce, it splits the residual load between the battery and grid, prioritizing the local energy storage.

The operation of the proposed fuzzy logic controller can be formally described as follows

$$\begin{aligned}
&\text{if } \mathit{rLoad} \leq 0: \qquad (i.e.\ P_{\text{pv}} \geq P_{\text{load}}) \qquad (5.11)\\
&\quad P_{\text{batt}-\text{load}} = 0,\\
&\quad P_{\text{pv}-\text{load}} = P_{\text{load}},\\
&\quad P_{\text{pv}-\text{batt}} = \min\{\mathit{flow} \cdot (P_{\text{pv}} - P_{\text{load}}), PB_{\max}\},\\
&\quad P_{\text{pv}-\text{grid}} = \min\{P_{\text{pv}} - P_{\text{load}} - P_{\text{pv}-\text{batt}}, P_{\text{feed}}^{\max}\},\\
&\quad P_{\text{grid}-\text{load}} = 0,\\
&\text{if } \mathit{rLoad} > 0: \qquad (i.e.\ P_{\text{pv}} < P_{\text{load}}) \qquad (5.12)\\
&\quad P_{\text{batt}-\text{load}} = \mathit{flow} \cdot BL_{\max},\\
&\quad P_{\text{pv}-\text{load}} = P_{\text{pv}},\\
&\quad P_{\text{pv}-\text{batt}} = 0,\\
&\quad P_{\text{pv}-\text{grid}} = 0,\\
&\quad P_{\text{grid}-\text{load}} = \max\{P_{\text{load}} - P_{\text{pv}} - P_{\text{batt}-\text{load}}, 0\},
\end{aligned}$$

$$P_{\text{batt}-\text{grid}} = 0, \qquad (5.13)$$

where $BL_{\max}$ and $PB_{\max}$ are coefficients representing the maximum possible power flow between the battery and load, and between the PV generation systems and battery respectively.

The fuzzy rule base consists of 15 IF-THEN rules that correspond to all possible combinations of the input variables

$$\begin{aligned} &\textsf{IF } \textit{rLoad} \text{ is NL and } \textit{soc} \text{ is L } \textsf{THEN } \textit{flow} \text{ is } \{\mathrm{F}_1\}, \\ &\qquad\vdots \\ &\textsf{IF } \textit{rLoad} \text{ is PL and } \textit{soc} \text{ is H } \textsf{THEN } \textit{flow} \text{ is } \{\mathrm{F}_{15}\}. \end{aligned}$$

The complete fuzzy rule base is summarized in table 5.1.

Table 5.1: Fuzzy rule base of the proposed controller

soc \ *rLoad*	NL	NS	Z	PS	PL
H	F_{11}	F_{12}	F_{13}	F_{14}	F_{15}
M	F_6	F_7	F_8	F_9	F_{10}
L	F_1	F_2	F_3	F_4	F_5

5.2.2 Baseline Controller

The optimum values of the output fuzzy sets, $F_1, \ldots, F_{15}$, are not known and must be found. However, a baseline control strategy can be obtained by setting

$$F_1 = F_2 = \ldots = F_{15} = 0. \tag{5.14}$$

It completely eliminates the use of local energy storage, and is thus called *zero control*. The control surface for the baseline strategy is shown in fig. 5.2.

5.2.3 Controller Evolution

To produce power flows similar to those obtained by linear programming, the fuzzy logic controller described in the previous section needs to be adjusted. In this work, the structure of the controller is retained to take advantage of its parsimony and thus ease of understanding. The optimum values of the output fuzzy singletons, $\{F_i\}$, are found by differential evolution.

The output fuzzy singletons are for the optimization procedure encoded into candidate vectors in a straightforward way so that:

$$\vec{x}_i = (\{F_1\}, \ldots, \{F_{15}\}), \tag{5.15}$$

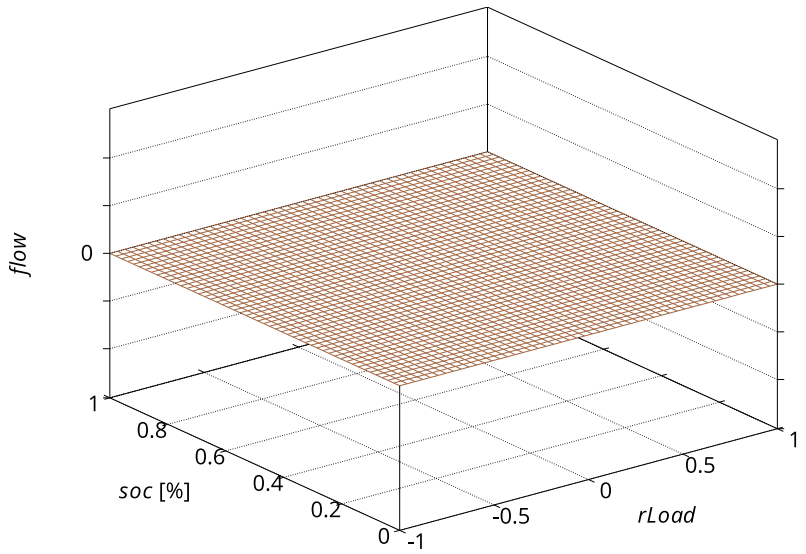

Figure 5.2: Control surface of the baseline controller.

and the controller optimization is cast as 15-dimensional real-parameter optimization problem. The candidate controllers are assessed according to the similarity of power flows they initiate to the optimum power flows determined by the IP. The similarity is evaluated as total RMSE between the power flows, which is used as the fitness function during the evolution.

The evolution uses the *DE/rand/1* variant of the algorithm with scaling factor $F = 0.9$, crossover probability $C = 0.9$, population size 20, and maximum number of 1500 generations. The parameters of the algorithm were set according to the best practices, past experience, and initial trials. Because the DE is a stochastic method, the evolution was executed 30 times independently.

5.3 Results and Discussion

The process of the FLC evolution is illustrated in Figure 5.3 depicting the mean RMSE and the 95% confidence intervals around it for each DE generation. It can be seen that the algorithm was able to find similar FLC configurations in all independent runs, *i.e.* the proposed approach is robust. Figure 5.3 also demonstrates that all DE runs converged to a stable solution in approx. 250 generations. The average final value of fitness (RMSE) was 13202.9 with the standard deviation of 142.4. The maximum and minimum fitness values over the 30 trials were 13933.9 and 13153.3, respectively.

The values of the output fuzzy singletons of the best evolved FLC controller

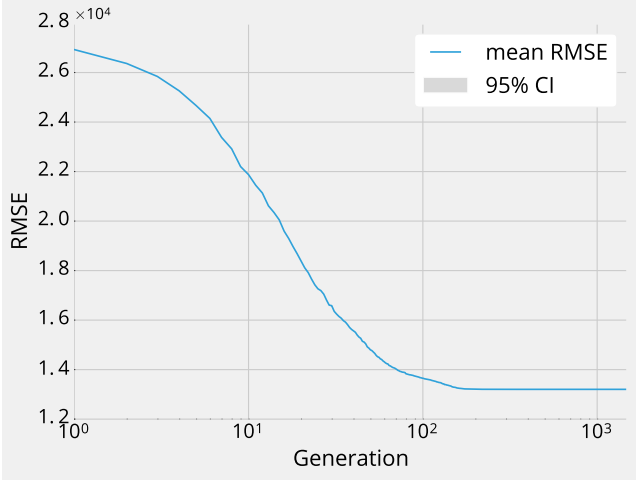

Figure 5.3: RMSE of the evolved FLC controllers in time. Note the logarithmic scale of the x axis.

(with the lowest RMSE, 13153.3) are listed in Table 5.2. The corresponding control surface is shown in Figure 5.4. It is composed of two half-surfaces that engage depending on the value of residual load, *rLoad*: when there is excess PV energy available (*i.e.* $rLoad \leq 0$, or $P_{\text{pv}} \geq P_{\text{load}}$), the controller charges the battery or sells energy to the grid, as shown in Figure 5.5, directing the available power according to the sequence in condition (5.12); when there is less PV power available than required by the load, *i.e.* $rLoad > 0$ or $P_{\text{pv}} < P_{\text{load}}$, the controller provides energy from the battery or from the grid, as shown in Figure 5.6, drawing the required power according to the sequence in condition (5.13).

Table 5.2: Values of output fuzzy singletons (best evolved controller)

soc \ *rLoad*	NL	NS	Z	PS	PL
H	1	1	0.0083	0.3002	1
M	0.9999	1	0.0670	0.2350	1
L	0	0	0	0	0

5.3.1 Controller Interpretation

The evolved controller implements the control surface depicted in Figure 5.4. For negative values of residual load, the controller directs all available PV power to the battery ($P_{\text{pv-batt}}$) and to the grid ($P_{\text{pv-grid}}$). This is controlled by the single output variable *flow*. The selection between battery and grid is made based on priority corresponding to the sequence of flows listed in equation (5.12). This means

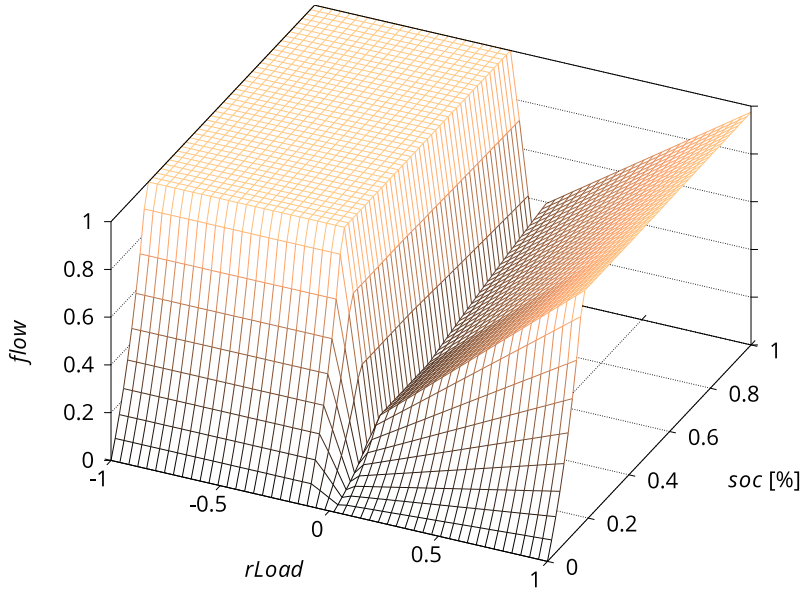

Figure 5.4: Control surface of the best evolved controller.

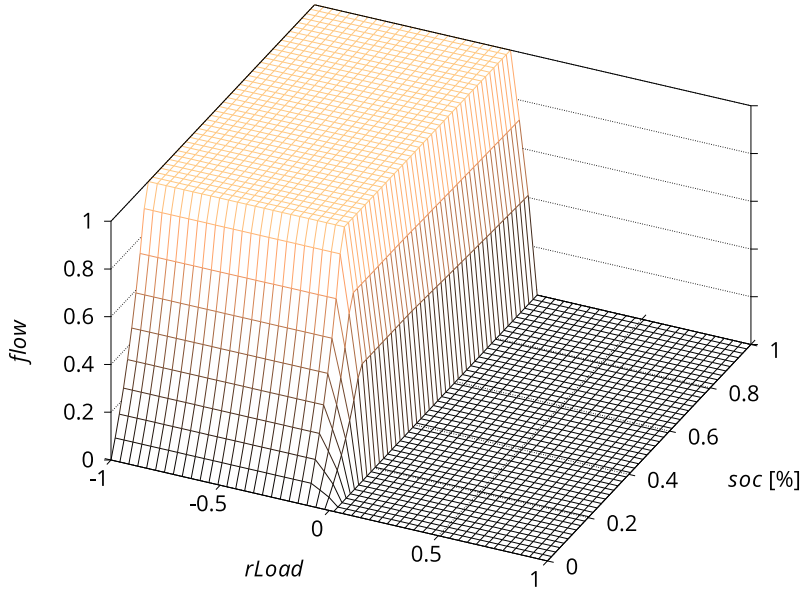

Figure 5.5: Control surface of the best evolved controller (control of $P_{\mathrm{pv-batt}} + P_{\mathrm{pv-gird}}$).

that surplus energy will be first fed to the battery, subject to the constraints of battery capacity SoC $\leq 95\%$ and the maximal charging power $PB_{\max}$. Due to the smoothing effect of the even fuzzy partition (cf. section 5.2), the control signal changes gradually from 0 (for $rLoad = 0$) to 1 (for $rLoad = -0.117$) and then remains at the plateau until the boundary ($rLoad = -1$). For positive residual load, the controller directly draws all the power required by the load from the battery

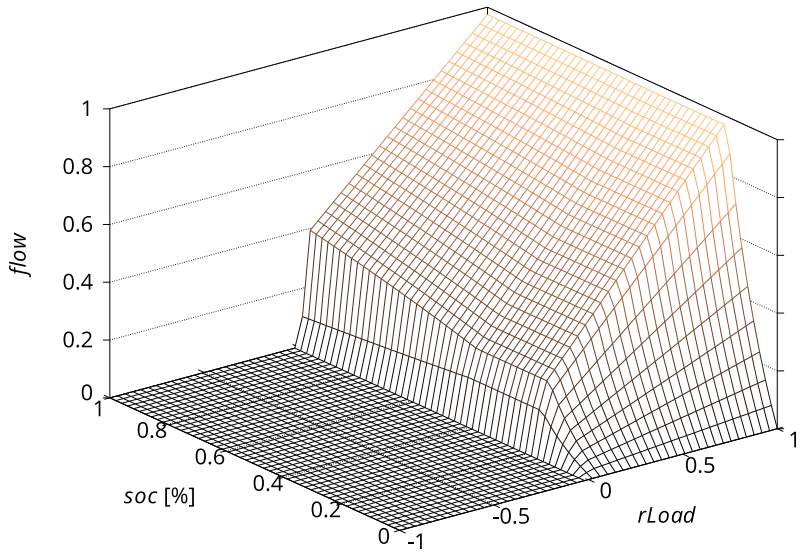

Figure 5.6: Control surface of the best evolved controller (control of $P_{\mathrm{batt-load}}$).

($P_{\mathrm{batt-load}}$) and from the grid ($P_{\mathrm{grid-load}}$). In this case, *flow* controls only $P_{\mathrm{batt-load}}$, while the value of $P_{\mathrm{grid-load}}$ is calculated as $\max\{P_{\mathrm{load}} - P_{\mathrm{pv}} - P_{\mathrm{batt-load}}, 0\}$. This means that the energy short-fall will be first satisfied by the battery, subject to the constraints of usable battery capacity SoC $> 5\%$ and the maximal discharging power BL_{max}. Compared to the the previous case, the character of the control surface is different, gradually changing between the values of *rLoad* $= -0.025$ and 1.0.

Another possible interpretation of the evolved controller involves merging the rules with (approximately) equal antecedents and replacing the values of fuzzy singletons $\{F_i\}$ by suitable linguistic labels. After applying these operations, the controller can be described as follows:

IF *rLoad* is negative and *soc* is medium or high THEN
flow from PV to battery (or grid) is high ,
IF *rLoad* is zero THEN
flow from PV to battery (or grid) is zero ,

IF *rLoad* is positive small and *soc* is medium or high THEN

flow from battery to load is small ,

IF *rLoad* is positive large and *soc* is medium or high THEN

flow from battery; to load is large .

The last row of the control matrix (cf. Table 5.2), corresponding to low *soc*, contains all zero values of *flow*. This is likely a consequence of training data points corresponding to days with high values of current and near future PV energy production. In these cases, the optimal solution prioritizes to sell the surplus energy to the grid rather than to store it. Only after reaching the feed-in limit is the surplus energy stored in the battery. This behavior occurs mostly during the summer, but the current controller cannot differentiate between different seasons. As these situations are rather rare, the corresponding rule is omitted from the simplified rule base listed above. Future work will explore this aspect of PV-BESS energy management strategy by including additional inputs to deal with the seasonality of the data.

5.3.2 Controller Evaluation

The evolved controller mimics the performance of the system with optimal power flows determined using linear programming. As described earlier in section 5.2, the main goal of designing the fuzzy logic controller was to develop a simple controller that would be easy to implement and understand. Therefore, deterioration of performance relative to the original optimized system was expected. At the same time, a significant improvement w.r.t. the baseline (zero) controller was presumed.

Results of simulations involving all three systems confirm these assumptions and show that the evolved fuzzy controller performs comparably well w.r.t. the LP-optimized system, as can be seen from the economical and self-consumption indicators listed in Table 5.3. Although the deterioration of performance of the evolved fuzzy controller is obvious, the gap between the optimal performance is not very large. The advantage of using the simple controller is that it does not require the use of energy production forecasts. In addition, the performance of the LP-optimized system cannot be attained in practice as it would require prior knowledge of all values of load and PV generation for the entire period of operation (1 year).

Table 5.3: Comparison of system performance

System	LP-optimized	zero-control	evo-control
RMSE	0	43691.6	13151.5
$C_{\text{buy\_E}}$	\$547.79	\$1275.15	\$792.75
$R_{\text{sell\_E}}$	\$624.80	\$955.53	\$543.33
ξ	75.72%	36.51%	64.52%

On the other hand, in comparison with the baseline controller, the evolved fuzzy logic controller reduced the total RMSE of the power flows by 55.82% and increased the self-consumption factor by 42.43%.

Figure 5.7 offers another view of how the three systems compare. The distribution of PV energy in the system among the load, battery, grid (left hand side), and composition of the sources of energy used to satisfy demand (right hand side) over the one year simulation period are shown. A simple visual inspection confirms a comparable performance of the LP-optimized system and evolved fuzzy logic controller proposed in this work. A more detailed look at the performance of the three systems is provided in the form of time series of all involved power flows in Appendix C.

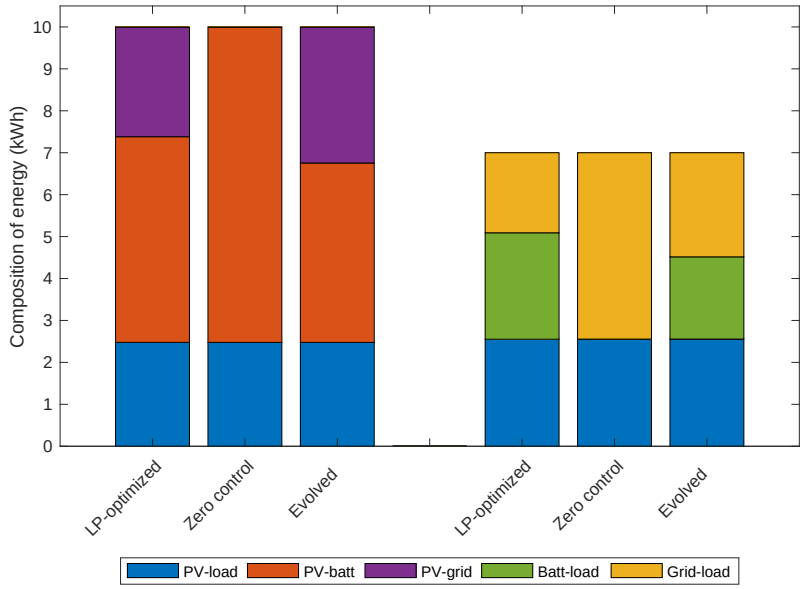

Figure 5.7: Composition of energy [kWh] generated by the PV system (left) and served to the load (right) over the one year period, comparing the three described approaches

5.4 Final Remarks

This chapter introduces a fuzzy logic controller implementing PV-BESS energy management based on optimal power flows determined for a real system using linear programming. The resulting controller, designed by differential evolution, offers performance comparable to the optimized system, At the same time, it is easy to implement for other systems, and can be interpreted to aid understanding of the PV-BESS behavior.

Chapter 6

Linear Battery Aging Model for Industrial Peak Shaving Applications

In power systems, the load profile can be characterized by the "peak load times" of the system – short periods of time when large amounts of power are required [108]. The peak load times can occur at different moments during the day, depending on the season of the year and the load composition (residential, commercial, or industrial). Peaks of demand impact the network planning because the electrical infrastructure of transmission and distribution systems must be designed to support the maximal demand of the system [139]. For this reason, the electrical power grid infrastructure may be underutilized most of the time, reaching its loading capacity limit only a few moments of the year. Consequently, commercial and industrial customers are charged not only by their total energy consumption but also by their highest power demand that dominates the line construction costs.

In this context, energy storage can be used to help customers flatten their demand profile by storing energy during off-peak periods and releasing this energy during peak load periods. Although the improvements of Battery Energy Storage System (BESS) efficiency and life cycle are increasing the interest in this type of storage [34], the high investment necessary for BESS installation still raises concerns about the economic viability of the use of this technology in power system applications. Therefore, an important aspect of the deployment of any BESS project is their proper power and energy sizing [42].

If a BESS is not sized properly, it can generate negative results from an economic perspective. While over-sizing of BESS may result in excessive aging-related

depreciation cost, small systems may not attain optimal cost-benefit ratio due to high initial investment cost.

In response to the need to size BESS properly, several studies aiming to find the optimal sizing of BESS have been conducted [66], [79], [80].

The necessity of proper BESS sizing has been highlighted in several studies. Most reports also recognize that aging of BESS cannot be neglected and point out battery deterioration as a major cost driver during the storage operation. To gain a better understanding of peak-shaving battery aging, this chapter proposes a new aging model suitable for BESS sizing for peak shaving applications in industrial settings and quantifies the battery aging for both naive and aging aware (LP based) operation strategies.

6.1 System Layout

The energy management system proposed in this study is derived from measured and simulated data for an exemplary BESS. The simulations involve a grid-connected system shown in a schematic diagram in Figure 6.1. The arrows in this figure illustrate the power flow direction for all component links.

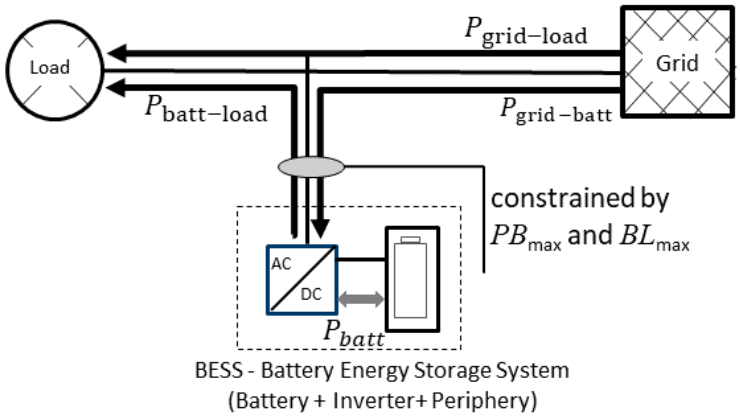

Figure 6.1: System configuration and power flows considered.

The electricity price in the commercial and industrial (C&I) sector is assumed to have the following components:

- Electricity generation (wholesale prices and retail costs); prices depend on negotiations between the customer and the utility company
- The network costs (transmission and distribution) is subdivided into two cat-

egories. First, power price per kW, based on the maximum power peak in the billing period; this is the only power specific price component. Prices vary with connected voltage level, billing period, distribution system operator and duration factor. Second, energy price per kWh, based on the total energy consumption.

- The total for industrial customer includes taxes, fees, surcharges (including renewable energy surcharge, electricity tax, CHP surcharge, etc.).

The overall cost $C_{storage}$ for the energy storage system with energy capacity E^{nom}_{batt}, and inverter with nominal power P^{nom}_{inv} can be expressed as:

$$\begin{aligned} C_{storage}(E^{nom}_{batt}, P^{nom}_{inv}) = C_{fix} + C_{OPEX,batt} \\ + (C_{var,batt} * E^{nom}_{batt}) \\ + (C_{var,inv} * P^{nom}_{inv}). \end{aligned} \tag{6.1}$$

where C_{fix} corresponds to the fixed cost including the housing of storage and all the peripheries, $C_{OPEX,batt}$ is the storage operation and maintenance (OPEX) cost within the battery lifetime, $C_{var,batt}$ denotes the energy specific cost of a storage system, and $C_{var,inv}$ represents the power specific cost of a storage system.

6.2 Battery Aging Model

Storage deterioration is a significant cost driver during storage operation. As a result, the aging of storage devices must be taken into consideration when simulating BESS operations. Lithium-ion batteries suffer from continuous aging. For most batteries of this type, it is possible to separate the degradation into a pure time-dependent irreversible loss of battery capacity called *calendric aging*, and an energy throughput dependent *cyclic aging* [128].

Accelerated aging tests performed at the Technical University Munich were used to build an equivalent circuit based aging model coupled with a thermic model [13] for a cell with graphite anode and nickel manganese cobalt (NMC). The maximum allowed C-rate of the cell is 1C for charging and -2C for discharging. The key factors that make this model appropriate are the analytic equations for estimating the cell degradation and the superposition of calendric and cyclic aging. Both are essential for an implementation of a linear model. The aging model and its linearization can be described as follows:

Calendric Aging

Considering that a BESS enclosure can maintain the temperature constant, it is possible to obtain a linear capacity fade for each time step. This is shown in Figure 6.2 where the piecewise line represents the calendric aging per time step dependent of the SoC, and the straight line shows its linearization with tstep = 15 minutes.

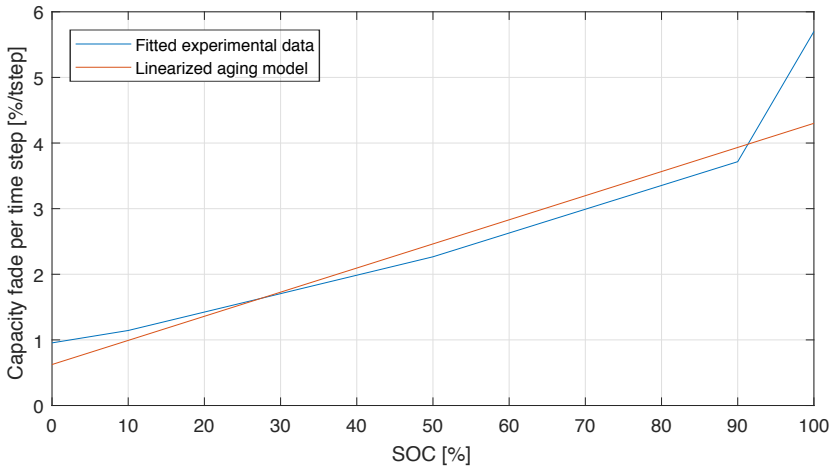

Figure 6.2: Calendric - Linearisation @ t=10 years

The linearization of the calendric aging for each time step i can be expressed as follows:

$$\mathrm{C}_{\mathrm{fade,cal,lin}}(\mathrm{SoC})_i = 3.676 \cdot 10^{-7} \cdot \mathrm{SoC} + 6.246 \cdot 10^{-6} \tag{6.2}$$

Cyclic Aging

For linearization of the cyclic aging, the C-rate dependency could be ignored for charging and discharging by averaging the C-rate factor. Consequently, the charge throughput can be linearized by evaluating it at a capacity fade of 20% under variation of C-rate and Depth of Discharge (DoD). After scaling it down to the capacity fade for each time step, the dependency of C-rate and DoD can now be quantified as shown in Figure 6.3.

An attempt to further linearize the cyclic aging would lead to a loss of parametric dependency of either C-rate or DoD. In the following, this model for accounting cyclic aging is named "DoD-cycle model." Another alternative is to consider the number of full equivalent cycles (FEC) that provides the overall energy throughput (counting only in either the charge or discharge direction) with any DoD per cycle

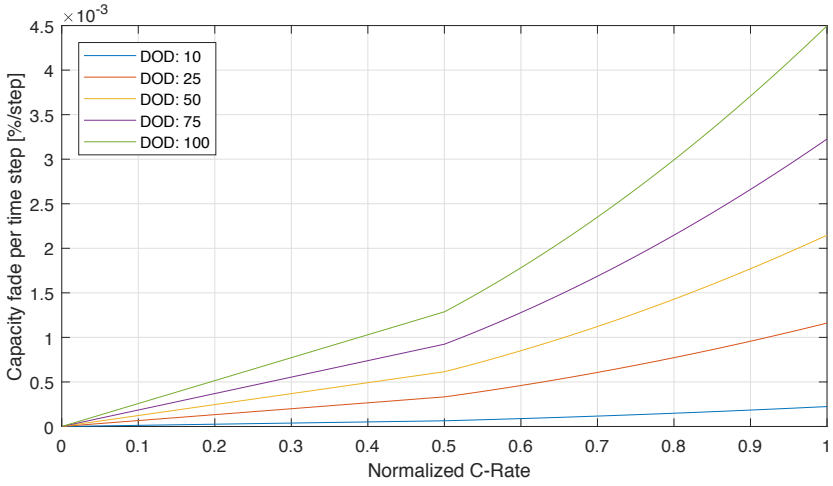

Figure 6.3: C-fade(C-Rate,DoD) - Linearized @ C-fade(EOL) = 20%

divided by the available capacity (in the following this model will be named the "FEC-cycle model") [29]. The number of FEC can be defined as:

$$\mathrm{FEC} = 0.5 \cdot \frac{1}{t} \int \mathrm{SoC}(t) dt \approx 0.5 \cdot \frac{\int |P_{\mathrm{batt}}|\, dt}{E_{\mathrm{batt}}^{\mathrm{nom}}} \tag{6.3}$$

The factor of 0.5 results from the conversion of charge throughput to full cycle counting. SoC denotes the state of charge, P_{batt} the power flow via the battery, and $E_{\mathrm{batt}}^{\mathrm{nom}}$ the nominal energy capacity of the battery. The maximum charge/discharge throughput is achieved at 80% of the SoH if there is no calendric aging.

As already mentioned, the use of BESS for peak shaving is a particular application which aims to reduce the cost of electricity by reducing the peak power. For instance, Figure 6.4 shows an industrial customer with 214.27 MWh annual load. Assuming a storage system with a nominal capacity of 57 kWh and inverter with nominal power of 171 kW, it is possible to reduce 30% of the annual peak power. In this example, the storage system is used in only 3 short moments during one year, meaning that the cycling aging has a minimal impact in peak shaving applications while the calendric aging is the most important factor. Figure 6.5 extends the battery operation to 10 years and confirms this assumption. It can be seen that the divergence between the capacity fade with DoD dependency and the capacity fade considering FEC is very small. At the end of the 10 year period, the DoD dependency and the FEC degradation represent only 0.51% and 0.54% of the SoH, respectively. On the other hand, the calendar aging with SoC dependency (equation (2.2)) represents 3.42% of the SoH.

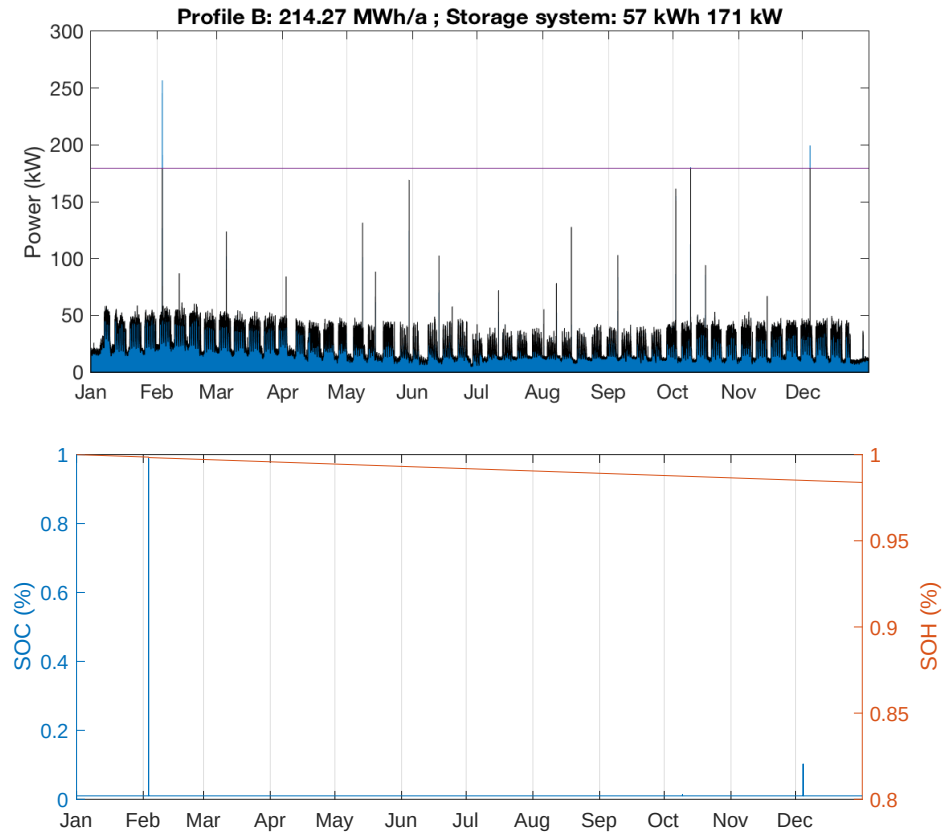

Figure 6.4: Industrial load profile (top), and battery SoC and SoH (bottom)

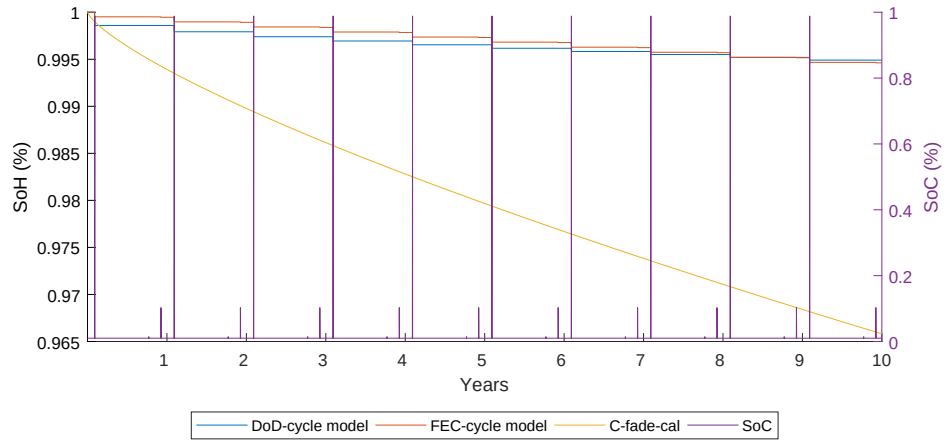

Figure 6.5: Cyclic capacity fade after 10 years - Comparison of depth of discharge dependency and number of full equivalent cycles

Although the cycling aging plays a minor role in the storage degradation for peak shaving, it cannot be neglected. For this reason, the next section introduces a sensitivity analysis to evaluate the cycling and calendric degradation for the peak shaving.

6.3 Case Study

6.3.1 Case Description

The structure of demand based energy tariffs is presented based on German electricity costs, where some customers have seen a rise of demand charge by up to 150% in the last five years evoking interest in demand charge management. Data used for simulations was adapted from real measurements in Germany and was averaged with a resolution of $\Delta t_{res} = 15$ min. This time discretization results from the fact that in the model region the 15 minutes demand average is registered and its maximum value is used for tariff calculation over a period of one month or one year [49].

The constraints considered in this model can be described as follows:

$$\begin{aligned}
P_{\mathrm{load}_i} &= P_{\mathrm{batt-load}_i} + P_{\mathrm{grid-load}_i} \\
P_{\mathrm{grid-load}_i} + P_{\mathrm{grid-batt}_i} &\leq P_{\mathrm{peak-shave}} \\
P_{\mathrm{batt}_i} &= \eta_{inv} \cdot P_{\mathrm{grid-batt}_i} - \frac{1}{\eta_{inv}} \cdot P_{\mathrm{batt-load}_i} \\
E_{\mathrm{batt}_i} &= (E_{\mathrm{batt}_{i-1}} \cdot \frac{\mathrm{SD}_{batt}}{d}) + (\eta_{batt} \cdot P_{\mathrm{batt}_i} \cdot \frac{1h}{\Delta t_{res}}) \\
E_{\mathrm{batt}}^{\mathrm{usable}} &\leq E_{\mathrm{batt}}^{\mathrm{nom}} \cdot (\mathrm{SoC}_{max} - \mathrm{SoC}_{min}) \\
E_{\mathrm{batt}_i} &\leq E_{\mathrm{batt}_i}^{\mathrm{usable}} \cdot \mathrm{SoH}_i \\
\mathrm{SoH}_i &= \mathrm{SoH}_{i-1} - (\mathrm{aging}_{\mathrm{cal}_i} + \mathrm{aging}_{\mathrm{cyc}_i}) \cdot 0.2
\end{aligned} \tag{6.4}$$

To meet the electrical demand P_{load_i}, the system is allowed to drain power from the battery or the grid. In the same way, the power imported from the grid in each time step i is restricted to the highest point of demand $P_{\mathrm{peak-shave}}$. The bidirectional power flow from the inverter to the battery is stored in an auxiliary variable P_{batt} and is subjected to the average one-way efficiency of the inverter η_{inv}. The battery energy content E_{batt_i} at i-th time step satisfies a recurrence relation, and $E_{\mathrm{batt}_i}^{\mathrm{usable}}$ is the total energy content of the battery installed which is confined by an upper and lower boundary (SoC_{max} and SoC_{min}). The energy content of the storage system is also restricted by an upper boundary that decreases upon usage and aging according to the SoH which also satisfies a recurrence relation. Subsequently, theSoC can be expressed as:

$$\mathrm{SoC}_i = \frac{E_{\mathrm{batt}_i}}{E_{\mathrm{batt}}^{usable} * \mathrm{SoH}_i}. \tag{6.5}$$

The calendric aging $\mathrm{aging}_{\mathrm{cal}_i}$ is defined according to eq. (6.2) and can be estimated

as:

$$\text{aging}_{\text{cal}_i} = 3.676{\cdot}10^{-7}{\cdot}\text{SoC}_i{+}6.246{\cdot}10^{-6}. \tag{6.6}$$

As such, the cyclic aging degradation $\text{aging}_{\text{cyc}_i}$ is a function depending of Crate and DoD:

$$\text{aging}_{\text{cyc}_i} = \frac{0.5.\int |P_{\text{batt}}|\, dt}{\text{Life}_{\text{cyc}}^{80\%}.\text{E}_{\text{batt}}^{\text{nom}}}. \tag{6.7}$$

where $\text{Life}_{\text{cyc}}^{80\%}$ represents a reference value for storage degradation to 80% SoH at 20°C temperature, when no calendric aging is applied.

Table 6.1: BESS/Inverter Performance Parameters and Price Information

Variable	Parameter	Unit	Value
η_{inv}	Average one way inverter efficiency	%	97.5
T_{inv}	Assumed inverter lifetime in years	years	20
η_{batt}	Battery round-trip efficiency	%	95
SD_{batt}	Self-discharge per day	%	0.02
	Usable SoC	%	5-95
$Life_{cal}^{80\%}$	Battery calendric life indicator	years	13
$Life_{cyc}^{80\%}$	Cycle life indicator in FEC	FEC	4500
$P_{\text{inv}}^{\text{nom}}$	Nominal power of the battery inverter	kW	117
$E_{\text{batt}}^{\text{nom}}$	Nominal battery capacity	kWh	39
C_{buy}	Retail electricity price	€/kWh	0.18
C_{power}	Power peak penalty price	€/kW	12.75
	Full equivalent cycles per years	#	5.28

This study considers a NMC BESS. Assuming that temperature is kept stable (approximately 20°C), the battery round trip efficiency (η_{batt}) and self-discharge per day (SD_{batt}) are 95% and 0.02% respectively. Table 6.1 provides an overview of the parameters and price information for the BESS/inverter system taken into account during simulations. Figure 6.6 shows the load profile considered in this study. This load profile is peak shaved at 2,112 kW which represents 5.05% of the total peak power without a battery installed.

Two battery usage strategies are considered to better understand the impacts of calendric and cycling degradation. The first strategy is naive and assumes that the BESS is always at full SoC capacity, as the battery is drained to provide enough power to peak shave, is fully charged again, and stays idle until the next peak of load. The second strategy is based in the optimal solution which is achieved through a linear programming (LP) algorithm. The LP solution respects all the constrains in Section 6.3 and aims to reduce the overall cost by minimizing the expenses for

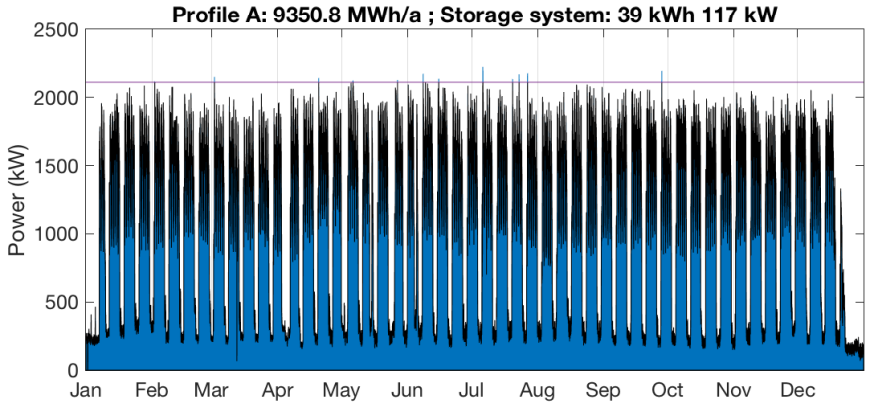

Figure 6.6: Industrial load profile - 9,350.8 MWh/a; Storage system: 39kWh 117kW. Peak shave at 2,112kW

energy purchase, as well as reducing the power peak penalty, *i.e.*:

$$\text{minimize} \qquad C_{\text{energy\_tot}} + C_{\text{power\_max}}. \tag{6.8}$$

The first component $C_{\text{energy\_tot}}$ comprises the cost of energy purchased from the grid, while the second component $C_{\text{power\_max}}$ is the penalty cost based on the highest point of demand (or peak) within the billing period. These two components are evaluated as follows:

$$C_{\text{energy\_tot}} = \sum_{i} C_{\text{buy}} * (P_{\text{grid}-\text{load}_\text{i}} + P_{\text{grid}-\text{batt}_\text{i}}) \tag{6.9}$$

$$C_{\text{power\_max}} = C_{\text{power}} * P_{\text{peak}-\text{shave}} \tag{6.10}$$

where C_{buy} and C_{power} are the retail electricity price and the power peak penalty price respectively.

6.3.2 Effect of Calendric and Cyclic Aging

Figure 6.7 illustrates the periodically changing charge level of the storage system (SoC), and the evolution of battery degradation (SoH) for cycling and calendar aging for a ten-year period. The upper image shows the variation when the naive strategy is followed. That means, the battery is kept at full nominal capacity and is drained when the load overcomes the peak shave limit of 2,112 kW to avoid the peaks of demand. Figure 6.7b (bottom) shows the SoC and SoH considering an optimal strategy. It can be noticed that the number of times that the battery needs to intervene to avoid peaks are the same. For this reason, the cycling aging is precisely the same in both cases.

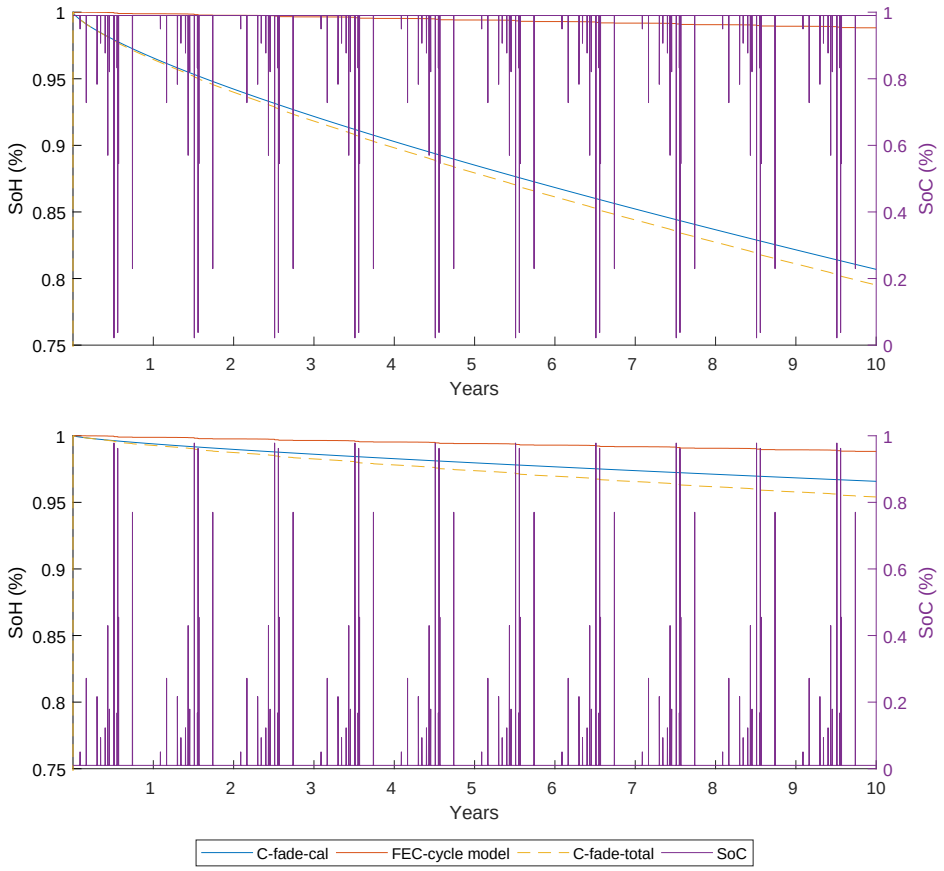

Figure 6.7: Time correlated evolution of battery state of charge (SoC) and resulting state of health (SoH) decline for the naive strategy (top) and optimal strategy (bottom).

In contrast, the calendric aging features distinctly because of the SoC dependency described in equation (2.2). As a result, the naive strategy depleted the battery 5 times faster than the optimal strategy. The optimal strategy also shows that the battery cycles can be short, meaning that the battery can be charged to the maximum necessary level just before being drained; but, a prediction algorithm needs to be implemented to guarantee the battery is going to have the required energy to avoid the peaks of demand.

6.4 Final Remarks

This chapter describes a linear model of BESS degradation for peak shaving applications. The obtained results show that the BESS is more susceptible to calendric aging than cyclic aging. The linear programming reveals the potential of reducing the calendric aging by five times when comparing with the naive strategy. Cyclic

aging is not determinant in peak shaving applications because the BESS has only a small number of charging/discharging cycles and energy is never stored in the battery for a long time. For this reason, the DoD dependency can be easily substituted by the FEC calculation to have an acceptable degradation estimate for BESS. However, it is important to notice that this chapter proposes a linear model that gives an approximation of the real degradation, and small variations will be present when compared with a real system.

Chapter 7

Optimal Component Sizing for Peak Shaving in Battery Energy Storage Systems for Industrial Applications

In power systems, the load profile can be characterized by the "peak load times" of the system—short periods of time when large amounts of power are required [108]. The peak load periods can occur at different times during the day, depending on the season of the year and the load composition (residential, commercial, or industrial). Peaks of demand impact the network planning because the electrical infrastructure of transmission and distribution systems must be designed to support the maximal demand of the system [139]. For this reason, the electrical power grid infrastructure may be underutilized most of the time, reaching its loading capacity limit at only a few moments of the year. Consequently, commercial and industrial customers are charged not only by their total energy consumption but also by their highest power demand that dominates the grid construction costs. The electricity charge can be discriminated in subcomponents like the generation cost, taxes, and fees which represent a small portion of the total electricity payment of the customers. Accordingly, commercial and industrial customers are interested in decreasing energy and power costs, which are the most significant part of the total charges, without lowering their energy consumption. In this context, Energy Storage Systems (ESS) can be used to help customers flatten their demand profile by storing energy during off-peak periods and releasing it during peak load periods.

The deployment of ESS can achieve another benefit besides the reduction of demand charges for customers. For instance, system operators can reduce the need

of network reinforcement by sizing the infrastructure for a more flat profile coupled with ESS, instead of designing it for the highest power demand [96]. Depending on the market conditions, other benefits can be achieved. The customers can take advantage of time of use energy price [147] by discharging the ESS when the energy price at the peak load periods is more expensive than the price during the off-peak periods. This can lead to an additional electricity bill reduction [136].

ESS technologies are used for a variety of applications [43], [61]. They can be classified in many different ways, according to the application area [38], based on the energy conversion [18], or depending on the quantity of energy that the ESS can provide [72]. For "power-type" applications like peak shaving, the ESS must maintain a constant delivery of power [67].

Although the improvements of Battery Energy Storage System (BESS) efficiency and life cycle are increasing the interest for this type of storage [34], the high investment costs necessary for BESS solutions still raise concerns about the economic viability of this technology in power system applications [52], [88], [98], [125]. Therefore, an important aspect of the deployment of any BESS project is their proper power and energy sizing. If a BESS is not sized properly, it can generate negative results from an economic perspective. While small BESS may result in excessive aging-related depreciation costs, over-sized systems may not attain an optimal cost-benefit ratio due to their relatively high initial investment cost.

This chapter proposes a linear optimization method to define a cost-optimal sizing of the battery and power electronics for peak shaving application in industrial settings. In addition, this chapter also presents a case study conducted with real industrial profiles, a techno-economic analysis evaluating the Return on Investment (ROI) of the system and battery degradation, and a linear programming (LP) approach allowing exact solution determination for BESS sizing. At the same time, the power flow optimization reveals the best storage operation considering energy purchase, peaks of consumption, and battery aging.

7.1 System Layout and Storage Model

This section summarizes all parameters relevant for the optimization of the components for peak shaving in BESS for industrial application. It describes the system layout, overviews technical parameters of the storage system, and specifies the economic and legal framework considered in this study.

7.1.1 System Layout

The energy management system proposed in this study is derived from measured and simulated data for an exemplary BESS. The simulations involve a grid-connected system shown in a schematic diagram in Figure 7.1a. The arrows in this figure illustrate the power flow direction for all component links. Additionally, Figure 7.1b illustrates all price components for industrial customers: the total energy consumption $\mathrm{E_{total}} = \sum \mathrm{load}_i$ where i denotes an averaged time segment of 15 min, the maximum power peak in the billing period P_{max}, and the maximum power peak after peak shaving P_{PS}. Other variables necessary for subsequent modeling are explained in more detail later along with the optimization problem definition.

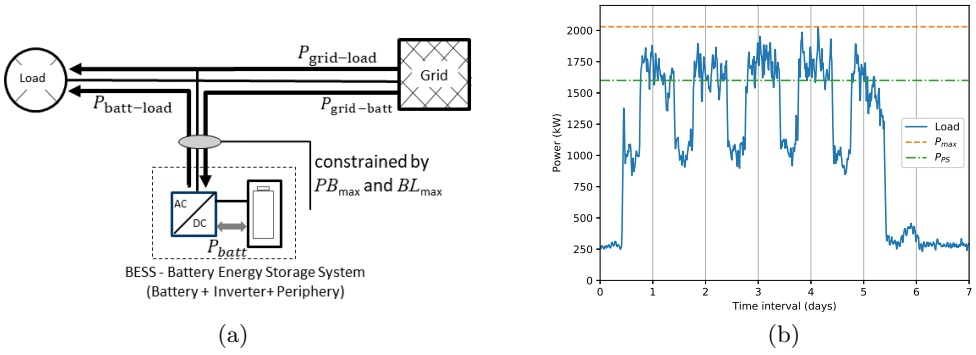

Figure 7.1: System configuration showing: (a) all considered power flows and (b) all customer load curves with price components.

7.1.2 Economic and Legal Framework for Industrial Customers

BESS are very flexible devices that can be used for many different applications [61]. Depending on the application, several factors influence the attractiveness for ESSs. Particularly in behind-the-meter-scenarios (BTM), the economic attractiveness of ESSs depends not so much on the electricity price itself, but on the pricing structure [19].

Peak shaving is a typical BTM application that concentrates on the reduction of the peak demand of consumers. Peak shaving systems are only attractive in markets where demand charges amount to a proportionally large part of the electricity price. Already at a very early stage of electricity system development, system operators

introduced electricity tariffs that included a demand based part added to the usage based part of electricity costs [26]. This scheme has been established to provide an incentive for efficient grid usage. This is a so-called cost reflective tariff, since the level of demand is the main driver of network costs, *i.e.* grid reinforcement and transformer overloading [90].

Battery storage is still a new technology associated with high perceived investment risk. This is likely the reason why most storage projects are currently conducted in well-developed countries [48]. According to a study by Azure International, the most attractive countries for demand charge management in the commercial and industrial (C&I) sector are Australia, France, the USA (California), Japan and Germany.

Electricity costs are paid via the utility company selected by the consumer. The utility company keeps a small percentage for itself to cover generation and retail costs; transfers taxes, fees, and surcharges to the relevant authorities; and transfers network costs to the system operator responsible for the corresponding system. Therefore, the location of the network connection point defines network costs. For instance, the two eastern transmission system operators (TSOs) in Germany charge significantly higher prices than the two western TSOs, but prices also differ from one distribution system operator to the next inside the same regulation zone. Specifically, commercial and industrial customers who (typically) exceed 100,000 kWh energy consumption per year or 500 kW of average power demand pay an additional power price per kW to the energy price per kWh. The electricity price in the C&I sector typically has the following components:

- Electricity generation (wholesale prices and retail costs); prices depend on negotiations between customer and utility company.

- The network costs (transmission and distribution) are subdivided into two categories. First, power price per kilowatt, based on the maximum power peak in the billing period; this is the only power-specific price component; prices vary with connected voltage level, billing period, distribution system operator and duration factor. Second, energy price per kilowatt hour, based on the total energy consumption.

- The total for standard rates including taxes, fees, surcharges (including renewable energy surcharge, electricity tax, CHP surcharge etc.).

These prices are based on a load profile considering a duration factor calculated as:

$$\Delta_{\text{feh}} = \frac{\sum_i P_{\text{grid-load}_i} \cdot \Delta t_{\text{res}}}{P_{\text{peak}}}, \tag{7.1}$$

where Δ_{feh} is equal to the full load equivalent hours, $\sum_i P_{\text{grid-load}_i}$ is the total energy consumption per year, and P_{peak} is the yearly peak power at network connection point.

Table 7.1: Electricity price for exemplary industrial customer in Germany [19], [73].

Full Load Equivalent Hours (Δ_{feh})	**<2500 h/a**	**>= 2500 h/a**
Electricity generation	0.035 €/kWh	
Network-energy price	0.055 €/kWh	0.005 €/kWh
Network-power price	12.78 €/kW	139.12 €/kW
Taxes, fees, surcharges	0.09 €/kWh	
Total	12.78 €/kW + 0.18 €/kWh	139.12 €/kW + 0.13 €/kWh

Table 7.1 summarizes the costs of electricity for industrial customers in Germany. For customers with $\Delta_{\text{feh}} \leq 2,500$ hours per year, the energy price of 0.18 €/kWh and power price of 12.78 €/kW are assumed. Customers with $\Delta_{\text{feh}} \geq 2,500$ hours per year are charged an energy price of 0.13 €/kWh and a power price of 139.12 €/kW. This pricing scheme produces a dependence of cost versus duration factor as shown in Figure 7.2. The total cost decreases as the duration factor increases.

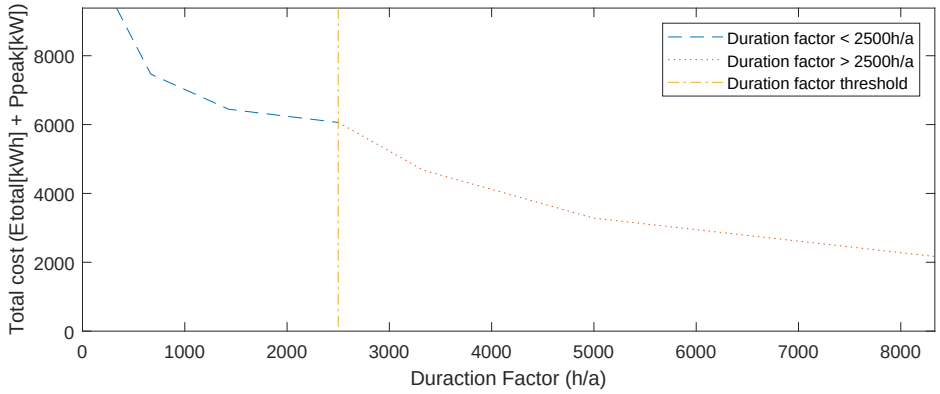

Figure 7.2: Network cost vs. duration factor at constant total energy consumption of 100 MWh in a given network area, medium voltage tariff, 2017.

A typical lithium-ion battery available on the market can provide up to 3 C (*i.e.* a 50 kWh battery can be discharged with 150 kW or in 1/3 h). As specific capacity costs are higher than specific power costs, load profiles with peaks below

1 hour are ideal for peak shaving with BESS. Typical loads producing steep peaks are power intensive plants and machinery with short start-up times or heat-up periods, like furnaces in the steel industry. Another precondition for the feasibility of peak shaving is periodic, predictable behavior of the load. Forecasting algorithms ensure that the storage system will be able to discharge its maximum energy when needed [113]. Although such prediction tasks are indispensable for achieving the best BESS operation, they are outside the scope of this work.

A non-representative study of nearly 300 industrial load profiles, conducted by Smart Power GmbH(www.smart-power.net) in 2017, showed that about 10% of all load profiles result in a static ROI of five years or less, and thus can be directly considered for peak shaving application (cf. Figure 7.3). Under the assumption that storage system prices will decrease by about 30% and demand rate will rise by about 30%, the number of loads applicable for peak shaving will rise to about 33% in the next few years [98].

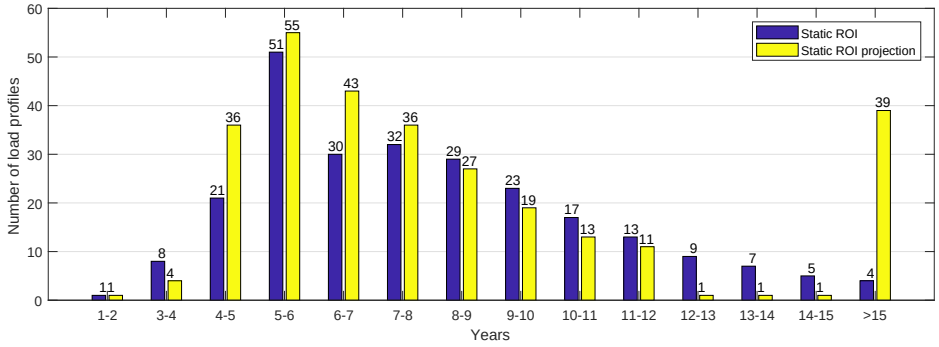

Figure 7.3: Static return on invest (ROI) of peak shaving storage systems in years based on 288 industrial load profiles analyzed by Smart Power in 2017 (blue), and the static ROI projection where the investment is reduced by 30% and the energy rate is raised by 30% (yellow).

Interestingly, Schmidt et al. [121] construct a comparative study for promising electrical energy storage technologies. The authors also investigate how the derived rates of future cost reduction influence when storage becomes economically competitive in transport and residential applications. In terms of price per energy capacity, the technology that brings the most energy density to market is likely to become the most cost-competitive. For instance, lithium-ion batteries can be used in multiple applications and secure high-capacity markets such as battery packs for electric vehicles.

For the sole battery storage investment without an inverter, the following price

structure is considered:

$$C_{batt}(E_{batt}^{nom}) = C_{fix} + C_{opex,batt} + (C_{var,batt} \cdot E_{batt}^{nom}), \tag{7.2}$$

where C_{batt} represents the total battery investment cost, C_{fix} corresponds to the fixed cost including the housing of storage and all the peripheries, $C_{var,batt}$ denotes the energy specific cost of a storage system, and $C_{opex,batt}$ is the storage operation and maintenance (OPEX) cost within the battery lifetime. As such, the overall cost $C_{storage}$ for the energy storage system can be expressed as:

$$C_{storage}(E_{batt}^{nom}, P_{inv}^{nom}) = C_{fix} + C_{opex,batt} + (C_{var,batt} \cdot E_{batt}^{nom}) + (C_{var,inv} \cdot P_{inv}^{nom}) \tag{7.3}$$

which includes battery storage with energy content E_{batt}^{nom}, and inverter with nominal power P_{inv}^{nom}. As container storage systems predominantly have battery racks and inverter units assembled to the same casing, no separate fixed costs for inverters are assumed, but are given as part of the overall storage fixed cost C_{fix}.

7.2 Case Study

This section presents the application of the introduced model for dimensioning BESS for industrial peak shaving application. The industrial customer is responsible for buying, installing, maintaining, and operating the storage system. In this model, the energy used to charge the battery and the energy used for immediate consumption have the same cost, and both are considered in the industrial customer peak power calculation. As a result, the usage of a storage system is transparent from the point of view of the utility company.

7.2.1 Linear Optimization of BESSs

The economically optimal battery storage component sizing for an industrial customer equipped with a storage system is obtained using LP. The load demand profiles considered in this study cover one full year to capture all seasons with their characteristics. As the intent is to minimize the overall electricity cost, three types of costs are considered: the energy cost C_{energy_tot}, the power cost C_{power_max}, and the battery degradation cost $C_{storage\_deg}$. The energy cost is composed of the base energy price, fees, taxes, and stock exchange price. The power cost is charged by the network operator on the basis of the duration factor. The battery degradation

cost, also called aging cost, is the major cost driver during storage operation, caused by cyclic and calendric aging.

The annual cost flow analysis presented here takes into account the discounted storage cost caused by degradation. As such, this simulation allows to estimate the profitability of a BESS for the full life of the battery. All variables and parameters considered in this study are described in Table 7.2.

Table 7.2: Variables and parameters used for the battery modeling and optimization routines.

Variable	**Description (At the Time Slot i)**	**Unit**	**Constraints/Comments**
P_{load_i}	load demand (historical data)	kW	$\geq$0; input data
$P_{\text{inv}}^{\text{nom}}$	Nominal power of the battery inverter	kW	Subject to optimization
$\text{E}_{\text{batt}}^{\text{nom}}$	Nominal battery capacity	kWh	Subject to optimization
$P_{\text{peak-shave}}$	Maximum power for the full year	kW	Subject to optimization
P_{batt}	Bidirectional power flow to the battery	kW	Result of optimization
$P_{\text{batt-load}_i}$	Power transferred from the battery to the load	kW	See Equation (7.4)
$P_{\text{grid-load}_i}$	Power imported from the grid to the load	kW	$\geq$0; see Equations (7.4) and (7.5)
$P_{\text{grid-batt}_i}$	Power imported from the grid to the battery	kW	$\geq$0; see Equation (7.5)
SoH_i	State of health	p.u.	$[0 \dots 1]$; see Equation (7.10)
E_{batt_i}	Battery energy content at time i	kWh	See Equations (7.8) and (7.9)
SoC_i	State of charge	p.u.	$[\text{SoC}_{\text{min}} \dots \text{SoC}_{\text{max}}]$

To meet the electrical demand, P_{load_i}, the system attempts to use power from the battery, $P_{\text{batt-load}_i}$, or draws power from the grid, $P_{\text{grid-load}_i}$, *i.e.*:

$$P_{\text{load}_i} = P_{\text{batt}-\text{load}_i} + P_{\text{grid}-\text{load}_i}. \tag{7.4}$$

In the same way, the power imported from the grid ($P_{\text{grid}-\text{load}_i} + P_{\text{grid}-\text{batt}_i}$) in each time step i is restricted to the maximum power for the period. The two constraints can be represented as:

$$P_{\text{grid}-\text{load}_i} + P_{\text{grid}-\text{batt}_i} \leq P_{\text{peak}-\text{shave}_j}, \tag{7.5}$$

where $P_{\text{peak}-\text{shave}_j}$ represents the highest point of demand in the billing period j. For instance, considering only the highest load of the year, all data points i should be limited to the same maximum annual limit $P_{\text{peak}-\text{shave}_j}$. However, if we consider the seasonal billing period where there are two independent thresholds, each season is limited to its own limit. The peak power is used to calculate the optimal solution power cost.

The bidirectional power flow from the storage inverter to the battery is stored in an auxiliary variable, P_{batt_i}, and correlated with the inverter efficiency, η_{inv}, as follows:

$$P_{\text{batt}_i} = (\eta_{\text{inv}} \cdot P_{\text{grid}-\text{batt}_i}) + (-\frac{1}{\eta_{\text{inv}}} \cdot P_{\text{batt}-\text{load}_i}), \tag{7.6}$$

where η_{inv} is the average one-way efficiency of the inverter. The reciprocal efficiencies are the battery charge power $P_{\text{grid}-\text{batt}_\text{i}}$ and the discharge power $P_{\text{batt}-\text{load}_\text{i}}$, both of which are limited by the nominal power flow from the inverter to the battery:

$$\begin{aligned} 0 \leq & P_{\text{grid}-\text{batt}_i} \leq P_{\text{inv}}^{\text{nom}}, \\ 0 \leq & P_{\text{batt}-\text{load}_i} \leq P_{\text{inv}}^{\text{nom}}, \end{aligned} \tag{7.7}$$

where $P_{\text{inv}}^{\text{nom}}$ corresponds to the inverter size. The battery energy content at time step i (E_{batt_i}) satisfies the recurrence relation:

$$\text{E}_{\text{batt}_i} = (\text{E}_{\text{batt}_{i-1}} \cdot \frac{\text{SD}_{\text{batt}}}{d}) + (\eta_{\text{batt}} \cdot P_{\text{batt}_i} \cdot \Delta t_{\text{res}}), \tag{7.8}$$

where SD_{batt} represents the self-discharge factor of the battery and $d = 96$ the conversion factor of time steps per day. The energy content of the storage system is furthermore confined by an upper boundary, that decreases upon usage and aging according to the State of Health (SoH). The SoH is defined as the irreversible capacity fade over time, related to the nominal battery capacity, and E_{batt_i} is a fraction of the total energy content of the battery installed:

$$\text{E}_{\text{batt}_i} \leq \text{E}_{\text{batt}}^{\text{nom}} \cdot \text{SoH}_i. \tag{7.9}$$

The SoH of the storage system at time step i also satisfies the recurrence relation:

$$\text{SoH}_i = \text{SoH}_{i-1} - 0.2 \cdot (\text{aging}_{\text{cal}_i} + \text{aging}_{\text{cyc}_i}). \tag{7.10}$$

Using Equations (6.2) and (6.3), the calendric and cyclic aging can be estimated as:

$$\text{aging}_{\text{cal}_i} = (3.676 \times 10^{-7} \cdot \text{SoC} + 6.246 \times 10^{-6}) \cdot (i \cdot \Delta t_{\text{res}}) \tag{7.11}$$

and

$$\text{aging}_{\text{cyc}_i} = \text{aging}_{\text{cyc}_{i-1}} + 0.5 \cdot \frac{|P_{\text{batt}_i} \cdot \Delta t_{\text{res}}|}{E_{\text{batt}_i}} \cdot \frac{1}{\text{Life}_{\text{Cyc}}^{80\%}}. \tag{7.12}$$

The calendric aging is affected by the storage temperature and its SoC level according to Swierczynski et al. [128]. Despite the fact that the charge/discharge process leads to dissipative heat generation and unavoidable temperature changes within the battery, the very low utilization ratio of the storage system and the restriction to a maximum C-rate of 3 limits the effects of temperature variations significantly.

As a result, the additional cyclic aging degradation of time step i is estimated by the energy throughput in time step i ($P_{\text{batt}_j} \cdot \Delta t_{\text{res}}$) divided by the energy content

of the system E_{batt_i} and is normalized with the factor of 0.5 and the technology specific cycle life indicator $\text{Life}_{\text{Cyc}}^{80\%}$. Similarly, the SoC can be expressed as:

$$\text{SoC}_i = \frac{\text{E}_{\text{batt}_i}}{\text{E}_{\text{batt}}^{\text{usable}} \cdot \text{SoH}_i}. \tag{7.13}$$

The inverter nominal power is limited to three times the battery nominal capacity:

$$\text{E}_{\text{batt}}^{\text{nom}} \geq 3 \cdot P_{\text{inv}}^{\text{nom}}. \tag{7.14}$$

The optimal solution must satisfy all constraints described above, aiming to reduce the overall cost by minimizing the expenses for energy purchase and implicit cost caused by battery degradation. This cost model is divided into three components, *i.e.*:

$$\text{minimize} \qquad C_{\text{energy\_tot}} + C_{\text{power\_max}} + C_{\text{storage\_deg}}. \tag{7.15}$$

The first component $C_{\text{energy\_tot}}$ comprises the cost of energy purchased from the grid, while the second component $C_{\text{power\_max}}$ is the peak induced cost based on the highest point of demand (or peak) within the billing period (monthly or annually). These two components are evaluated as follows:

$$C_{\text{energy\_tot}} = \sum_i C_{\text{buy}} \cdot (P_{\text{grid-load}_i} + P_{\text{grid-batt}_i}), \tag{7.16}$$

$$C_{\text{power\_max}} = C_{\text{power}} \cdot P_{\text{peak-shave}}, \tag{7.17}$$

where C_{buy} and C_{power} are the retail electricity price and peak-power tariff respectively. The third component estimates the storage system degradation cost that can be represented as:

$$C_{\text{storage\_deg}} = \frac{\Delta\text{SoH}}{(1 - \alpha_{\text{Replace}})} \cdot \text{E}_{\text{batt}}^{\text{nom}} + P_{\text{inv}}^{\text{nom}} \cdot \frac{\Delta t}{T_{\text{inv}}}, \tag{7.18}$$

where Δt denotes the time span covered with the simulation (one year) and ΔSoH is the total battery aging. The full battery related cost is then calculated in consideration of the initial installation investment cost.

7.2.2 Case Description

Four industrial load profiles (A–D) shown in Figure 7.4 are used to verify the effectiveness of the proposed model. Data used for the simulations was adapted from real measurements and averaged with a resolution of $\Delta t_{\text{res}} = 15$ min [8]. This time

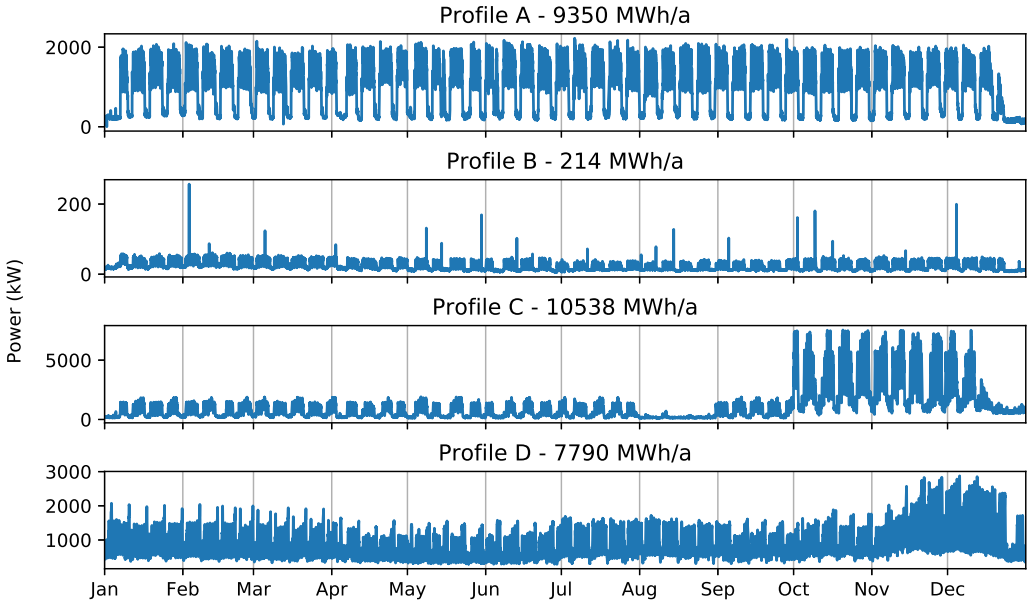

Figure 7.4: Load profiles.

discretization results from the fact that, in the model region, the 15 minutes demand average is registered and its maximum value is used for tariff calculation over a period of one month or one year [49]. It is assumed that temperature is kept stable at approximately 25 °C. Parameters and price information for the BESS/inverter system used in the simulations are listed in Table 7.3.

As described in Section 7.1, the electricity cost has two main components: the total energy consumption and the power peak cost in the billing period. According to German law StromNEV §19I, every grid operator is obligated to offer a monthly billing scheme, *i.e.* instead of the highest load of the year, the highest load of the month is the basis for the price per kW. Hence, this study considers both yearly and monthly billing schemes. The results presented in the next section describe not only the optimal BESS/inverter component sizes, but also the optimal billing scheme.

7.2.3 Effect of Sizing, Considering BESS Degradation Costs

The objective function and the constraints structured in this study have linear relationships. This means that the effect of changing a decision variable is proportional to its magnitude. For this reason, the economically optimal battery storage component sizing for peak shaving is obtained using LP. The linear optimization was implemented in MATLAB (MathWorks, Natick, MA, USA) code using a dual-simplex algorithm, which is based on a conventional simplex algorithm on the dual

Table 7.3: Battery Energy Storage System(BESS)/inverter performance parameters and price information

Variable	Parameter	Unit	Value
η_{inv}	Average one way inverter efficiency	%	97.5
T_{inv}	Assumed inverter lifetime in years	years	20
η_{batt}	Battery round-trip efficiency	%	95
SD_{batt}	Self-discharge per day	%	0.02
$[\text{SoC}_{\text{min}} \dots \text{SoC}_{\text{max}}]$	Usable SoC	%	5–95
$\text{Life}_{\text{cal}}^{80\%}$	Battery calendric life indicator	years	13
$\text{Life}_{\text{cyc}}^{80\%}$	Cycle life indicator in FEC	FEC	4500
$C_{\text{var,inv}}$	Variable inverter cost	€/kW	1306
$C_{\text{var,batt}}$	Variable battery cost	€/KWh	577
C_{fix}	Fixed cost for storage (housing, cooling, and periphery)	€	580

problem [132]. Each one-year simulation considered a 15-min time resolution, co-optimized the storage and inverter size, and took on average 700 s on a workstation with Intel Core i5 processor at 3.5 Ghz and 16 GB of memory.

The optimal storage and inverter size for each profile (A–D), as well as a number of relevant technical and economical indicators, are presented in Table 7.4.

Table 7.4: Economical and technical comparison of system optimization results.

Profile	Profile A		Profile B		Profile C		Profile D	
Scheme	Year	Month	Year	Month	Year	Month	Year	Month
Peak Loading Capping	5%	6%	30%	13%	8%	1%	0%	0%
Battery Size (kWh)	39	51	57	21	1109	18	0	0
Inverter size (kW)	117	152	171	63	3326	55	0	0
Δ_{feh} (h/a)	4431	4453	1195	957	1517	1407	2709	2709
Investment (€)	72,601	91,962	97,187	42,351	3,266,112	37,126	0	0
Operation Cost (€)	1156	1512	1663	674	39,577	583	0	0
Saving Grid charges (€)	15,880	16,735	992	6666	7613	6173	0	0
Total Savings (€)	14,725	15,223	−671	5992	−31,964	5591	0	0
Total return (IRR)	19%	14%	−169%	11%	−171%	12%	0%	0%
Amortization Time (years)	5	6	–	7	–	7	0	0
Full equivalent cycles (FEC)	5	51	1	32	11	25	0	0
Number of capped peaks	20	243	5	751	176	185	0	0
SoH at the end of year	98.78%	97.76%	98.88%	98.19%	98.66%	98.34%	0.00%	0.00%

The investment comprises the overall cost $\text{C}_{\text{storage}}$ described in Equation (7.3). The operation cost, $\text{C}_{\text{opex,batt}}$, reflects the German market and is calculated as 0.6% of the investment plus 6 €/kW. Table 7.5 shows the OPEX components considered in this paper.

The total return equal to the Internal Return Rate (IRR) [11], is calculated without inflation or price changes based on the total savings of the first year. Likewise,

Table 7.5: Operation cost (OPEX) composition.

Insurance	0.30%
System management	0.20%
Service contract	1 €/kW
Maintenance reserve	5 €/kW
Administrative costs	0.10%

total savings and amortization time are static calculations:

$$\text{TotalSavings} = \text{SavingsGridCharges} - \text{OPEX}, \tag{7.19}$$

$$\text{AmortizationTime} = \frac{\text{Investment}}{\text{TotalSavings}} \cdot \tag{7.20}$$

'Profile A' has an annual load of 9,350 MWh and features weekday peaks and small loading during weekends. As shown in Table 7.4, this profile exhibits similar results for yearly and monthly billing schemes. Figures 7.5 and 7.6 illustrate the results obtained for the two billing schemes.

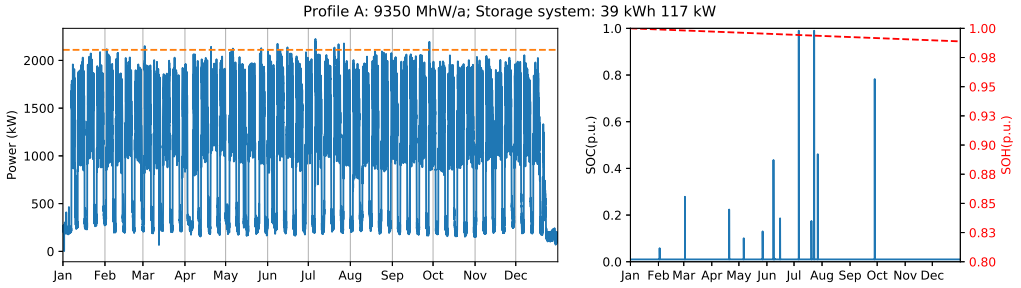

Figure 7.5: Industrial load profile A with yearly billing scheme (**left**), and battery state of charge and state of health (**right**).

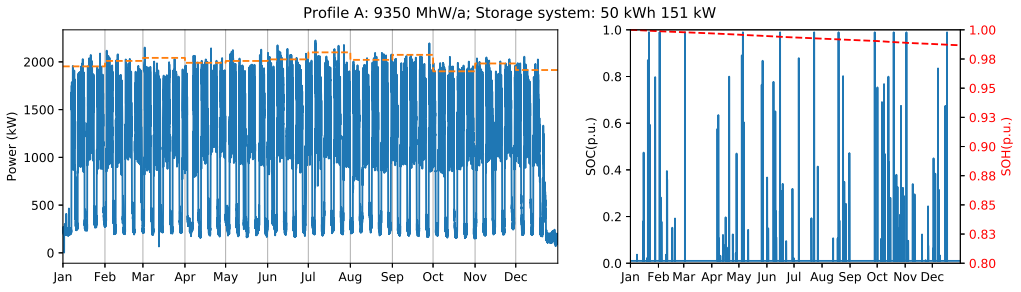

Figure 7.6: Industrial load profile A with monthly billing scheme (**left**), and battery state of charge and state of health (**right**).

The yearly billing scheme requires an initial investment of almost €20,000 less compared to the cost of the system optimized for monthly billing, and it can generate

an additional 5% of total return in a shorter time. Although the monthly billing scheme with a 51 kWh battery and 152 kW inverter (Figure 7.6) can increase the peak load capping, it also shortens the battery end of life by seven years (Figure 7.7). Therefore, all things considered, the yearly billing scheme is more suitable for 'Profile A' because it delays the battery replacement and provides several extra years of saving grid charges before it becomes necessary to invest in a new battery system.

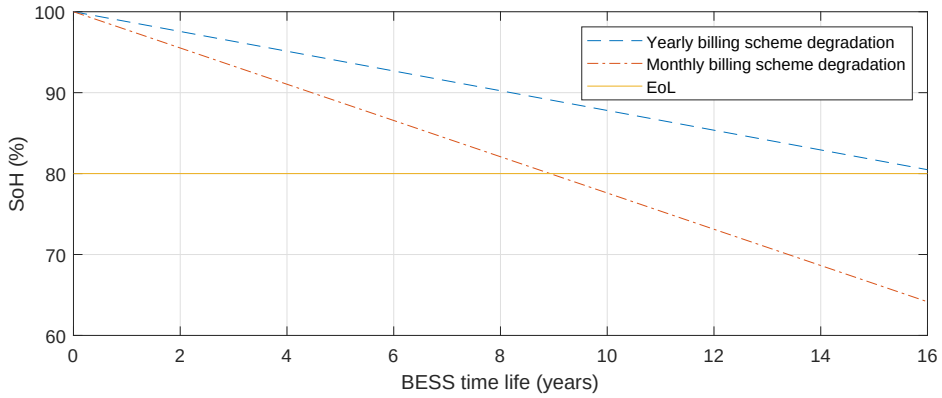

Figure 7.7: Extrapolation of the one-year results to represent the degradation after 10 years of usage for Profile A.

Further considering the monthly billing scheme, the optimizer determines the optimal storage size of 51 kWh and inverter nominal power of 152 kW. Figure 7.8 illustrates the power flows for a three-day period during the first week of May. The left panel shows the load consumption, the power flow imported from the grid for direct use or to charge the battery, as well as the maximum power peak after shaving. The right panel shows the periodically changing charge level of the storage system (SoC), and the evolution of battery degradation (SoH). It clearly shows that the capacity fade is stronger when the energy throughput is high. Figure 7.9 shows the battery power profile and the same capacity fade in the terms of C-rate.

In contrast to 'Profile A,' results for 'Profile B' show that the yearly billing scheme is not suitable for profiles with low average load and relatively high peaks. Although it is possible to reduce 30% of the peak load using a 57 kWh BESS with 171 kW inverter, this system configuration provides no savings to support the initial investment. In this case, the monthly scheme is more profitable, resulting in a peak reduction of 13% with a 21 kWh battery and 63 kW inverter.

Similarly, 'Profile C' has a negative IRR when considering the yearly billing scheme. This is caused by the seasonal nature of the load. As can be seen in Fig-

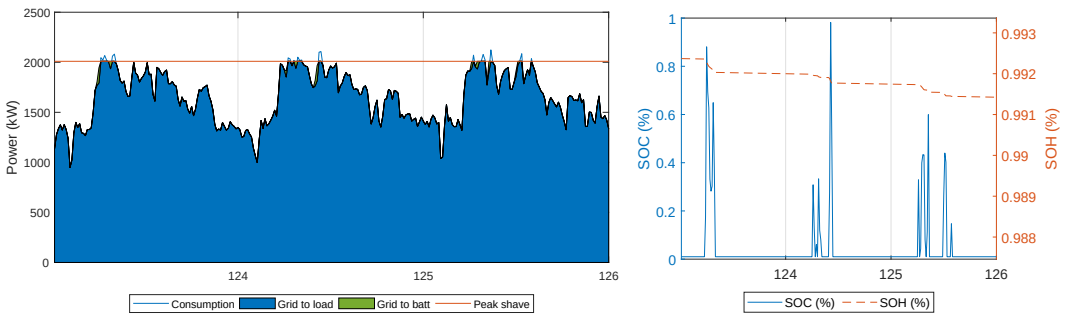

Figure 7.8: Power flow analysis for a three-day period: load and power flows within the system (**left**); time correlated evolution of battery state of charge (SoC) and resulting state of health (SoH) decline (**right**).

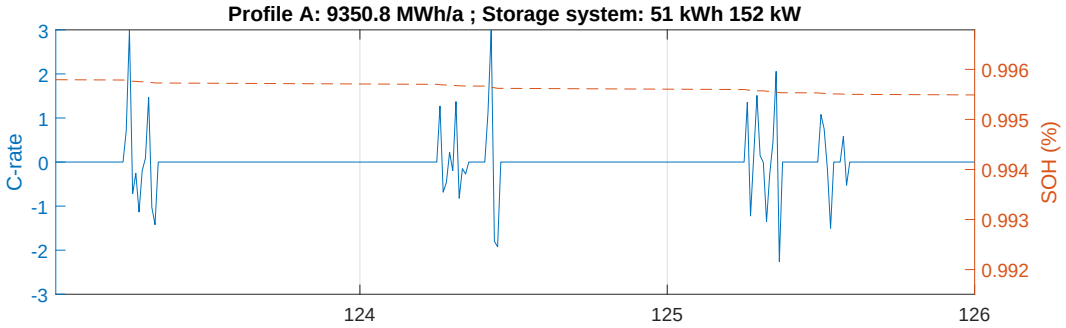

Figure 7.9: Battery power profile analysis for a three-day period and resulting state of health decline.

ure 7.4, the consumption in the last three months of the year is very high compared to the rest of the year. Analyzing the total return value in Table 7.4, the monthly billing scheme appears to be the right choice for this profile. However, a peak load reduction of only 1% is too slow to justify the installation of a BESS.

Finally, 'Profile D' presents the most extreme case. Considering the exposed investment cost for BESS and price schemes, there is no advantage to installing a BESS for peak shaving purpose for this profile. Figure 7.10 illustrates the optimal annual peak shaving limit for the profiles B, C, and D, as well as the state of charge and state of health for the storage system used in each case. Similarly, Figure 7.11 shows the optimal monthly peak shaving limit, the SoC, and SoH for the same three profiles. Appendix B provides the battery power profiles for all investigated scenarios.

It can be seen that the optimization process minimizes expenses using the capacity of the storage system to decrease the peak power. The optimal power flow

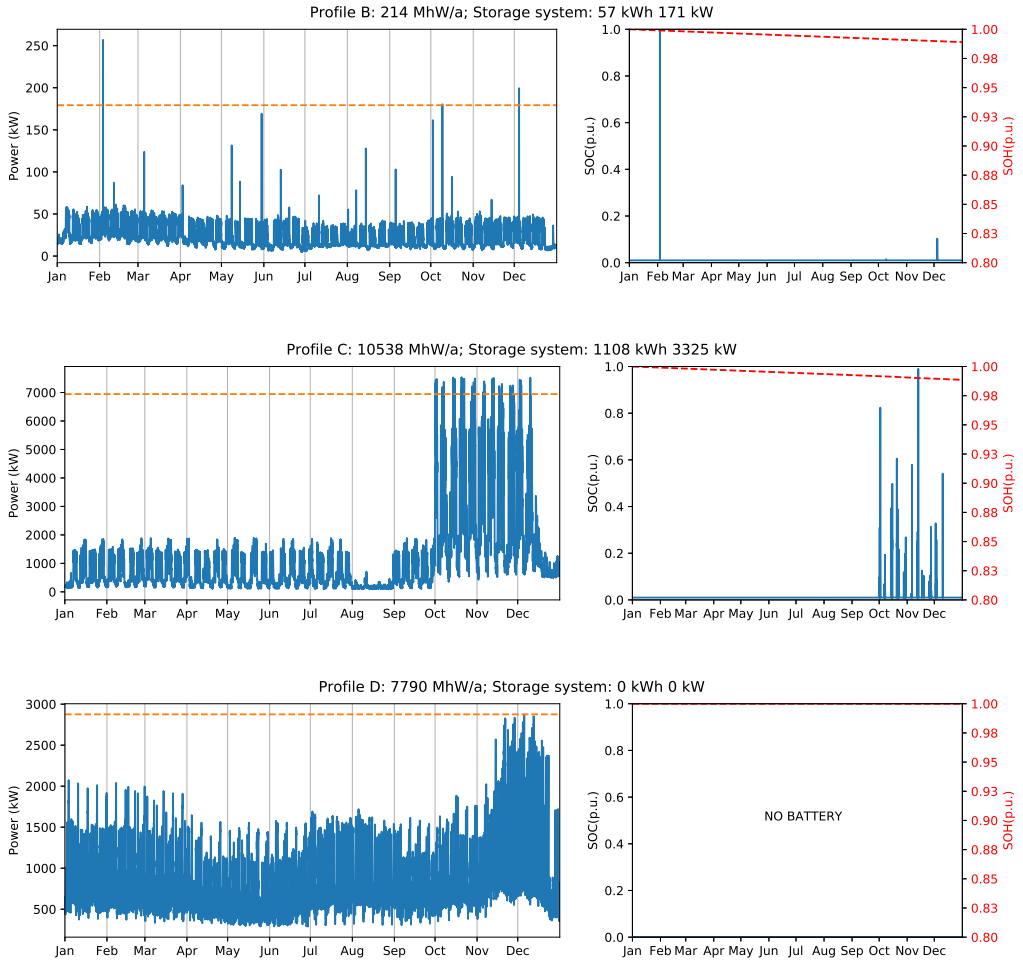

Figure 7.10: Industrial load profile B,C, and D with yearly billing scheme (**left**), and battery state of charge and state of health (**right**).

shows that the battery cycles are short, meaning that the battery is charged to the maximum necessary level just before being drained. This occurs due to the presence of SoC-dependent calendric degradation as one of the optimization criteria. At the same, cyclic aging is not a determinant in peak shaving applications because the BESS has only a low number of charging/discharging cycles and energy is never stored in the battery for a long time. For this reason, calendric degradation is the most important cost driver in storage systems for peak shaving applications.

To analyze the relation between load size and return of investment, consider Table 7.6. Optimization runs were performed, scaling the load size of Profile A from 10 to 40,000 MWh/a. The relation between the peaks and the loads were kept the same as in the original profile, resulting in exactly the same shape of battery

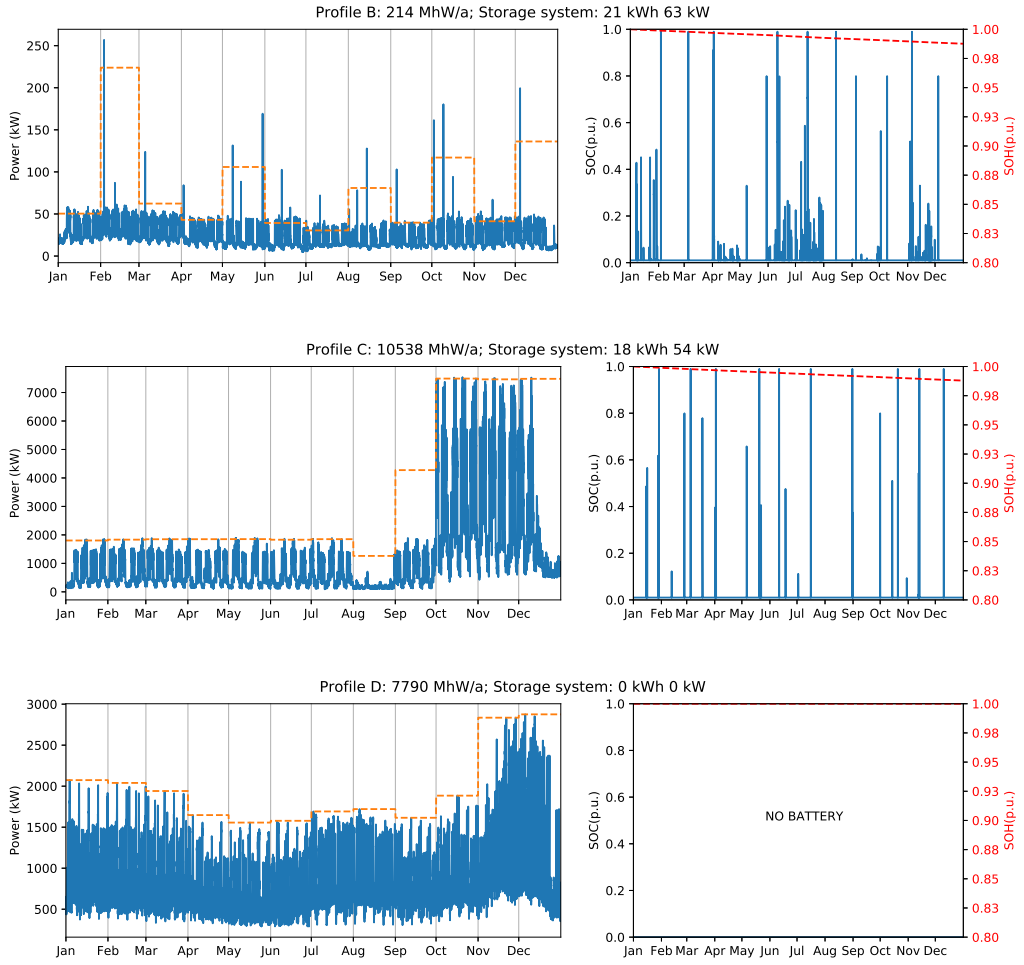

Figure 7.11: Industrial load profile B, C, and D with monthly billing scheme (**left**), and battery state of charge and state of health (**right**).

Table 7.6: Profile A with yearly billing scheme and duration factor of 4,431 h/a. Peak load capping of 5% which represents 20 capped peaks per annum.

Load (MWh/a)	Optimal Battery Size	Optimal Inverter Size	Recommended Battery Size	Recommended Inverter Size	Investment	Operation Cost	Saving Grid Charges	Total Savings (EBITDA)	Internal Rate of Return (IRR)	Payback (Years)	EoL (Years)	FEC (First Year)
10	0	0	0	0	€0	€0	€0	€0	0%	0.00	0.00	0.00
25	0	0	0	0	€0	€0	€0	€0	0%	0.00	0.00	0.00
50	0	0	0	10	€0	€0	€0	€0	0%	0.00	0.00	0.00
100	0	0	0	10	€0	€0	€0	€0	0%	0.00	0.00	0.00
250	1	3	10	10	€18,370	€170	€425	€254	−15%	72.23	18.00	1.00
500	2	6	10	10	€18,370	€170	€849	€679	−7%	27.06	18.00	1.00
750	3	9	10	10	€18,370	€170	€1274	€1103	−1%	16.65	18.00	2.00
1000	4	13	10	20	€18,370	€230	€1698	€1468	2%	12.51	18.00	3.00
2500	10	31	20	40	€31,901	€431	€4246	€3814	8%	8.36	18.00	4.00
5000	21	63	30	70	€42,351	€674	€8491	€7817	17%	5.42	18.00	5.00
10,000	42	126	50	130	€86,737	€1300	€16,983	€15,682	16%	5.53	18.00	6.00
20,000	84	251	90	260	€175,619	€2614	€33,966	€31,352	16%	5.60	18.00	7.00
30,000	126	377	130	380	€222,974	€3618	€50,948	€47,331	20%	4.71	18.00	7.00
40,000	168	503	170	510	€286,941	€4782	€67,931	€63,150	21%	4.54	18.00	7.00

SoC profile. As an overall trend, customers with large loads require BESS with large storage size and large nominal power of the inverter. Loads smaller than 1,000 MWh/a have a negative IRR and an extensive payback period, rendering them

unsuitable for BESS-based peak shaving applications. On the other hand, larger load profiles have a substantial improvement in the payback period. The results show that the BESS can be used for almost 18 years before reaching end of life at 80% of SoH. Although the peak capping is the same in all simulations, the battery usage differs for each load size because of the assumed discrete sizing of BESS and inverters in steps of 10 kWh and 10 kW respectively.

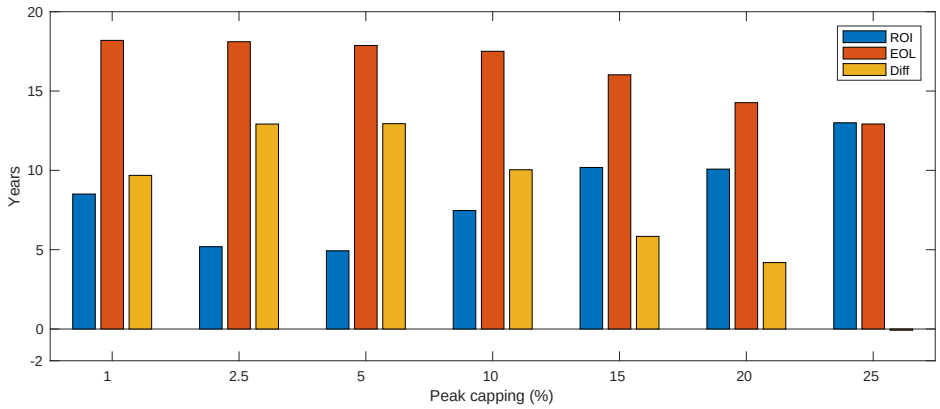

Figure 7.12: Profile A-Impacts of peak capping variation. Initial investment Amortization time (ROI), the number of years before the battery end of life (EOL), and the number of years the BESS will keep being used and generating savings through peak shaving after ROI being achieved.

It is clear that larger load sizes can benefit from BESS-based peak shaving with better economical results. In addition, it is interesting to analyze the impact of the peak capping variation on the payback period as well as the battery life time. Refer to Figure 7.12 and Table 7.7 for a detailed comparison. To generate these results, an additional constraint was added to the linear model described in Section 7.2.1:

$$P_{\text{peak-shave}} = \max(P_{\text{load}}) \cdot (1 - \text{PC}); \text{PC} = [0.01, 0.025, 0.05, 0.10, 0.15, 0.20, 0.25, 0.30], \tag{7.21}$$

where PC is the fixed amount of the peak that must be shaved. As shown in Table 7.7, all scenarios are profitable. However, the best IRR is obtained for peak capping equal to 5% of the total load. Smaller peak capping values extend the battery lifetime, but also extend the payback time as less savings of peak power reduction may be attained. In contrast, larger peak capping values increase the payback, but shorten the battery life.

As an overall trend, the increase of inverter size has a direct relation to the peak shaved load, *i.e.* 2.5% load shaving needs a 60 kW inverter, and 25% load shaving

requires ten times more. It is a straightforward relation because the inverter is sized according to the load power peak. Interestingly, the battery sizing does not follow the same trend because it is related to the number of peaks that must be shaved. In contrast to the optimal result where the battery is charged closer to the load peaks, larger peak load capping results in a smaller C-rate because the battery is charged slowly to avoid violating the maximum power peak allowed, and the battery must keep energy content for a longer period.

Table 7.7: Profile A wich peak load capping variating from 1% to 25%.

Peak Load Capping	Number of Capped Peaks	H/A	Load (MWh/a)	Recommended		Investment	Total Savings (EBITDA)	IRR	Payback (Years)	End of Life (Years)	Cycles
				Battery Size	Inverter Size						
1%	1	4246	9351	10	30	€23,595	€2773	8%	8.51	18.19	1
3%	6	4311	9351	20	60	€37,126	€7154	18%	5.19	18.11	2
5%	20	4431	9351	40	120	€72,601	€14,721	19%	4.93	17.87	5
10%	217	4670	9351	250	230	€211,317	€28,300	10%	7.47	17.51	11
15%	1298	4945	9351	610	360	€424,782	€41,714	5%	10.18	16.02	34
20%	4185	5254	9351	1420	480	€560,915	€55,651	5%	10.08	14.27	69
25%	8008	5605	9351	2720	600	€945,282	€68,099	1%	13.88	12.92	101

7.3 Final Remarks

This article describes a linear optimization model to size the most cost-effective BESS for a variety of industrial load profiles and multiple billing schemes. The optimization approach formulated in this work minimizes the storage degradation cost and the maximum power peak in the billing period.

The optimal BESS size and the number of capped peaks are directly related to the load profile. As an overall trend, for the exemplary load profiles under investigation, the monthly billing scheme is more attractive for industrial customers because of the number of peaks that can be capped with acceptable BESS sizes. For instance, a 51 kWh/152 kW BESS can shave 243 peaks which represents 6% of the maximum load peak and results in a 15,223 €of annual savings. As a general remark, considering the current cost of storage and retail energy tariff valid in Germany for 2016, most scenarios favor storage system installation. The expected increases of electricity prices and the reduction of BESS costs are likely to accelerate this trend. Although this work uses parameters corresponding to German market conditions and regulations, the described methodology can be easily adapted to other jurisdictions that use or consider peak power penalties, albeit with different billing period schemes and retail electricity tariff models.

Chapter 8

Battery Energy Storage as a Service for Peak Shaving Applications With Multiple Industrial Clients

Industrial electricity customers are not only charged for their energy consumption but also for the demand in a billing cycle. The demand charge can represent up to 50% of the customer electricity bill [91]. The load power peaks usually occur during short periods of time when large amounts of power are required and can impact the network planning because the electrical infrastructure must support these peaks of demand [139]. Consequently, the electricity charge contains the costs of energy, transmission and distribution fees, taxes, and other fees that represent a small portion of the total electricity bill of the customers.

Accordingly, industrial customers wants to reduce their energy and demand charges, but without decreasing the overall energy consumption. In this context, shaving the peak demand will benefit both the customer, by significantly reducing the peak demand payments, as well as the entire grid system, by helping reduce the network congestion and possibly lowering marginal energy prices. There are various methods to shave peak demand. However, one common method is to use an energy storage system (ESS).

The ESS can be used to help customers to flatten their demand profile by storing energy during off-peak periods and realizing this energy during peak load periods [18]. As a result, the use of ESS does not affect the customer load because the shaved demand is supplied by the ESS discharged power, but the net load seen from the utility side is changed. For instance, if the distribution provider considers

a flat profile coupled with ESS, the infrastructure can be designed with less network reinforcement [96]. Time of use energy price is another benefit that can be achieved [147] by charging the ESS during low price hours and discharging during high price hours [136].

Although the interest in battery energy storage system (BESS) is increasing in recent years [34], it comes at the expense of a high capital cost. The costs associated with purchasing, installing, and maintaining a storage system solution make the deployment of BESS in power system applications debatable [52], [88], [98], [125].

In response to the need to make BEES economically viable, several studies focus on finding the battery storage system optimal operation [14], [15], [21] to minimize the electricity charges. The BESS size is assumed to be known, and the optimal sizing problem is not considered. Therefore, several studies address the need to properly size BESS [42], [61]. The work described in [1], [80] focuses on commercial applications. Different methods have been used to determine the optimal size including iterative methods [92], [115]. Magnor et al. [66] and Merei et al. [79] optimize the size of home storage systems in the context of island grids using genetic algorithms. The minimization of electric chargers in the customer side is formulated with nonlinear model considering both energy charge and demand charge, where Markov decision processes, and particle swarm optimization are used in [58], [99], respectively. A general framework to find the optimal BESS size considering peak shaving applications is presented by Martins et al. [71]. This study discusses the economic advantages of peak load shaving and identifies the best storage operation patterns considering a trade-off between energy purchase, peak-power tariff, and battery aging.

Most existing studies focus on finding the optimal sizing as well as control strategies for BESS for individual customers. While these studies prove that it is possible to flatten the load and reduce demand charge, it is noticed that the storage system is underused, staying idle most of the time. Contrasting the important contributions mentioned above, this work proposes a strategy to reduce the inactive time of the storage system by sharing the same BESS between multiple industrial customers. In this new business model, the battery energy storage system is offered as a service by a third party who has a contract with the industrial load owners to avoid the power peaks. At the same time, the company providing BESS as a service (BESaS) is considered an industrial customer and is charged by the energy consumption as

well as by the power demand.

This chapter also introduces a techno-economic analysis evaluating the ROI of the system and battery degradation, and presents a linear programming(LP) approach for exact determination of optimal size and operation strategy of BESS. In addition, the break even point to balance the BESaS charges and clients expenses is discussed. The results show the profit margin for negotiation and identify cases when the service is not appealing.

8.1 Economic and Legal Framework for Industrial Customers

BESS are very flexible devices that can be used for many different applications [61]. The energy management system proposed in this study involve a grid-connected system shown in a schematic diagram in Figure 8.1. This figure demonstrates the power flow direction for all component links.

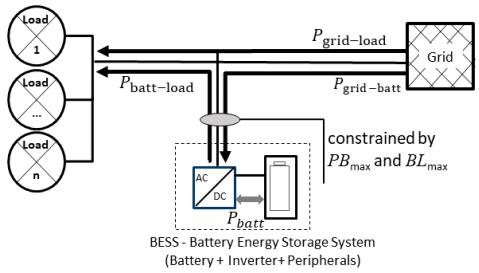

Figure 8.1: Power flows considered.

Since the early times of power systems, system operators introduced electricity tariffs to incentivize efficient grid usage. Typically, they add a demand charge to the total bill [26]. Industrial customers who exceed 100 MWh/year or 500 kW of average power demand have to pay an additional power price per kW. Electricity costs typically can be divided in the following components: electricity generation (wholesale prices and retail costs), the total for standard rates including taxes and fees, the power price per kilowatt (the maximum power peak in the billing period), and the energy price per kilowatt hour, based on the total energy consumption.

Figure 8.2 illustrates the price components for industrial customers: the total energy consumption $E_{total} = \sum Load_i$ averaged in time slots of 15 minutes, the power peak P_{max}, and the power peak after peak shave P_{PS}. The optimization definition and additional variables are explained in detail later.

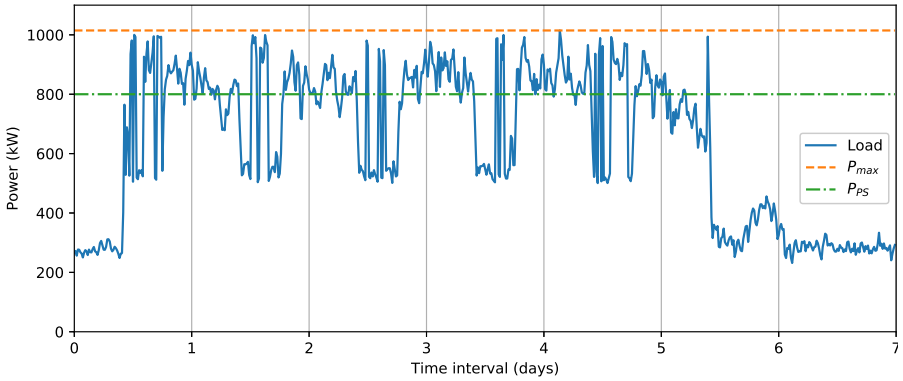

Figure 8.2: Customer load curve

In this context, three distinct parties are involved in the proposed peak shaving model that can be described as follows:

- Utility owns and operates the distribution feeder lines that carry the electricity from local sub-stations to neighborhood transformer boxes, and to industrial end users. It also manages the electrical meters situated at end users to measure their electricity usage.
- BESS owner is responsible for charging the BESS according to the projected peak shave demand of the customers, and feeding the end-use customers.
- End users contract the utility to purchase electricity for their day-by-day consumption, and also contract the BESS owner to supply power to avoid the contracted peak of demand.

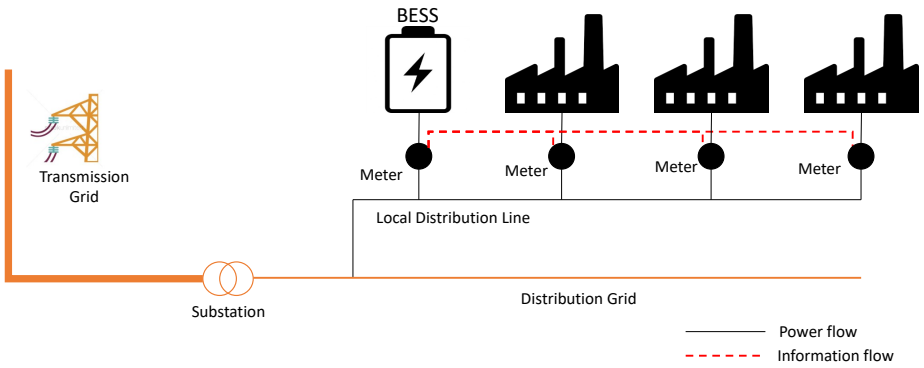

Figure 8.3: Virtual net metering model

This model considers the local distribution system as a virtual metering model. Figure 8.3 illustrates the structure of this model. Electricity stored in the BESS

feeds directly into the local distribution grid through a meter. The net metering is charged to each end user in the local distribution grid to offset its electricity usage. At the same time, the industrial customers are charged individually by the BESS owner for the electricity supplied to avoid their peak of demand.

In this thesis, it is assumed that the BESS is located in a close proximity of the load (e.g. in an industrial park) and thus power losses are not considered. Similar assumption of proximity can be made also for residential applications, e.g. with a community energy storage system.

Table 8.1: Electricity price for exemplary industrial customer

	Customer Charge	Demand Charge		Energy Charge
		For the first 500 kW of billing demand	For all billing demand over 500 kW	
Transmission	-	26.70 ¢/kW/day	30.39 ¢/kW/day	1.09 ¢/kWh
Distribution	50.09 ¢/day	28.89 ¢/kW/day	20.07 ¢/kW/day	-
Service	$2.7464 /day	-	0.72 ¢/kW/day	-
Total Price	**$3.2473 /day**	**55.59 ¢/kW/day**	**51.18 ¢/kW/day**	**1.09 ¢/kWh**

Table 8.1 describes the costs for industrial customers in Alberta, Canada. The billing period has a fixed distribution and service charge of $3.2473 per day. The charge for the first 500 kW peak demand is 55.59¢\kW per day in the billing period, and after 500 kW the peak demand cost 51.18¢\kW per day. The energy price is 1.09¢/kW. Using the costs from Table 8.1, the total charges C_{total} in one billing period can be calculated as follow:

$$C_{\text{total}} = 3.2473 \cdot \Delta_{\text{days}} + 0.5559 \cdot P_{\text{peak}}^{<=500kW} + 0.5118 \cdot P_{\text{peak}}^{>500kW} + 0.0109 \cdot E_{\text{load}}, \quad (8.1)$$

i.e. considering an industrial customer with total load $E_{\text{load}} = 486MWh$ in a 30 day (Δ_{days}) billing period, and with peak power of 1044 kW, the total charges C_{total} in this period are

$$C_{\text{total}} = 3.2473 \cdot 30days + 0.5559 \cdot 500kW + 0.5118 \cdot 544kW + 0.0109 \cdot 486MWh \approx \$5951.$$

As described in Table 8.1 and equation 8.1, demand charges are billed for the peak kW use averaged over 15 minutes increments of time. The highest demand recorded during the billing period is used to level out the recovery of the fixed costs necessary to serve the demand set.

A large amount of investment in transmission lines and other facilities may be dedicated to attend industrial customers. To reduce the risks serving customers who have potentially large swings in demand during the year, the imposition of a

demand ratchet allows the utility to earn a fair return on its investment, even when the demand falls to low levels. For instance, a ski resort may have significant energy requirements for only few months of the year, but the utility have to prepare the grid infrastructure to attend the resort when needed. A minimum billing will be calculated based on a given percentage of their peak use, for example 85% of the January billing, and the resort will be billed at least this much in the next 12-month period, even if they use little or no energy. This insures that the utility is properly compensated for the year-round expenses it incurs to serve this customer.

Figure 8.4 illustrates the ratchet rate. The utility notices when a high peak of demand occurs. Considering the ratchet is 85%, the utility sets a minimum billed demand for 85% of the maximum recorded peak kW for the next 11 months. Thus, the customer will be billed 85% of the previous peak, even if the customer uses a smaller amount of power during a succeeding month.

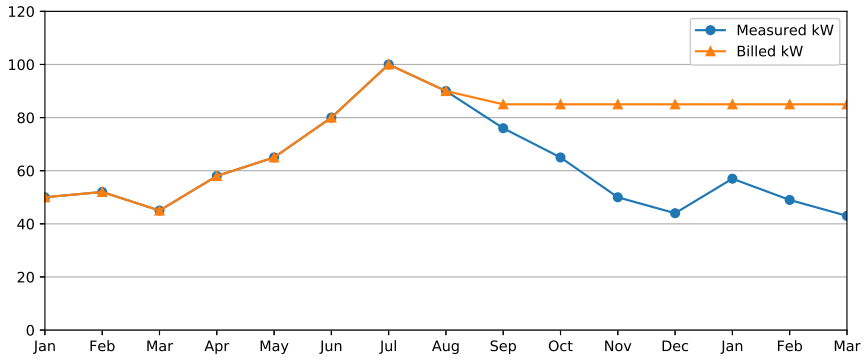

Figure 8.4: Measured kW vs Billed at 85% Ratchet (started in July)

This study analyzes the economic potential and technical capabilities of BESS where the investment costs of battery and the inverter are analyzed independently. The total battery investment cost without inverter C_{batt} comprises the fixed cost C_{fix}, the storage system energy cost C_{batt}^{var}, and the storage operation and maintenance (OPEX) cost ($C_{opex,batt}$). The total cost $C_{storage}$ for the energy storage system can be described as

$$C_{storage}(E_{batt}^{nom}, P_{inv}^{nom}) = C_{fix} + C_{opex,batt} + (C_{batt}^{var} * E_{batt}^{nom}) + (C_{inv}^{var} * P_{inv}^{nom}), \quad (8.2)$$

where E_{batt}^{nom} and P_{inv}^{nom} represent respectively, the energy content and the inverter nominal power of the storage system.

8.2 Battery Energy Storage Model

The battery energy storage system model considered in this paper is derived from previous study [71]. Typical loads producing steep peaks are ideal for peak shaving with BESS. Another condition for the feasibility of peak shaving is predictable behavior of the load. Forecasting algorithms ensure that the storage system will have enough energy when needed [113]. Although such prediction tasks are indispensable for achieving the best BESS operation performance, they are outside the scope of this work.

Storage aging is a significant cost driver during energy storage operation and cannot be neglected. It is common to separate battery degradation between *calendric aging*, and *cyclic aging* [118], [120], [138]. The battery cyclic and calendric lifetime indicators ($\text{Life}^{80\%}_{\text{Cyc}}$, $\text{Life}^{80\%}_{\text{Cal}}$) determinate the current state of health (SoH). This paper considers that the BESS must be replaced when the SoH achieves 80% of the nominal capacity.

As lithium-ion batteries have been developed to maturity, they have begun to approach their theoretical energy density limits (200-250 Wh/kg) [4]. Ongoing electrochemical research on lithium-ion batteries aims at increasing cycle life, safety, and other performance characteristics [55]. The aging model and its linearization are described in Chapter 6, and Table 8.2 summarizes the parameters and price information for the BESS/inverter system used in the optimization model.

Table 8.2: BESS/inverter performance parameters and price information

Variable	Parameter	Unit	Value
η_{inv}	Average one way inverter efficiency	%	97.5
T_{inv}	Inverter lifetime	years	20
η_{batt}	Battery round-trip efficiency	%	95
SD_{batt}	Battery self-discharge per day	%	0.02
$[SoC_{min} \dots SoC_{max}]$	SOC limits	%	5-95
$Life^{80\%}_{cal}$	Battery calendric life	years	13
$Life^{80\%}_{cyc}$	Battery cyclic life	FEC	4500
$\text{C}^{\text{var}}_{\text{inv}}$	Inverter cost (variable)	\$/kW	239
$\text{C}^{\text{var}}_{\text{batt}}$	Battery cost (variable)	\$/kWh	889
C_{fix}	Fixed cost for storage (housing, cooling, and periphery)	\$	893.2

8.3 Linear Optimization of BESS

The economically optimal power flows and battery storage component sizing can be obtained using linear programming. The goal is to minimize the overall electricity

cost, three types of costs are considered. First, the energy cost $C_{\text{energy\_tot}}$ that is composed of the base energy price, fees, and taxes. Second, the power cost $C_{\text{power\_max}}$ that is charged by the retailer of franchisee in each billing period on the basis of the ratchet rate. Third, the battery degradation cost $C_{\text{storage\_deg}}$, also called aging cost, that is the major cost driver during storage operation, caused by cyclic and calendric aging. All variables and parameters considered in this study are described in Table 8.3.

Table 8.3: Variables and parameters used for the battery modeling and optimization routines

Variable	**Description (at the time slot i)**	**Unit**
$P_{\text{load}_{ij}}$	Load demand (historical data)	kW
$P_{\text{inv}}^{\text{nom}}$	Nominal power of the battery inverter	kW
$E_{\text{batt}}^{\text{nom}}$	Nominal battery capacity	kWh
$P_{\text{peak-shave}_{jk}}$	Maximum power in the billing cycle k	kW
$P_{\text{peak-shave}_k}^{\text{batt}}$	Maximum power in the billing cycle k for the storage system	kW
P_{batt}	Bidirectional power flow to the battery	kW
$P_{\text{batt-load}_{ij}}$	Power transferred from the battery to load j	kW
$P_{\text{grid-load}_{ij}}$	Power imported from the grid to load j	kW
$P_{\text{grid-batt}_i}$	Power imported from the grid to the battery	kW
SoH_i	State of health ($[0 \dots 1]$)	p.u.
E_{batt_i}	Battery energy content at time i	kWh
SoC_i	State of charge ($[\text{SoC}_{\text{min}} \dots \text{SoC}_{\text{max}}]$)	p.u.

To meet the electrical demand for industrial load j in each time step i, $P_{\text{load}_{ij}}$, the system attempts to use power from the battery, $P_{\text{batt-load}_{ij}}$, or draw power from the grid, $P_{\text{grid-load}_{ij}}$, *i.e.*:

$$P_{\text{load}_{ij}} = P_{\text{batt-load}_{ij}} + P_{\text{grid-load}_{ij}}. \tag{8.3}$$

In the same way, the power imported from the grid to load j at time i ($P_{\text{grid-load}_{ij}}$) is restricted to the maximum power for the billing cycle k. This constrain can be represented as:

$$P_{\text{grid-load}_{ij}} \leq P_{\text{peak-shave}_{jk}}, \tag{8.4}$$

where $P_{\text{peak-shave}_{jk}}$ represent the highest point of demand in the billing cycle k. For instance, considering the highest load of the month, all data points i for the load j should be limited to the same maximum limit $P_{\text{peak-shave}_{jk}}$. The peak power is used to calculate the optimal solution power cost. Similarly, the power imported from the grid to the battery at time i ($P_{\text{grid-batt}_i}$) is also restricted to the maximum

power for the billing cycle k:

$$P_{\text{grid}-\text{batt}_i} \leq P^{\text{batt}}_{\text{peak}-\text{shave}_k}. \tag{8.5}$$

The battery charge power, $P_{\text{grid}-\text{batt}_i}$ and the discharge power, $P_{\text{batt}-\text{load}_{ij}}$, are both limited by the nominal power flow from the inverter to the battery

$$0 \leq P_{\text{grid}-\text{batt}_i} + P_{\text{batt}-\text{load}_{ij}} \leq P^{\text{nom}}_{\text{inv}}, \tag{8.6}$$

where $P^{\text{nom}}_{\text{inv}}$ corresponds to the inverter size. The battery energy content at time step i (E_{batt_i}) is a fraction of the total energy content of the battery installed and satisfies the recurrence relation

$$E_{\text{batt}_i} = (E_{\text{batt}_{i-1}} * \frac{\text{SD}_{batt}}{d}) + (\eta_{batt} * P_{\text{batt}_i} * \Delta t_{res}), \tag{8.7}$$

where SD_{batt} is the self-discharge factor of the battery, and $d = 96$ is the conversion factor to 15 minutes time slots. $P_{\text{batt}_i}$is an auxiliary variable used to store the bidirectional power flow from the storage inverter to the battery. It is correlated with the average one-way efficiency of the inverter, η_{inv}, as follows

$$P_{\text{batt}_i} = (\eta_{inv} * P_{\text{grid}-\text{batt}_i}) + (-\frac{1}{\eta_{inv}} * P_{\text{batt}-\text{load}_{ij}}). \tag{8.8}$$

The energy content of the storage system is further confined by an upper boundary, which decreases upon usage and aging according to the SoH. The SoH is defined as the irreversible capacity fade over time, related to the nominal battery capacity, and $E^{\text{usable}}_{\text{batt}}$ represents a fraction of the total energy content of the battery installed limited to the maximum and minimum state of charge (SoC) that the battery can achieve. The two constrains can be represented as

$$E_{\text{batt}_i} \leq E^{\text{usable}}_{\text{batt}} * \text{SoH}_\text{i}, \tag{8.9}$$

$$E^{\text{usable}}_{\text{batt}} \leq E^{\text{nom}}_{\text{batt}} * (\text{SoC}_{max} - \text{SoC}_{min}). \tag{8.10}$$

The state of health (SoH) also meets the recurrence relation

$$\text{SoH}_i = \text{SoH}_{i-1} - (\text{aging}_{\text{cyc}_i} + \text{aging}_{\text{cal}_i}) \cdot 0.2. \tag{8.11}$$

where $\text{aging}_{\text{cyc}_i}$ is the energy throughput dependent *cyclic aging*, and $\text{aging}_{\text{cal}_i}$ is the pure time-dependent irreversible loss of battery capacity called *calendric aging* [118], [120], [128], [138]

$$\text{aging}_{\text{cyc}_i} = \text{aging}_{\text{cyc}_{i-1}} + 0.5 \cdot \frac{|P_{\text{batt}_i} \cdot \Delta t_{res}|}{E_{\text{batt}_i}} \cdot \frac{1}{\text{Life}^{80\%}_{\text{Cyc}}}, \tag{8.12}$$

$$\text{aging}_{\text{cal}_i} = (3.676 \cdot 10^{-7} \cdot \text{SoC} + 6.246 \cdot 10^{-6}) \cdot (i \cdot \Delta t_{\text{res}}). \tag{8.13}$$

SoH estimates the overall aging using the superposition principle [120]. A theoretical maximum charge throughput is defined via $\text{Life}_{\text{Cyc}}^{80\%}$, i.e. the number of full equivalent cycles until 80% capacity is reached if there were no calendric aging.

The optimal solution aims to reduce the overall cost by minimizing the expenses for service charges and implicit cost caused by battery degradation. At the same time, it must satisfy all constraints described above. This cost model is divided into three components, *i.e.*:

$$\text{minimize} \qquad C_{\text{charge}}^{\text{grid}} + C_{\text{charge}}^{\text{batt}} + C_{\text{storage\_deg}}. \tag{8.14}$$

The first component $C_{\text{charge}}^{\text{grid}}$ comprises the sum of the customer charge, the peak induced cost based on the highest point of demand (or peak) within billing period, and the cost of energy purchased from the grid which is directly used to attend the industrial load j or charge the battery. This component can be represented as

$$\begin{aligned} C_{\text{charge}}^{\text{grid}} = & \sum_k C_{\text{fix}} \cdot \Delta\text{days}_k + \\ & \sum_j \sum_k C_{\text{power}_j} \cdot P_{\text{peak-shave}_{jk}} + \\ & \sum_k C_{\text{power}} \cdot P_{\text{peak-shave}_k}^{\text{batt}} + \\ & \sum_i \sum_j C_{\text{buy}} \cdot P_{\text{grid-load}_{ij}} + \\ & \sum_i C_{\text{buy}} \cdot P_{\text{grid-batt}_i}, \end{aligned} \tag{8.15}$$

where C_{fix} represents the fixed daily charge, Δdays_k is related to the number of days in the billing period k, C_{power} is the peak-power tariff, and C_{buy} is the retail electricity price. The second component $C_{\text{charge}}^{\text{batt}}$ represents the amount that each industrial load pays for energy coming from the storage system. It is defined as

$$C_{\text{charge}}^{\text{batt}} = \sum_i \sum_j \frac{\text{C}_{\text{batt}}^{\text{var}}}{Life_{cyc}^{80\%}} \cdot P_{\text{batt-load}_{ij}}, \tag{8.16}$$

where $\text{C}_{\text{var}}^{\text{batt}}$ is the energy specific cost of a storage system, and $Life_{cyc}^{80\%}$ denotes the theoretical maximum charge throughput, *i.e.* the number of FEC until 80% capacity is reached if there is no calendric aging. The third component estimates the storage system degradation cost that can be represented as

$$C_{\text{storage\_deg}} = \frac{\Delta\text{SoH}}{(1 - \alpha_{Replace})} \cdot (E_{\text{batt}}^{nom}) + (P_{\text{inv}}^{nom}) \cdot \frac{\Delta t}{T_{\text{inv}}}, \tag{8.17}$$

where Δt describes the time covered with the simulation and ΔSoH the battery aging.

8.4 Case Study

This section presents an application of the developed methodology for dimensioning BESaS for industrial peak shaving. The industrial customer has no responsibility over the storage system, which is offered as a service. In this model, the BESS is considered an industrial customer by the utility company. As a result, the energy used to charge the battery and the energy used for immediate consumption have the same cost, and both have to take into consideration the industrial customer peak power calculation.

8.4.1 Case Description for Multiple Industrial Customers

Figure 8.5 shows the industrial load profiles considered in this case of study. The simulations consider real demand averaged with a resolution of Δt_{res}= 15 min [8]. The maximum value in each 15 minutes time spam is used for demand charge over the billing cycle.

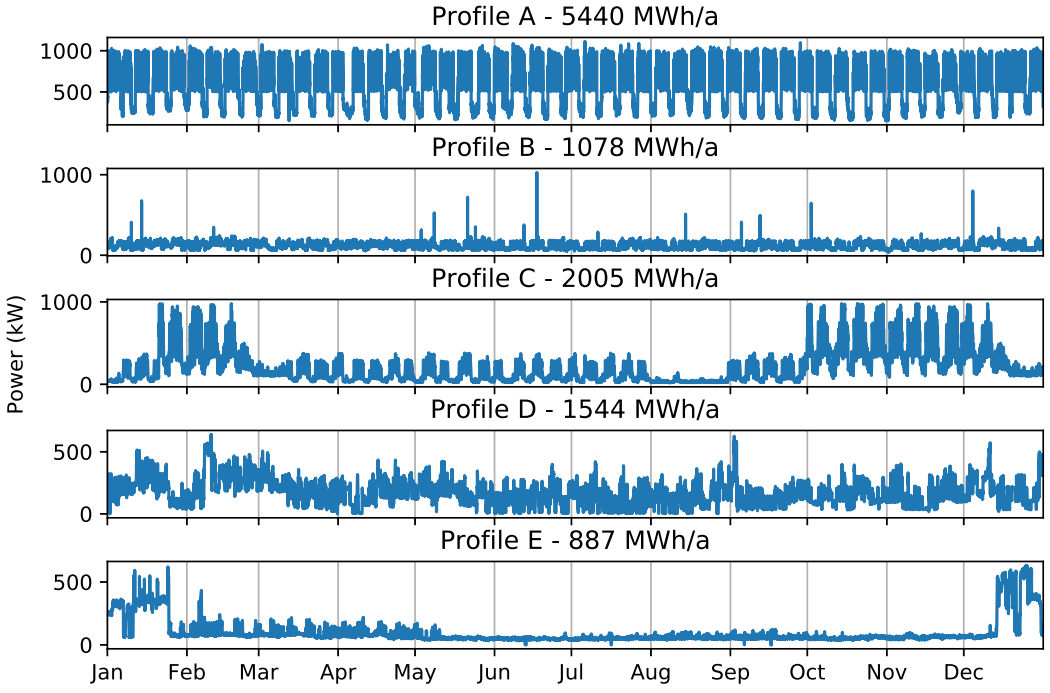

Figure 8.5: Load profiles.

The results presented in the next sections describe the optimal BESS component

sizes, the optimal operation strategy, the degradation impact, and the economic analysis for different combinations of industrial clients.

8.4.2 Effect of Sizing and Degradation of the BESS for Multiple Industrial Customers

The main goal of this work is to decrease the peak of demand of multiple clients with one BESS solution. The optimal storage and inverter size for each profile (A-E), as well as the total load, the number of full equivalent cycles and the storage degradation at the end of one year, and the number of years before end of life (EoL), are presented in Table 8.4.

Table 8.4: BESS sizing and degradation comparison of system optimization results.

#	Profiles					Total load	Battery	Inverter	Number	SoH at the	Number of Years
	A	B	C	D	E	(MhW/a)	size	size	of FEC	end of year	before EoL
1	x					5,441	118	111	31	98.22%	11
2		x				270	189	203	5	98.79%	16
3			x			2,005	580	193	10	98.68%	15
4				x		1,545	381	127	12	98.63%	14
5					x	887	212	71	7	98.75%	16
6	x	x				5,710	197	203	23	98.38%	12
7	x		x			7,446	580	193	15	98.57%	13
8	x			x		6,985	348	127	22	98.42%	12
9	x				x	6,328	342	114	16	98.56%	13
10		x	x			2,275	619	206	11	98.67%	15
11		x		x		1,814	374	204	14	98.59%	14
12		x			x	1,157	498	203	6	98.78%	16
13			x	x		3,550	600	200	18	98.51%	13
14			x		x	2,893	580	193	14	98.60%	14
15				x	x	2,432	390	130	16	98.55%	13
16	x	x	x			7,716	619	206	15	98.57%	13
17	x	x		x		7,255	373	204	22	98.41%	12
18	x	x			x	6,598	496	203	13	98.62%	14
19	x		x	x		8,991	601	200	21	98.43%	12
20	x		x		x	8,333	585	195	18	98.50%	13
21	x			x	x	7,873	383	128	23	98.39%	12
22		x	x	x		3,820	625	208	18	98.51%	13
23		x	x		x	3,162	619	206	14	98.60%	14
24		x		x	x	2,702	530	204	13	98.61%	14
25			x	x	x	4,437	601	200	20	98.45%	12
26	x	x	x	x		9,260	625	208	21	98.43%	12
27	x	x	x		x	8,603	620	207	18	98.50%	13
28	x	x		x	x	8,143	525	204	18	98.49%	13
29	x		x	x	x	9,878	604	201	24	98.38%	12
30		x	x	x	x	4,707	625	208	20	98.45%	12
31	x	x	x	x	x	10,148	625	208	23	98.38%	12

According to this table, the cyclic aging (number of FEC) has a small impact in the SoH. For instance, in simulation '1' which considers only the industrial 'Profile A,' the total number of FEC after one year is less than 1% of $Life_{cyc}^{80\%}$. To

gain a better understanding of the impacts of calendric and cycling degradation in peak-shaving applications, two battery usage strategies are considered. The first strategy is based on the optimal solution obtained using the linear programming (LP) algorithm. The second strategy is naive and assumes that the BESS is always at full SoC capacity, drained to provide enough power to peak shave, fully charged again, and then stays idle until the next peak of load.

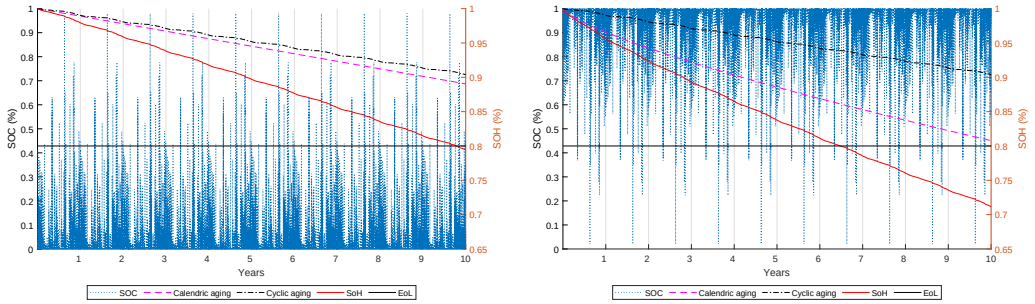

(a) Optimal strategy (b) Naive strategy

Figure 8.6: Time correlated evolution of battery state of charge (SoC) and resulting state of health (SoH) decline for the optimal strategy (left) and naive strategy (right).

Figure 8.6 illustrates the periodically changing charge level of the storage system (SoC), and the evolution of battery degradation (SoH) for cycling and calendar aging for a ten-year period. The image at the right shows the variation when the optimal strategy is followed, and the image at the left shows the SoC and SoH considering a naive strategy. That means, the battery is kept at full nominal capacity and then drained when the load reaches above the peak shave limit. It can be noticed that the number of times that the battery needs to intervene to avoid peaks remains the same. For this reason, the cycling aging is exactly the same in both cases. In contrast, the calendric aging distinctly differs because of the SoC dependency described in equation (2.2). As a result, the naive strategy depleted the battery 30% faster than the optimal strategy. The optimal strategy also shows that the battery cycles can be short, meaning that with adequate forecasting the battery can be charged to the maximum necessary level just before the need to be drained.

Next, to better understand how the battery usage impacts the industrial clients, consider Table 8.5 which shows the monthly peak load capping for simulations with 'Profile A,' 'Profile B,' and 'Profile C.' In general, it is possible to notice that the peak load shaved increased. For instance, a peak reduction of 7.78% on average

Table 8.5: Profile A and profile B simulations. Total peak load shaved per billing cycle and total number of capped peaks in one year.

#	Profiles					Total load MhW/a	Peak load capping (%)												Number capped peaks
	A	B	C	D	E		Jan	Feb	Mar	Apr	May	Jun	Jul	Aug	Sep	Oct	Nov	Dec	
1	x					5441	6.42	8.35	9.96	9.40	7.68	8.84	9.96	5.55	10.10	6.28	4.51	6.25	782
2		x				270	69.98	38.69	12.07	15.26	71.93	79.10	38.40	64.58	64.24	70.99	35.68	74.62	1,137
3			x			2005	13.59	10.43	18.14	15.45	10.66	17.21	12.79	43.15	34.36	6.17	8.25	18.69	651
6	x					5710	6.44	8.35	9.98	9.40	7.69	9.07	11.41	5.57	11.02	6.40	4.63	6.24	856
		x					70.02	39.71	12.97	16.30	72.20	79.10	39.57	65.08	64.60	71.17	36.28	74.74	1,351
7	x					7446	6.73	8.44	10.27	9.78	7.72	9.02	11.53	5.86	9.57	6.52	5.15	6.68	885
			x				13.59	10.43	18.59	15.54	11.29	17.50	14.33	42.10	34.36	6.40	8.31	18.61	669
10		x				2275	70.02	39.71	12.97	16.89	72.20	80.29	39.51	65.46	64.64	71.17	36.40	74.82	1,441
			x				13.59	10.43	18.14	15.45	10.69	17.21	13.93	44.90	36.64	6.40	8.25	18.69	676
16	x					7716	6.73	8.46	10.27	9.78	7.79	9.07	11.53	5.96	9.75	6.43	5.15	6.68	896
		x					70.02	39.71	12.97	16.89	72.24	80.29	39.90	65.46	64.73	71.17	36.46	74.82	1,464
			x				13.59	10.43	18.59	15.54	11.23	17.44	14.37	43.91	36.29	6.43	8.31	18.69	685
26	x					9260	6.73	8.50	10.23	9.73	7.79	9.27	11.80	5.61	9.57	6.54	5.33	6.75	901
		x					70.02	39.71	12.97	16.89	72.28	81.16	39.90	65.46	64.86	71.27	36.40	74.78	1,488
			x				13.62	10.66	20.89	17.53	12.53	19.79	15.93	41.95	37.04	6.81	8.82	19.81	759
				x			19.50	13.82	25.73	27.25	23.44	29.68	33.20	27.10	23.14	26.12	21.39	17.82	888
27	x					8603	6.80	8.61	10.28	9.82	7.81	9.07	11.53	5.61	9.75	6.58	5.22	6.79	908
		x					70.07	39.71	12.82	16.89	72.20	80.47	39.90	65.46	64.73	71.22	36.40	74.82	1,467
			x				14.45	11.16	18.97	16.54	11.55	17.63	14.50	44.10	36.37	6.62	8.50	18.88	724
					x		21.39	21.48	17.54	25.49	34.94	34.26	23.57	14.29	14.64	30.62	12.79	4.52	889
31	x					10148	6.81	8.50	10.23	9.78	7.79	9.27	11.80	5.61	9.57	6.31	5.33	6.75	899
		x					70.07	39.71	12.97	16.89	72.24	81.16	39.96	65.46	64.86	71.27	36.40	74.78	1,493
			x				14.45	11.10	20.98	17.66	12.53	19.79	15.93	41.95	37.04	6.87	8.82	19.81	776
				x			19.52	13.96	25.90	27.28	23.44	29.73	33.20	27.10	22.64	26.22	21.39	17.82	895
					x		21.64	22.03	17.95	26.03	35.35	34.51	23.82	14.29	14.75	31.71	13.40	4.63	933

which represents 782 capped peaks can be achieved when 'Profile A' is BESaS's only customer. This average increases to 8.15% and 899 capped peaks when all five profiles are present. Similarly, 'Profile B' has an increase of 0.85% on average, and 'Profile C' peak reduction goes from 17.41% when it is the sole client to 18.91% when coupled with the other four profiles. The number of capped peaks in 'Profile B' are smaller but represent a significant portion of the demand charges. On average, 'Profile B' consumes 31 kWh, but its monthly demand peaks vary from 54 kW to 257 kW. These large demand spikes represent an excellent opportunity for peak shaving. For this reason, 'Profile B' has the most significant peak load capping.

Further considering 'Profile A' with 5,441 MWh/a, the optimizer determines the optimal storage size of 118 kWh and inverter nominal power of 111 kW. Figure 8.7 illustrates the power flows for a five-day period during the second week of July. The left panel shows the load consumption, the power flow imported from the grid for direct use or to charge the battery, as well as the maximum power peak after shaving. The right panel shows the power profile of the storage system in the terms of C-rate, and the evolution of battery capacity fade (SoH). It clearly shows that the capacity fade is stronger when the energy throughput is high.

Furthermore, the battery is an industrial client that is charged based on the energy consumption and the power demand. For this reason, the optimizer avoids

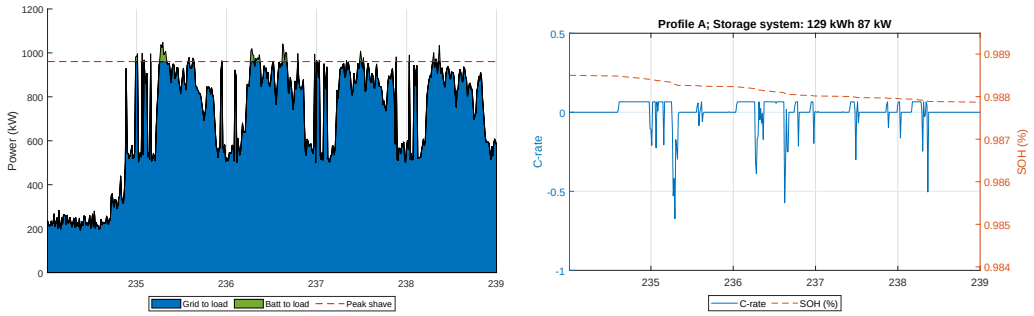

(a) Load Profile (b) Power Profile and SoH decline

Figure 8.7: Power flow analysis for a five-day period: load and power flows within the system (left); time correlated evolution of battery power profile and resulting state of health (SoH) decline (right).

charging the battery using large power spikes, resulting in the flat charging profile seen in Figure 8.7b.

8.4.3 Economic Analysis

This section discusses a number of relevant economic indicators. Table 8.6 shows the optimal storage, the inverter size, and the economic results for simulations including 'Profile A,' 'Profile B,' and 'Profile C.' The total BESS investment comprises the

Table 8.6: Profile A, profile B and profile C economic comparison of system optimization results.

#	Profiles					Battery	Inverter	Total BESS	BESS	Individual	Operation	Saving Grid	BESaS	Total	Origial grid	%
	A	B	C	D	E	size	size	investment	share	Investment	Cost	charges	Charges	Savings	charges	Savings
1	x					118	111	99963	100%	9,088	1,265	16,868	10300	5,303	274,763	2%
2		x				189	203	163092	100%	10,193	2,198	16,619	10683	3,738	29,279	13%
3			x			580	193	434405	100%	28,960	3,767	19,408	32103	-16,462	149,841	-11%
6	x					197	203	168782	51%	7,192	1,141	17,411	8261	8,009	274,763	3%
		x							49%	6,873	1,091	16,710	7453	8,166	29,279	28%
7	x					580	193	434405	47%	15,818	1,783	17,593	17666	-1,856	274,763	-1%
			x						53%	17,598	1,984	19,591	19955	-2,348	149,841	-2%
10		x				619	206	463263	46%	14,137	1,839	16,779	15363	-423	29,279	-1%
			x						54%	16,747	2,178	19,818	19055	-1,415	149,841	-1%
16	x					619	206	463263	33%	11,601	1,308	17,655	13138	3,209	274,763	1%
		x							31%	10,990	1,239	16,788	11978	3,571	29,279	12%
			x						37%	13,045	1,470	19,870	15079	3,321	149,841	2%
26	x					625	208	468285	23%	8,848	921	17,703	10425	6,357	274,763	2%
		x							21%	8,380	872	16,831	9401	6,557	29,279	22%
			x						27%	10,404	1,083	20,843	12654	7,106	149,841	5%
				x					29%	11,392	1,185	22,849	13548	8,115	113,923	7%
27	x					620	207	464339	28%	9,887	1,115	17,707	11404	5,189	274,763	2%
		x							26%	9,341	1,053	16,796	10300	5,443	29,279	19%
			x						32%	11,364	1,281	20,372	13457	5,635	149,841	4%
					x				14%	5,126	578	9,156	6085	2,493	58,926	4%
31	x					625	208	468285	20%	7,877	820	17,688	9407	7,461	274,763	3%
		x							19%	7,466	777	16,831	8447	7,608	29,279	26%
			x						24%	9,374	975	21,077	11618	8,483	149,841	6%
				x					26%	10,145	1,056	22,838	12245	9,538	113,923	8%
					x				11%	4,162	433	9,321	5162	3,725	58,926	6%

overall cost C_{storage} described in Equation (8.2). The BESS share factor $\Delta^{share}_{\text{storage}_j}$ represents the fraction of peak of demand for each industrial customer j. It can be

estimated as:

$$\Delta^{share}_{\text{storage}_j} = \frac{\Delta_{\text{peak}_j}}{\sum_j \Delta_{\text{peak}_j}}, \tag{8.18}$$

$$\Delta_{\text{peak}_j} = \frac{\sum_k (P_{\text{load-max}_{jk}} - P_{\text{peak-shave}_{jk}})}{k}, \tag{8.19}$$

where $(P_{\text{load-max}_{\text{jk}}} - P_{\text{peak-shave}_{\text{jk}}})$ describes the difference between the maximum load peak without peak shaving and the maximum load peak after peak shaving per billing period k, and $\Delta_{\text{peak}_{\text{j}}}$ is the average of this difference in all billing periods. The BESS share factor is used to define the individual investment each client must commit annually:

$$\text{C}^{share}_{\text{storage}_j} = \frac{\text{C}_{\text{storage}}}{\text{EoL}} \cdot \Delta^{share}_{\text{storage}_j}, \tag{8.20}$$

where the total storage cost $\text{C}_{\text{storage}}$ is divided by the estimated number of years before end of life (EoL) (Table 8.4). The operation cost, $\text{C}_{\text{opex,batt}}$, is calculated as 0.6% of the investment plus 6\$/kW and divided amongst the industrial customers according to the respective BESS share factor. Table 8.7 shows the OPEX components considered in this work.

Table 8.7: Operation cost (OPEX) composition.

Insurance	0.30%
System management	0.20%
Service contract	1 \$/kW
Maintenance reserve	5 \$/kW
Administrative costs	0.10%

The saving grid charges represent the amount each customer saves by using the BESaS system:

$$\text{Savings}_{\text{grid-charges}_j} = C_{\text{buy}} \cdot \sum_i P_{\text{batt-load}_{ij}} + \Big(C_{\text{power}_k} \cdot (P_{\text{load-max}_{jk}} - P_{\text{peak-shave}_{jk}})\Big), \tag{8.21}$$

where C_{buy} and $C_{\text{power}_{\text{k}}}$ are the energy and power cost respectively. Additionally, the cost of using the BESaS ($\text{BESaS}_{\text{charges}_j}$) is extracted from the parameter of the cost function (equation (7.15)) and it can be expressed as follows:

$$\text{BESaS}_{\text{charges}_j} = \left(\left(\sum_i \frac{\text{C}^{\text{var}}_{\text{batt}}}{Life^{80\%}_{cyc}} \cdot P_{\text{batt-load}_{ij}}\right) + \left(C_{\text{power}} \cdot \sum_k P^{\text{batt}}_{\text{peak-shave}_k} \cdot \Delta^{share}_{\text{storage}_j}\right) + \text{C}^{share}_{\text{storage}_j}\right) \cdot \Delta_{\text{profit}}, \tag{8.22}$$

where the first component denotes the energy cost, and the second component denotes the power cost for the billing period k. The share factor $\Delta^{share}_{\text{storage}_{\text{j}}}$ is also

considered to define the fraction of the storage demand peak to which each customer must commit. The charges are subject to the profit margin that the BESaS owner must apply. To make it easier to find the break even point, the results in Table 8.6 consider $\Delta_{\text{profit}} = 1$. Therefore, the total savings is a static calculation:

$$\text{TotalSavings}_j = \text{Savings}_{\text{grid}-\text{charges}_j} - (\text{OPEX}_j + \text{BESaS}_{\text{charges}_j}). \tag{8.23}$$

The original charges C_{total} (equation (8.1)) represents the electricity bill without storage. Finally, the last column '% savings' describes how much of the original grid charges can be saved using BESaS using:

$$\text{FracSavings}_j = \frac{\text{TotalSavings}_j}{C_{\text{total}}}. \tag{8.24}$$

Table 8.6 shows that 'Profile C' has a negative savings balance when contracting BESaS alone or individually coupled with 'Profiles A' or 'Profile B.' This is happening because of the seasonal shape of its load profile. In contrast, BESaS starts to become more attractive to this profile when more clients are involved, and the total load shape reduces the seasonal impact of 'Profile C.'

The profit margin can vary between different BESaS providers. Figure 8.8 illustrates this variation for four scenarios presented in Table 8.6. In these examples, the grid charges savings and the operation costs are constant.

Figure 8.8a confirms that having only client A and client B is not desirable. At the same time, Figure 8.8b shows that adding 'Profile C' makes contracting a BESaS more attractive, but with a small margin for negotiation ($\Delta_{\text{profit}} \leq 22\%$). Indeed, the scenario with all five profiles is the most appealing because the margin profit can variates the most. For instance, for scenario 21, if the maximum profit margin $\Delta_{\text{profit}} = 22\%$ is kept, customer E and customer D can save approximately \$3000 and \$7000, respectively. Maximizing the number of clients also allows individual negotiation with each customer. For instance, Profile E may looses interest in hiring a BESaS when $\Delta_{\text{profit}} \geq 70\%$, but the negotiations with customer B can be extended to $\Delta_{\text{profit}} \leq 90\%$

After confirming that contracting a BESaS becomes more attractive when the number of industrial customers increases, it is necessary to perform the economic analysis from the BESaS perspective. Table 8.8 summarizes the economic aspects of providing a BESaS in the same scenarios as presented in Table 8.6. This table shows the BESS and inverter sizes, the operation cost, and the BESS charge with

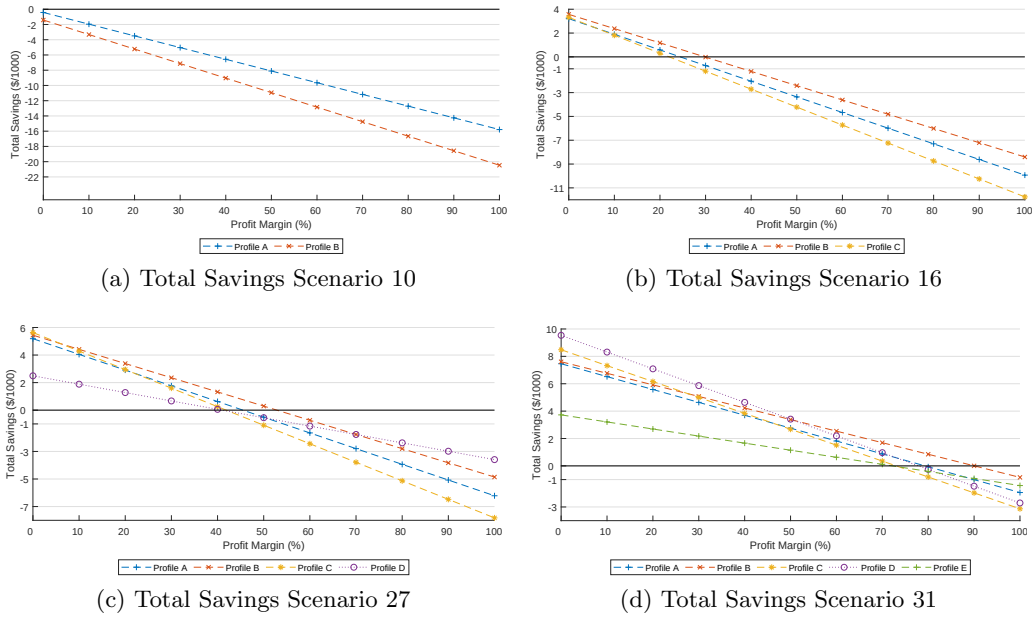

(a) Total Savings Scenario 10

(b) Total Savings Scenario 16

(c) Total Savings Scenario 27

(d) Total Savings Scenario 31

Figure 8.8: Economic analysis of four selected scenarios. The profit margin varies from 0% (reference scenario) to 100% of the BESaS charges. Each panel shows the total savings (equation (8.23)).

$\Delta_{\text{profit}} = 1$. Additionally, there is the total return equal to the Internal Return Rate (IRR) [11] calculated without inflation or price changes based on the total savings for the first year. Likewise, the pay back is a static calculation:

$$\text{PayBack} = \frac{\text{C}_{\text{storage}}}{\sum_j \text{BESaS}_{\text{charges}_j}}. \tag{8.25}$$

As mentioned before, the profit margin can be individually negotiated with each client. The payback can be decreased by doing that. However, this paper neglects this option and considers the same profit margin variation applied to all clients within a scenario. To show the impact of Δ_{profit} in the pay back period, refer

Table 8.8: BESaS economic comparison from the provider point of view

#	Profiles					Battery Size	Inverter size	Operation Cost	BESS charges	Total return (IRR)	Payback (years)
	A	B	C	D	E						
1	x					118	111	1,265	10,300	8%	10
2		x				189	203	2,198	10,683	2%	15
3			x			580	193	3,767	32,103	3%	14
6	x	x				197	203	2,232	15,714	6%	11
7	x		x			580	193	3,767	37,621	5%	12
10		x	x			619	206	4,017	34,418	3%	13
16	x	x	x			619	206	4,017	40,195	5%	12
26	x	x	x	x		625	208	4,061	46,028	7%	10
27	x	x	x		x	620	207	4,027	41,246	5%	11
31	x	x	x	x	x	625	208	4,061	46,879	7%	10

to Figure 8.9. As expected, the payback period decreases when the profit margin increases.

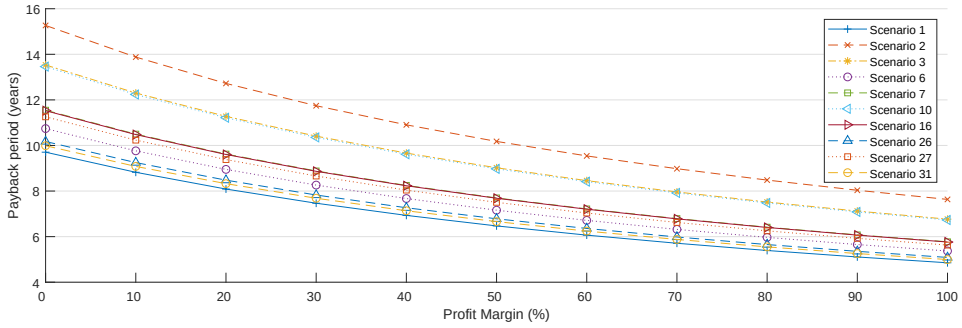

Figure 8.9: Payback margin.

Looking only to Table 8.8 and Figure 8.9 the BESaS provider needs to make the profit margin as high as possible. In contrast, the industrial customers want to keep the profit margin as low as possible to reduce their expenses. As a result, it can be assumed that the negotiations can be concluded once a balance is found. To find this balance, it is necessary to consider the BESaS income after the BESS pay off and before the BESS EoL, *e.g.*:

$$\text{BESaS}_{\text{Profit}} = \text{BESaS}_{\text{charges}} \cdot (Life_{cal}^{80\%} - \text{PayBack}). \tag{8.26}$$

In the same way, the total savings during the BESaS life time are considered from the industrial client perspective:

$$\text{Life}_{\text{Savings}} = \sum_{j} \text{TotalSavings}_{\text{j}} \cdot Life_{cal}^{80\%}. \tag{8.27}$$

After plotting the two lines resulting from equations 8.26 and 8.27, it is possible to find the balance between the profit of BESaS provider and savings of the industrial client. Figure 8.10 shows the break even points for the four sample scenarios.

As previously highlighted, Scenario 10 is not profitable for the industrial clients. For this reason, the lines in Figure 8.10a never cross. However, the other three sample scenarios show balance points at various locations. Scenario 16 with 3 load profiles and scenario 27 with 4 load profiles have the balance point at $\Delta_{\text{profit}} = 7\%$ and $\Delta_{\text{profit}} = 16\%$, respectively. Following this trend, scenario 31 witch considers five industrial profiles strikes the balance for profit margin at $\Delta_{\text{profit}} = 28\%$. Figure 8.10 further supports the hypothesis that the higher the number of customers contracting a BESaS service, the greater the negotiation margin.

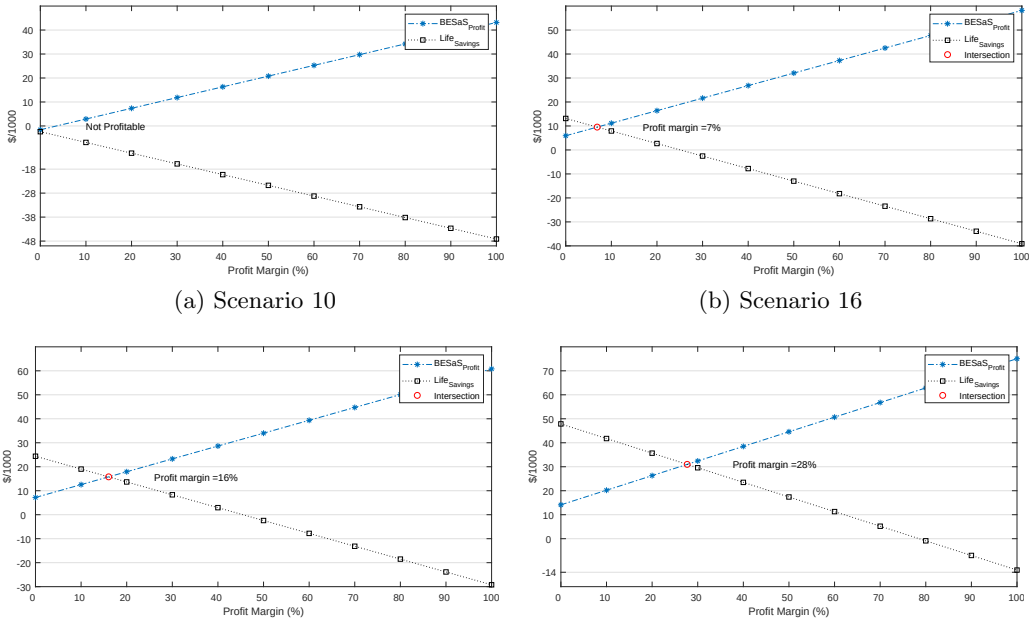

(a) Scenario 10

(b) Scenario 16

(c) Scenario 27

(d) Scenario 31

Figure 8.10: Break even point analysis of four selected scenarios. Each panel shows the BESS profit (equation (8.26)) and the total savings during the BESaS life time (equation (8.27)).

8.5 Final Remarks

This chapter describes a linear model to determine the optimal size of BESS for industrial peak shaving applications. The main contribution is the introduction of the concept of providing Battery Energy Storage as a Service (BESaS), and design of a novel system for sharing a single BESS between multiple industrial customers. The proposed approach significantly decreases the idle time of the BESS and makes a strong business for their peak shaving applications.

The optimization approach formulated in this work also minimizes the storage degradation cost and the maximum power peak for all clients. The model finds not only the best component sizes and pricing from the point of view of industrial customers, but also from the perspective of BESS service provider. The desirability of contracting a BESaS is not only dependent on the characteristics of the load profile(s), but is also directly proportional to the number of clients sharing the BESS service. As a general trend derived from the load profiles under investigation, a seasonal load profile is not suitable for peak shaving because of concentration of a number of peaks in a small time window. However, combining various load profiles

produces a featureless seasonal shape and makes the aggregated load more amenable for peak shaving.

The number of customers also impacts the economic balance. The simulation results have shown that the same optimally-sized BESS system could support different combinations of industrial clients. For instance, in scenario 30, a 625kWh/208kW BESS attending 4 clients can shave 4,086 peaks and provide $20,176 of annual savings. A BESS of the same size is found to be optimal for scenario 31 with 5 clients, shaving a total of 4,996 peaks and providing $29,354 of annual savings. The fact that when a additional customer shares the BESS costs, there is a resulting 45% increase in the total savings. It is an interesting consequence of relying on BESaS. In terms of profit margin for the BESaS provider, the extra customer translates to an increase from 11% in scenario 30 to 28% in scenario 31.

As a general remark, most scenarios favor storage system, even considering the current cost of storage and retail energy tariff used in this study. The expected increases in electricity prices and the reduction of BESS costs are likely to accelerate this trend in the future. Although this work uses parameters corresponding to market conditions in Alberta, Canada, the described methodology can be easily adapted to different retail electricity tariff models and applied to other jurisdictions that use or consider peak power penalty.

Chapter 9

Conclusion and Future Studies

This thesis highlighted the necessity for finding the most cost-effective BESS dimensioning using a variety of residential load demand and local PV generation profiles. At the same time, it shows the importance of considering costs caused by battery degradation in the search for the optimal solution. Additionally, the linear programming based predictive energy management system and the fuzzy logic controlled energy management system were shown to provide superior technical and economic performance compared to other common operational strategies.

The research contributions of this thesis can be summarized as follows:
Optimal component sizing for battery system and power electronics:

- A comparison of the three storage systems reveals that different storage technologies perform best for specific combinations of PV generation and local demand. NMC technology appears most economical for households with very small local demand. PbA chemistry shows some advantages for a mid-scale demand and high PV generation. LFP batteries provide better results than PbA and NMC at higher local electricity demand coincident with higher PV generation.

- In peak shaving applications, the optimal BESS size and number of capped peaks are directly related to the industrial load profile.

- As an overall trend, for the exemplary load profiles under investigation, the monthly billing scheme is more attractive for industrial customers because of the number of peaks that can be capped with acceptable BESS sizes.

- The optimization approach formulated for BESSaS approach minimizes the storage degradation cost and the maximum power peak for all clients. The

model finds not only the best component sizes and pricing from the point of view of industrial customers, but also from the perspective of BESS service provider.

- The desirability of contracting a BESaS is not only dependent on the characteristics of the load profile(s), but is also directly proportional to the number of clients sharing the service.

- The number of customers also impacts the economic balance. The simulation results have shown that the same optimally-sized BESS system could support different number of industrial clients. When additional customers share the BESS costs, the total savings increase.

Energy management system:

- A linear programming-based predictive energy management system (LP-PEMS) controller for residential PV-BESS provides superior technical and economical performance compared to other common operational strategies.

- A fuzzy logic controller implementing PV/BESS energy management based on optimal power flows (determined for a real system using linear programming) was designed by differential evolution. It offers performance comparable to the optimized system.

- The proposed approach is robust as the algorithm was able to find similar FLC configurations in all independent runs.

- At the same time, it is easy to implement for other systems, and can be interpreted to aid understanding of the PV/BESS behavior.

- From energy management perspective, offering BESSaS allows to decrease the idle time of the storage system by sharing the storage among multiple industrial clients.

The impact of battery degradation:

- The linear programming results reveal the potential of reducing the calendric aging by five times when comparing with the naive strategy.

- The research confirms that the depth of discharge cyclic aging dependency is not relevant to peak shaving applications, and can be easily substituted by the full equivalent cycle calculation to obtain an acceptable degradation estimate for BESS.

- The linear model proposed for peak shaving applications gives an approximation of the real degradation, and small variations will be present when compared with a real system.

- The linear aging model can be used in the design of a general framework for sizing of battery energy storage systems in peak shaving applications.

9.1 Future Research Direction

There is opportunity for further research in the topics addressed in this thesis. The studies proposed in this work are limited to specific methodologies or parameterizations to keep the scope of the research manageable, and these limitations provide avenues for further research.

The Economic study on residential BESS optimization uses parameters corresponding to German market conditions and regulations, the described methodology can be easily adapted to other countries that use feed-in and retail electricity tariff models, *e.g.* Australia, Canada, France, Greece, and many others. German regulations for the PV-to-grid feed-in limit and the complex scheme for storage systems subsidies results in various constraints and challenging model scenarios. The adaptation to other regions is the subject of present work. This study is limited to the optimization of storage systems using historical data on specific load demand and PV generation profiles. A well parameterized energy management controller for a BESS will also need accurate forecasting of load demand and PV generation [112] to achieve the best operation. Although such forecasting tasks are outside the scope of this work, they will be considered and used for energy management strategies in future.

The LP-Based management system considers historical data as the sort-term energy production and consumption forecasts. Future work will concentrate on the determination of the optimal prediction horizon and on the combination of energy management with other system components including controllable loads and different types of energy storage devices.

Similarly, the evolutionary fuzzy controller uses the optimal power flow for a specific household to find the best parameters for the rule-based system, and with additional research, it is likely our model could be refined or improved. The controller can be improved using a more refined rule base and additional input and/or control variables. In addition to that, data from multiple houses could be consider to make the initial fuzzy system more generic, and allow a faster convergence to a stable solution.

When constructing the optimization model to size the most cost-effective BESS it is necessary to know in advance the industrial customer load profile signal shape, as well as average peaks to define potential shaving opportunities. To consider the load profiles as uncertainty leads to new research opportunities. Future research could employ machine learning strategies to adapt the storage system size according to a short time forecast. Additionally, the BESS could be used in other application so as to balance the reactive power in the grid, or supply energy to residential customers.

References

[1] I. Alsaidan, W. Gao, and A. Khodaei, "Battery energy storage sizing for commercial customers," in *2017 IEEE Power Energy Society General Meeting*, 2017, pp. 1–5. DOI: 10.1109/PESGM.2017.8274380. 95

[2] S. Amin and B. Wollenberg, "Toward a smart grid: Power delivery for the 21st century," *Power and Energy Magazine, IEEE*, vol. 3, no. 5, pp. 34–41, 2005, ISSN: 1540-7977. DOI: 10.1109/MPAE.2005.1507024. 38, 50

[3] K. Bank., "Förderprogram erneuerbare energien-speicher.," Available online: (accessed on 14 July 2016)., 2016, [Online]. Available: https://www.kfw.de/Download-Center/F\%C3\%B6rderprogramme-(Inlandsf\%C3\%B6rderung)/PDF-Dokumente/6000002700_M_275_Speicher.pdf. 24

[4] C. Barchasz, F. Molton, C. Duboc, J.-C. Leprêtre, S. Patoux, and F. Alloin, "Lithium/sulfur cell discharge mechanism: An original approach for intermediate species identification," *Analytical Chemistry*, vol. 84, no. 9, pp. 3973–3980, 2012, PMID: 22482872. DOI: 10.1021/ac2032244. eprint: https://doi.org/10.1021/ac2032244. [Online]. Available: https://doi.org/10.1021/ac2032244. 100

[5] B. Battke, T. S. Schmidt, D. Grosspietsch, and V. H. A. r. a. Hoffmann, "And probabilistic model of lifecycle costs of stationary batteries in multiple applications," *Renew. Sustain. Energy Rev*, pp. 240–250, 2013. DOI: http://dx.doi.org/10.1016/j.rser.2013.04.023. 27

[6] B. der Energie-und Wasserwirtschaft e.V. Bdew Strompreisanalyse Mai, *Available online:*, 2016, (accessed on 4 May 2017). [Online]. Available: https://www.bdew.de/internet.nsf/res/886756C1635C3399C1257FC500326489/$file/160524_BDEW. 24

[7] T. Beck, H. Kondziella, G. Huard, and T. Bruckner, "Assessing the influence of the temporal resolution of electrical load and pv generation profiles on self-consumption and sizing of pv-battery systems," *Appl. Energy*, pp. 331–342, 2016. DOI: http://dx.doi.org/10.1016/j.apenergy.2016.04.050. 26

[8] ——, "Assessing the influence of the temporal resolution of electrical load and {pv} generation profiles on self-consumption and sizing of pv-battery systems," *Applied Energy*, vol. 173, pp. 331 –342, 2016. 40, 51, 84, 104

[9] M. Benz, "Online-rechner f"ur senec.ies stormspeicher," *Available online: (accessed online)*, vol. 4, 2017. 11, 18

[10] J. Bergner, J. Weniger, T. Tjaden, and V. Quaschning, "Feed-in power limitation of gridconnected pv battery systems with autonomous forecast-based operation strategies," *29th European Photovoltaic Solar Energy Conference and Exhibition*, 2014. DOI: 10.4229/EUPVSEC20142014-5CO.15.1. 41

[11] R. A. Brealey and S. C. Myers, "Principles of corporate finance (mcgraw-hill higher education, new york, ny)," 2003. 86, 111

[12] Bundesnetzagentur, "Dateneldungen und eeg-verg"utungss"atze f"ur photovoltaikanlagen.," 2017, Available online. (accessed on 4 May 2017). [Online]. Available: https://www.bundesnetzagentur.de/DE/Sachgebiete/ElektrizitaetundGas/Unternehmen_. 24

[13] C. Campestrini, S. F. Schuster, R. C. Karl, C. Ni, and A. Jossen, "Equivalent circuit based modelling and prediction of the ageing behaviour of lithium-ion cells," *European Battery, Hybrid and Fuel Cell Electric Vehicle Congress Brussels, Belgium*, 2015. 14, 66

[14] G. Carpinelli, S. Khormali, F. Mottola, and D. Proto, "Optimal operation of electrical energy storage systems for industrial applications," in *2013 IEEE Power Energy Society General Meeting*, 2013, pp. 1–5. DOI: 10.1109/PESMG.2013.6672905. 95

[15] G. Carpinelli, F. Mottola, and L. Perrotta, "Energy management of storage systems for industrial applications under real time pricing," in *2013 International Conference on Renewable Energy Research and Applications (ICRERA)*, 2013, pp. 884–889. DOI: 10.1109/ICRERA.2013.6749876. 95

[16] J. Carroquino, J.-L. Bernal-Agustín, and R. Dufo-López, "Standalone renewable energy and hydrogen in an agricultural context: A demonstrative case," *Sustainability*, vol. 11, no. 4, p. 951, 2019. 2

[17] M. Castillo-Cagigal, E. Caamaño-Martín, E. Matallanas, D. Masa-Bote, A. Gutiérrez, F. Monasterio-Huelin, and J. Jiménez-Leube, "PV self-consumption optimization with storage and active DSM for the residential sector," *Solar Energy*, vol. 85, no. 9, pp. 2338 –2348, 2011, ISSN: 0038-092X. DOI: http://dx.doi.org/10.1016/j.solener.2011.06.028. 14

[18] H. Chen, T. N. Cong, W. Yang, C. Tan, Y. Li, and Y. Ding, "Progress in electrical energy storage system: A critical review," *Progress in Natural Science*, vol. 19, no. 3, pp. 291 –312, 2009, ISSN: 1002-0071. DOI: http://dx.doi.org/10.1016/j.pnsc.2008.07.014. [Online]. Available: http://www.sciencedirect.com/science/article/pii/S100200710800381X. 76, 94

[19] N. Consulting, *Energy storage trends and opportunities in emerging markets*, English, Journal, 2017. 77, 79

[20] S. E. D. Corporation, *Sony Energy Devices Quality, Operations and Management*. Available online. [Online]. Available: http://www.sonyenergy-devices.co.jp/en/csr/quality.php(accessedon4May2017). 132

[21] M. Dabbagh, A. Rayes, B. Hamdaoui, and M. Guizani, "Peak shaving through optimal energy storage control for data centers," in *2016 IEEE International Conference on Communications (ICC)*, 2016, pp. 1–6. DOI: 10.1109/ICC.2016.7511242. 95

[22] R. Dufo-Lopez, J. L. Bernal-Agustin, and J. Contreras, "Optimization of control strategies for stand-alone renewable energy systems with hydrogen storage," *Renewable Energy*, vol. 32, no. 7, pp. 1102 –1126, 2007, ISSN: 0960-1481. DOI: http://dx.doi.org/10.1016/j.renene.2006.04.013. 38, 51

[23] A. P. Engelbrecht, *Computational Intelligence: An Introduction*, 2nd. Wiley Publishing, 2007, ISBN: 0470035617. 15

[24] X. Fang, S. Misra, G. Xue, and D. Yang, "Smart grid—the new and improved power grid: A survey," *IEEE communications surveys & tutorials*, vol. 14, no. 4, pp. 944–980, 2012. 1

[25] H. Farhangi, "The path of the smart grid," *IEEE power and energy magazine*, vol. 8, no. 1, 2010. 1

[26] A. Faruqui, *The global movement toward cost-reflective tariffs*, English, Journal, 2015. 78, 96

[27] G. Fitzgerald, J. Mandel, J. Morris, and H. Touati, *The economics of battery energy storage*. 2015. 11, 18, 19

[28] G. Fuchs, B. Lunz, M. Leuthold, and D. U. Sauer, "Technology overview on electricity storage, overview on the potential and on the deployment perspectives of electricity storage technologies.," *Available online: (accessed online)*, vol. 16, 2016. [Online]. Available: http://www.sefep.eu/activities/projects-studies/120628_Technology_Overview_Electricity_Storage. 22

[29] G. Fuchs, B. Lunz, M. Leuthold, and D. U. Sauer, *Technology overview on electricity storage*, English, Journal, Berlin, 2012. 68

[30] M. M. Fuhs, "Home-speicher," *PV-Magazine*, vol. 2016, pp. 35–39, 11, 19, 23, 24

[31] N. Garimella and N.-K. C. Nair, "Assessment of battery energy storage systems for small-scale renewable energy integration," pp. 1–6, 2009. 11, 18

[32] F. Geth, J. Tant, E. Haesen, J. Driesen, and R. Belmans, "Integration of energy storage in distribution grids," *In Proceedings of theIEEE Power and Energy Society General Meeting, Providence, RI, USA*, vol. 29, no. 2010, pp. 1–6, 2010. 10, 11

[33] F. Geth, J. Tant, E. Haesen, J. Driesen, and R. Belmans, "Integration of energy storage in distribution grids," in *Power and Energy Society General Meeting, 2010 IEEE*, IEEE, vol. 2010, 2010, pp. 1–6. 12

[34] S. O. Geurin, A. K. Barnes, and J. C. Balda, "Smart grid applications of selected energy storage technologies," in *Innovative Smart Grid Technologies (ISGT), 2012 IEEE PES*, IEEE, 2012, pp. 1–8. 64, 76, 95

[35] V. storage GmbH. Varta-Storage Berechnungstool. Available online, 2017. [Online]. Available: https://www.varta-storage.com/de/produkte/heimspeichersysteme/berechnungstool.html(accessedon4May2017). 11, 18

[36] C. Goebel, H. Hesse, M. Schimpe, A. Jossen, and H.-a. Jacobsen, "Model-based dispatch strategies for lithium-ion battery energy storage applied to pay-as-bid markets for secondary reserve," *IEEE Trans. Power Syst*, 2016. DOI: http://dx.doi.org/10.1109/TPWRS.2016.2626392. 23, 132

[37] C. Goebel, H. Hesse, M. Schimpe, A. Jossen, and H. A. Jacobsen, "Model-based dispatch strategies for lithium-ion battery energy storage applied to pay-as-bid markets for secondary reserve," *IEEE Transactions on Power Systems*, vol. 32, no. 4, pp. 2724–2734, 2017, ISSN: 0885-8950. DOI: 10.1109/TPWRS.2016.2626392. 13

[38] M. A. Guerrero, E. Romero, F. Barrero, M. I. Milanes, and E. Gonzalez, "Overview of medium scale energy storage systems," in *2009 Compatibility and Power Electronics*, 2009, pp. 93–100. DOI: 10.1109/CPE.2009.5156019. 76

[39] R. Hassan and G. Radman, "Survey on smart grid," in *IEEE SoutheastCon 2010 (SoutheastCon), Proc. of the*, 2010, pp. 210–213. DOI: 10.1109/SECON.2010.5453886. 38, 50

[40] R. Hassan and G. Radman, "Survey on smart grid," in *IEEE SoutheastCon 2010 (SoutheastCon), Proceedings of the*, IEEE, 2010, pp. 210–213. 1

[41] H. C. Hesse, M. Schimpe, D. Kucevic, and A Jossen, "Lithium-ion battery storage for the grid – A review of stationary battery storage system design tailored for applications in modern power grids," *Energies*, vol. 12, no. 10, 2017. DOI: 10.3390/en10122107. 13

[42] H. C. Hesse, R. Martins, P. Musilek, M. Naumann, C. N. Truong, and A. Jossen, "Economic optimization of component sizing for residential battery storage systems," *Energies*, vol. 10, no. 7, 2017, ISSN: 1996-1073. DOI: 10.3390/en10070835. [Online]. Available: http://www.mdpi.com/1996-1073/10/7/835. iv, 42, 64, 95

[43] H. C. Hesse, M. Schimpe, D. Kucevic, and A. Jossen, "Lithium-ion battery storage for the grid—a review of stationary battery storage system design tailored for applications in modern power grids," *Energies*, vol. 10, no. 12, 2017, ISSN: 1996-1073. DOI: 10.3390/en10122107. [Online]. Available: http://www.mdpi.com/1996-1073/10/12/2107. 76

[44] M. Hesse H.; Müller, "Price and market trends for battery stationary storage systems," Unpublished work., 2017. 23

[45] R. Hidalgo, D. Siguenza, C. Sanchez, J. Leon, P. Jácome-Ruiz, J. Wu, and D. Ortiz Villalba, "A survey of battery energy storage system (bess), applications and environmental impacts in power systems," pp. 1–6, Oct. 2017. 2

[46] J. Hoppmann, J. Volland, T. S. Schmidt, and V. H. Hoffmann, "The economic viability of battery storage for residential solar photovoltaic systems–a review and a simulation model," *Renew. Sustain. Energy Rev*, vol. 2014, pp. 1101–1118, DOI: http://dx.doi.org/10.1016/j.rser.2014.07.068. 10, 11

[47] J. Hoppmann, J. Volland, T. S. Schmidt, and V. H. Hoffmann, "The economic viability of battery storage for residential solar photovoltaic systems–a review and a simulation model," *Renewable and Sustainable Energy Reviews*, vol. 39, pp. 1101–1118, 2014. 12

[48] A. International, *Energy storage world markets report*, English, Journal, 2017. 78

[49] F. ISI, *European electricity prices and their components*, English, Journal, 2013. 70, 85

[50] A. Jossen and W. Weydanz, "Moderne akkumulatoren richtig einsetzen," *Reichardt: Untermeitingen*, vol. 1, 2006. 132

[51] K.-P. Kairies, D. Haberschusz, J. van Ouwerkerk, J. Strebel, O. Wessels, D. Magnor, J. Badeda, and D. U. Sauer, *Wissenschaftliches Mess-und Evaluierungsprogramm Solarstromspeicher-Jahresbericht 2016*. 2016. 11, 18, 19, 34

[52] K. Kairies, D Haberschusz, J van Ouwerkerk, J Strebel, O Wessels, D Magnor, J Badeda, and D. Sauer, "Wissenschaftliches mess-und evaluierungsprogramm solarstromspeicher-jahresbericht 2016," *Institut für Stromrichtertechnik und Elektronische Antriebe (ISEA), RWTH Aachen, Aachen, Jahresbericht*, 2016. 11, 76, 95

[53] F. Karray and C. De Silva, *Soft Computing and Intelligent Systems Design: Theory, Tools, and Applications*. Pearson/Addison Wesley, 2004, ISBN: 9780321116178. [Online]. Available: https://books.google.ca/books?id=mqYw-Xig0IsC. 15

[54] K. R. Khalilpour and A. Vassallo, *Community energy networks with storage: modeling frameworks for distributed generation*. Springer, 2016. 2

[55] V. S. Kolosnitsyn and E. V. Karaseva, "Lithium-sulfur batteries: Problems and solutions," *Russian Journal of Electrochemistry*, vol. 44, no. 5, pp. 506–509, 2008, ISSN: 1608-3342. DOI: 10.1134/S1023193508050029. [Online]. Available: https://doi.org/10.1134/S1023193508050029. 100

[56] D. Lauinger, P. Caliandro, J. van Herle, and D. A Kuhn, "Linear programming approach to the optimization of residential energy systems," *J. Energy Storage*, pp. 24–37, 2016. DOI: http://dx.doi.org/10.1016/j.est.2016.04.009. 11, 19

[57] M. Lödl, R. Witzmann, and M. Metzger, "Operation strategies of energy storages with forecast methods in low-voltage grids with a high degree of decentralized generation," in *2011 IEEE Electrical Power and Energy Conference*, 2011, pp. 52–56. DOI: 10.1109/EPEC.2011.6070252. 38

[58] T. Y. Lee, "Operating schedule of battery energy storage system in a time-of-use rate industrial user with wind turbine generators: A multipass iteration particle swarm optimization approach," *IEEE Transactions on Energy Conversion*, vol. 22, no. 3, pp. 774–782, 2007, ISSN: 0885-8969. DOI: 10.1109/TEC.2006.878239. 95

[59] X. Luo, J. Wang, M. Dooner, and J. Clarke, "Overview of current development in electrical energy storage technologies and the application potential in power system operation," *Applied energy*, vol. 137, pp. 511–536, 2015. 2

[60] ——, "Overview of current development in electrical energy storage technologies and the application potential in power system operation," *Applied energy*, vol. 137, pp. 511–536, 2015. 11, 18, 132

[61] ——, "Overview of current development in electrical energy storage technologies and the application potential in power system operation," *Applied energy*, vol. 137, pp. 511–536, 2015. 14, 76, 77, 95, 96

[62] B. Lv and W. Yan, "Coordinated planning model of bess and controllable switches in distribution," *Electronics Letters*, vol. 50, no. 20, pp. 1479–1480, 2014, ISSN: 0013-5194. DOI: 10.1049/el.2014.1361. 2

[63] L. Magdalena, "Fuzzy Rule-Based Systems," in *Springer Handbook of Computational Intelligence*, J. Kacprzyk and W. Pedrycz, Eds., Berlin Heidelberg: Springer, 2015, ch. 13, pp. 203–218. 16

[64] D. Magnor and D. U. Sauer, "Optimization of pv battery systems using genetic algorithms," *Energy Procedia*, vol. 2016, pp. 332–340, DOI: http://dx.doi.org/10.1016/j.egypro.2016.10.123. 11, 12

[65] D. Magnor and D. U. Sauer, "Optimization of pv battery systems using genetic algorithms," *Energy Procedia*, vol. 99, pp. 332–340, 2016. 12

[66] ——, "Optimization of pv battery systems using genetic algorithms," *Energy Procedia*, vol. 99, pp. 332 –340, 2016, 10th International Renewable Energy Storage Conference, IRES 2016, 15-17 March 2016, Düsseldorf, Germany, ISSN: 1876-6102. DOI: http://dx.doi.org/10.1016/j.egypro.2016.10.123. [Online]. Available: http://www.sciencedirect.com/science/article/pii/S1876610216310840. 65, 95

[67] D. Manz, J. Keller, and N. Miller, "Value propositions for utility-scale energy storage," in *2011 IEEE/PES Power Systems Conference and Exposition*, 2011, pp. 1–10. DOI: 10.1109/PSCE.2011.5772524. 76

[68] R. Martins, P. Kreimer, and P. Musilek, "Lp-based predictive energy management system for residential pv/bess," in *2017 IEEE International Conference on Systems, Man, and Cybernetics (SMC)*, 2017, pp. 3727–3732. DOI: 10.1109/SMC.2017.8123213. iv

[69] R. Martins, P. Musilek, and H. C. Hesse, "Optimization of photovoltaic power self-consumption using linear programming," in *EEEIC 2016 - International Conference on Environment and Electrical Engineering*, 2016. 15, 39, 48, 51

[70] R. Martins, P. Musilek, H. C. Hesse, J. Jungbauer, T. Vorbuchner, and A. Jossen, "Linear battery aging model for industrial peak shaving applications," in *2018 IEEE International Conference on Environment and Electrical Engineering and 2018 IEEE Industrial and Commercial Power Systems Europe (EEEIC / I CPS Europe)*, 2018, pp. 1–6. DOI: 10.1109/EEEIC.2018.8494584. v

[71] R. Martins, H. C. Hesse, J. Jungbauer, T. Vorbuchner, and P. Musilek, "Optimal component sizing for peak shaving in battery energy storage system for industrial applications," *Energies*, vol. 11, no. 8, 2018, ISSN: 1996-1073. DOI: 10.3390/en11082048. [Online]. Available: http://www.mdpi.com/1996-1073/11/8/2048. v, 95, 100

[72] T. M. Masaud, K. Lee, and P. K. Sen, "An overview of energy storage technologies in electric power systems: What is the future?" In *North American Power Symposium 2010*, 2010, pp. 1–6. DOI: 10.1109/NAPS.2010.5619595. 76

[73] Maximilian Zängl, *Netzentgelte für entnahmestellen mit leistungsmessung - jahresleistungspreis - (preisblatt lg jlp)*, Bayernwerk Netz GmbH, Ed., Regensburg, Germany, 2017. [Online]. Available: https://www.bayernwerk-netz.de/cps/rde/xbcr/bayernwerk-netz/20161216_Preisblatt_Strom_LG-JLP.pdf. 79

[74] N. K. Meena, A. Swarnkar, N. Gupta, and K. R. Niazi, "Optimal accommodation and management of high renewable penetration in distribution systems," *The Journal of Engineering*, vol. 2017, no. 13, pp. 1890–1895, 2017, ISSN: 2051-3305. DOI: 10.1049/joe.2017.0659. 2

[75] *Mercedes-Benz*. Mercedes-Benz Energy Storage. Available online. [Online]. Available: https://www.mercedes-benz.com/en/mercedes-benz-energy/products/(accessedon4May2017). 19

[76] G. Merei, C. Berger, and D. U. Sauer, "Optimization of an off-grid hybrid pv-wind-diesel system with different battery technologies using genetic algorithm," *Sol. Energy*, pp. 460–473, 2013. DOI: http://dx.doi.org/10.1016/j.solener.2013.08.016. 11, 12

[77] G. Merei, J. Mosh"ovel, D. Magnor, and D. U. Sauer, "Optimization of self-consumption and techno-economic analysis of pv-battery systems in commercial applications," *Appl. Energy*, pp. 171–178, 2016. DOI: http://dx.doi.org/10.1016/j.apenergy.2016.01.083. 11

[78] G. Merei, C. Berger, and D. U. Sauer, "Optimization of an off-grid hybrid pv–wind–diesel system with different battery technologies using genetic algorithm," *Solar Energy*, vol. 97, pp. 460–473, 2013. 12

[79] ——, "Optimization of an off-grid hybrid pv–wind–diesel system with different battery technologies using genetic algorithm," *Solar Energy*, vol. 97, pp. 460 –473, 2013, ISSN: 0038-092X. DOI: http://dx.doi.org/10.1016/j.solener.2013.08.016. [Online]. Available: http://www.sciencedirect.com/science/article/pii/S0038092X13003265. 65, 95

[80] G. Merei, J. Moshövel, D. Magnor, and D. U. Sauer, "Optimization of self-consumption and techno-economic analysis of pv-battery systems in commercial applications," *Applied Energy*, vol. 168, pp. 171 –178, 2016, ISSN: 0306-2619. DOI: http://dx.doi.org/10.1016/j.apenergy.2016.01.083. [Online]. Available: http://www.sciencedirect.com/science/article/pii/S0306261916300708. 65, 95

[81] T. Motors, *The Tesla Home Battery*. Available online. [Online]. Available: https://www.tesla.com/powerwall(accessedon4May2017). 19

[82] V. Muenzel, I. Mareels, J. D. Hoog, A. Vishwanath, S. Kalyanaraman, and A. P. g. a. Gort, "And demand mismatch: Evaluating the potential of residential storage," in *Proceedings of the 2015 IEEE Power & Energy Society Innovative Smart Grid Technologies Conference (ISGT)*, DC, USA: Washington, 2015, pp. 18–20. 11, 19

[83] T. Munakata, *Fundamentals of the New Artificial Intelligence: Neural, Evolutionary, Fuzzy and More (Texts in Computer Science)*, 2nd ed. Springer Publishing Company, Incorporated, 2008, ISBN: 184628838X. 15

[84] M. Muselli, G. Notton, and A. Louche, "Design of hybrid-photovoltaic power generator, with optimization of energy management," *Solar Energy*, vol. 65, no. 3, pp. 143 –157, 1999, ISSN: 0038-092X. DOI: http://dx.doi.org/10.1016/S0038-092X(98)00139-X. 38, 50

[85] P. Musilek, P. Krömer, and R. H. C. H. Martins, "Optimal energy management of residential pv/hess using evolutionary fuzzt control," in *2017 IEEE Congress on Evolutionary Computation, CEC 2017*, 2017. iv, 15, 40

[86] M. Naumann and P. T. Keil, *institute for electrical storage technology internal calendric aging studies*. Unpublished work. 132

[87] M. Naumann, R. C. Karl, C. N. Truong, A. Jossen, and H. C. Hesse, "Lithium-ion battery cost analysis in pv-household application," *Energy Procedia*, vol. 73, pp. 37–47, 2015. 11, 18, 33, 36

[88] M. Naumann, R. C. Karl, C. N. Truong, A. Jossen, and H. C. Hesse, "Lithium-ion battery cost analysis in pv-household application," *Energy Procedia*, vol. 73, pp. 37 –47, 2015, ISSN: 1876-6102. DOI: http://dx.doi.org/10.1016/j.egypro.2015.07.555. 76, 95

[89] M. Negnevitsky, *Artificial Intelligence: A Guide to Intelligent Systems*, 1st. Boston, MA, USA: Addison-Wesley Longman Publishing Co., Inc., 2001, ISBN: 0201711591. 16

[90] S. P. Networks, *Annual report / sa power networks*, English, Journal, 2013. 78

[91] J. Neubauer and M. Simpson, "Deployment of behind-the-meter energy storage for demand charge reduction," DOI: 10.2172/1168774. 94

[92] T. A. Nguyen, M. L. Crow, and A. C. Elmore, "Optimal sizing of a vanadium redox battery system for microgrid systems," *IEEE Transactions on Sustainable Energy*, vol. 6, no. 3, pp. 729–737, 2015, ISSN: 1949-3029. DOI: 10.1109/TSTE.2015.2404780. 95

[93] *Nissan. xStorage by Nissan-Clean Power Energy. 2017*. Available online. [Online]. Available: https://www.nissan.co.uk/experience-nissan/electric-vehicle-leadership/xstorage-by-nissan.html(accessedon4May2017). 19

[94] J. Nocedal and S. Wright, *Numerical Optimization*, S. S. B. Media, Ed. New York, NY, USA, 2006. 30

[95] V. Novák, J. Mockor, and I. Perfilieva, *Mathematical principles of fuzzy logic*, ser. Kluwer international series in engineering and computing science. Boston, MA: Kluwer, 1999. [Online]. Available: https://cds.cern.ch/record/425778. 16

[96] S. Nykamp, A. Molderink, J. L. Hurink, and G. J. M. Smit, "Storage operation for peak shaving of distributed pv and wind generation," in *2013 IEEE PES Innovative Smart Grid Technologies Conference (ISGT)*, 2013, pp. 1–6. DOI: 10.1109/ISGT.2013.6497786. 76, 95

[97] B. Nykvist and M. Nilsson, "Rapidly falling costs of battery packs for electric vehicles," *nature climate change*, vol. 5, no. 4, p. 329, 2015. 11, 18

[98] B. Nykvist and M. Nilsson, "Rapidly falling costs of battery packs for electric vehicles," *Nature Clim. Change*, vol. 5, no. 4, pp. 329–332, 2015, Letter, ISSN: 1758-678X. [Online]. Available: http://dx.doi.org/10.1038/nclimate2564. 76, 80, 95

[99] E. Oh, S.-Y. Son, H. Hwang, J.-B. Park, and K. Y. Lee, "Impact of demand and price uncertainties on customer-side energy storage system operation with peak load limitation," *Electric Power Components and Systems*, vol. 43, no. 16, pp. 1872–1881, 2015. DOI: 10.1080/15325008.2015.1057883. eprint: https://doi.org/10.1080/15325008.2015.1057883. [Online]. Available: https://doi.org/10.1080/15325008.2015.1057883. 95

[100] N. Omar, M. A. Monem, Y. Firouz, J. Salminen, J. Smekens, O. Hegazy, and J. Van Mierlo, "Lithium iron phosphate based battery—assessment of the aging parameters and development of cycle life model," *Appl. Energy*, pp. 1575–1585, 2014. DOI: http://dx.doi.org/10.1016/j.apenergy.2013.09.003. 132

[101] W. Pedrycz, *Fuzzy Control and Fuzzy Systems*, 2nd. New York, NY, USA: John Wiley & Sons, Inc., 1993, ISBN: 0471934755. 16

[102] *Photovoltaik4all*. Available online. [Online]. Available: http://www.photovoltaik4all.de/en/wechselrichter(accessedon7September2016). 24

[103] A. Piepenbrinck, "E3/dc system calculator.," Available online: http://s10.e3dc.com/E3dcWeb/SystemCalculator/syscalc.php (accessed on 4 May 2017)., [Online]. Available: http://s10.e3dc.com/E3dcWeb/SystemCalculator/syscalc.php(accessedon4May2017). 11, 18

[104] G. I. Power, *Handbuch f"ur Verschlossene Gel-Blei-Batterien*. ; Exide Technologies GmbH.: B"udingen, Germany, 2013. 132

[105] K. V. Price, R. M. Storn, and J. A. Lampinen, *Differential Evolution A Practical Approach to Global Optimization*, ser. Natural Computing Series. Berlin, Germany: Springer-Verlag, 2005. 16

[106] V. Quaschning, *Unabhängigkeitsrechner*. Accessed on 9 February 2017. [Online]. Available: pvspeicher.htw-berlin.de/unabhaengigkeitsrechner/. 11, 18

[107] ——, *Representative Electrical Load Profiles of Residential Buildings in Germany with a Temporal Resolution of One Second*, H. B.-U. of Applied Sciences, Ed. Berlin, Germany, 2015. 29, 30

[108] C. Rahmann, B. Mac-Clure, V. Vittal, and F. Valencia, "Break-even points of battery energy storage systems for peak shaving applications," *Energies*, vol. 10, no. 7, 2017, ISSN: 1996-1073. DOI: 10.3390/en10070833. [Online]. Available: http://www.mdpi.com/1996-1073/10/7/833. 2, 12, 64, 75

[109] T. Reddy, *Linden's Handbook of Batteries*. 4th ed.; McGraw-Hill: New York, NY, USA, 2011. 132

[110] M. J. Reno, K. Coogan, S. Grijalva, R. J. Broderick, and J. E. Quiroz, "Pv interconnection risk analysis through distribution system impact signatures and feeder zones," in *PES General Meeting— Conference & Exposition, 2014 IEEE*, IEEE, 2014, pp. 1–5. 1

[111] M. Resch, B. Ramadhani, J. Buhler, and A. Sumper, "Comparison of control strategies of residential pv storage systems," *9th International Renewable Energy Storage Conference and Exhibition (IRES 2015)*, 2015. DOI: 10.13140/RG.2.1.3668.2084. 41, 44

[112] J. Rodway, P. Musilek, E. Lozowski, M. Prauzek, and J. Heckenbergerova, "Pressure-based prediction of harvestable energy for powering environmental monitoring systems," in *Proceedings of the 2015 IEEE 15th International Conference on Environment and Electrical Engineering (EEEIC)*, I. Rome, Ed., 2015, pp. 10–13. 117

[113] J. Rodway, P. Musilek, E. Lozowski, M. Prauzek, and J. Heckenbergerova, "Pressure-based prediction of harvestable energy for powering environmental monitoring systems," in *Environment and Electrical Engineering (EEEIC), 2015 IEEE 15th International Conference on*, IEEE, 2015, pp. 725–730. 80, 100

[114] S. Rohjans, M. Uslar, R. Bleiker, J. González, M. Specht, T. Suding, and T. Weidelt, "Survey of smart grid standardization studies and recommendations," in *Smart grid communications (SmartGridComm), 2010 first IEEE international conference on*, IEEE, 2010, pp. 583–588. 1

[115] M. Ross, R. Hidalgo, C. Abbey, and G. Joós, "Analysis of energy storage sizing and technologies," in *2010 IEEE Electrical Power Energy Conference*, 2010, pp. 1–6. DOI: 10.1109/EPEC.2010.5697212. 95

[116] M. Rylander, J. Smith, and W. Sunderman, "Streamlined method for determining distribution system hosting capacity," *IEEE Transactions on Industry Applications*, vol. 52, no. 1, pp. 105–111, 2016. 1

[117] J. Schiffer, D. Sauer, H. Bindner, T. Cronin, P. Lundsager, and R. Kaiser, "Model prediction for ranking lead-acid batteries according to expected lifetime in renewable energy systems and autonomous power-supply systems," *J. Power Sources*, pp. 66–78, 2007. DOI: http://dx.doi.org/10.1016/j.jpowsour.2006.11.092. 22

[118] J. Schiffer, D. U. Sauer, H. Bindner, T. Cronin, P. Lundsager, and R. Kaiser, "Model prediction for ranking lead-acid batteries according to expected lifetime in renewable energy systems and autonomous power-supply systems," *Journal of Power Sources*, vol. 168, no. 1, pp. 66 –78, 2007, 10th EUROPEAN LEAD BATTERY CONFERENCE, ISSN: 0378-7753. DOI: http://dx.doi.org/10.1016/j.jpowsour.2006.11.092. [Online]. Available: http://www.sciencedirect.com/science/article/pii/S0378775306025122. 100, 102

[119] J. Schmalstieg, S. K"abitz, M. Ecker, and D. U. A Sauer, "Holistic aging model for li(nimnco)o_2 based 18650 lithium-ion batteries," *J. Power Sources*, pp. 325–334, 2014. DOI: http://dx.doi.org/10.1016/j.jpowsour.2014.02.012. 23

[120] J. Schmalstieg, S. Käbitz, M. Ecker, and D. U. Sauer, "A holistic aging model for li(nimnco)o2 based 18650 lithium-ion batteries," *Journal of Power Sources*, vol. 257, pp. 325 –334, 2014, ISSN: 0378-7753. DOI: http://dx.doi.org/10.1016/j.jpowsour.2014.02.012. [Online]. Available: http://www.sciencedirect.com/science/article/pii/S0378775314001876. 13, 100, 102, 103

[121] O. Schmidt, A. Hawkes, A. Gambhir, and I. Staffell, "The future cost of electrical energy storage based on experience rates," vol. 6, 17110 EP –, 2017, Analysis. [Online]. Available: http://dx.doi.org/10.1038/nenergy.2017.110. 80

[122] S. Schuster, T. Bach, E. Fleder, J. M"uller, M. Brand, G. Sextl, and A. Jossen, "Nonlinear aging characteristics of lithium-ion cells under different operational conditions," *J. Energy Storage*, pp. 44–53, 2015. DOI: http://dx.doi.org/10.1016/j.est.2015.05.003. 132

[123] T. Senjyu, D. Hayashi, N. Urasaki, and T. Funabashi, "Optimum configuration for renewable generating systems in residence using genetic algorithm," *Energy Conversion, IEEE Transactions on*, vol. 21, no. 2, pp. 459–466, 2006, ISSN: 0885-8969. DOI: 10.1109/TEC.2006.874250. 15

[124] E. Society, *Potentiale Elektrochemischer Speicher in Elektrischen Netzen in Konkurrenz zu Anderen Technologien und Systeml"osungen (ESPEN)*. Goslar, Germany, 2016. 132

[125] A. Stephan, B. Battke, M. D. Beuse, J. H. Clausdeinken, and T. S. Schmidt, "Limiting the public cost of stationary battery deployment by combining applications," vol. 1, 16079 EP –, 2016, Article. [Online]. Available: http://dx.doi.org/10.1038/nenergy.2016.79. 76, 95

[126] M. Sterner and I. Stadler, *Energiespeicher. Bedarf, Technologien, Integration.* 1st ed.; Springer: Berlin/Heidelberg, Germany, 2014. 132

[127] J. Struth, K. P. Kairies, M. Leuthold, A. Aretz, M. Bost, S. G. M. Cramer, E. Szczechowicz, B. Hirsch, and A. S. D. U. Sauer, "Pv-benefit: A critical review of the effect of grid integrated pv-storage-systems," *8th International Renewable Energy Storage Conference and Exhibition (IRES 2013)*, 2013. 43

[128] M. Swierczynski, D. I. Stroe, A. I. Stan, R. Teodorescu, and S. K. Kaer, "Lifetime estimation of the nanophosphate $LiFePO_4$ battery chemistry used in fully electric vehicles," *IEEE Transactions on Industry Applications*, vol. 51, no. 4, pp. 3453–3461, 2015, ISSN: 0093-9994. DOI: 10.1109/TIA.2015.2405500. 13, 66, 83, 102

[129] J. Tant, F. Geth, D. Six, P. Tant, and J. Driesen, "Multiobjective battery storage to improve pv integration in residential distribution grids," *IEEE Trans. Sustain. Energy*, pp. 182–191, 2013. DOI: http://dx.doi.org/10.1109/TSTE.2012.2211387. 11

[130] ——, "Multiobjective battery storage to improve PV integration in residential distribution grids," *IEEE Transactions on Sustainable Energy*, vol. 4, no. 1, pp. 182–191, 2013, ISSN: 1949-3029. DOI: 10.1109/TSTE.2012.2211387. 12

[131] J. Tant, F. Geth, D. Six, P. Tant, and J. Driesen, "Multiobjective battery storage to improve pv integration in residential distribution grids," *IEEE Transactions on Sustainable Energy*, vol. 4, no. 1, pp. 182–191, 2013. 12

[132] T. Tjaden, J. Bergner, J. Weniger, and V. Quaschning, "Representative electrical load profiles of residential buildings in germany with a temporal resolution of one second," 2015. 86

[133] R. Tonkoski, D. Turcotte, and T. H. El-Fouly, "Impact of high pv penetration on voltage profiles in residential neighborhoods," *IEEE Transactions on Sustainable Energy*, vol. 3, no. 3, pp. 518–527, 2012. 1

[134] C. N. Truong, M. Naumann, R. C. Karl, M. Müller, A. Jossen, and H. C. Hesse, "Economics of residential photovoltaic battery systems in germany: The case of tesla's powerwall," *Batteries*, vol. 2, no. 2, p. 14, 2016. 11, 20, 33

[135] Y. Ueda, K. Kurokawa, K. Kitamura, K. Akanuma, M. Yokota, and H. Sugihara, "Study on the overvoltage problem and battery operation for grid-connected residential pv systems," *22nd European Photovoltaic Solar Energy Conference*, 2017. 43

[136] C. Venu, Y. Riffonneau, S. Bacha, and Y. Baghzouz, "Battery storage system sizing in distribution feeders with distributed photovoltaic systems," in *2009 IEEE Bucharest PowerTech*, 2009, pp. 1–5. DOI: 10.1109/PTC.2009.5282093. 76, 95

[137] J. Vetter, P. Novák, M. Wagner, C. Veit, K.-C. Möller, J. Besenhard, M. Winter, M. Wohlfahrt-Mehrens, C. Vogler, and A. Hammouche, "Ageing mechanisms in lithium-ion batteries," *Journal of Power Sources*, vol. 147, no. 1, pp. 269 –281, 2005, ISSN: 0378-7753. DOI: https://doi.org/10.1016/j.jpowsour.2005.01.006. [Online]. Available: http://www.sciencedirect.com/science/article/pii/S0378775305000832. 22

[138] ——, "Ageing mechanisms in lithium-ion batteries," *Journal of Power Sources*, vol. 147, no. 1, pp. 269 –281, 2005, ISSN: 0378-7753. DOI: http://dx.doi.org/10.1016/j.jpowsour.2005.01.006. [Online]. Available: http://www.sciencedirect.com/science/article/pii/S0378775305000832. 100, 102

[139] Z. Wang and S. Wang, "Grid power peak shaving and valley filling using vehicle-to-grid systems," *IEEE Transactions on Power Delivery*, vol. 28, no. 3, pp. 1822–1829, 2013, ISSN: 0885-8977. DOI: 10.1109/TPWRD.2013.2264497. 64, 75, 94

[140] J. Weniger, T. Tjaden, J. Bergner, and V. Quaschning, "Sizing of battery converters for residential pv storage systems," *Energy Procedia*, pp. 3–10, 2016. DOI: http://dx.doi.org/10.1016/j.egypro.2016.10.092. 11, 19

[141] J. Weniger, J. Bergner, and V. Quaschning, "Economics of residential pv battery systems in the self-consumption age," *29th European Photovoltaic Solar Energy Conference and Exhibition*, 2014. DOI: 10.4229/EUPVSEC20142014-7DO.14.3. 38

[142] ——, "Integration of PV power and load forecasts into the operation of residential PV battery systems," *4th Solar Integration Workshop on Integration of Solar Power into Power Systems*, 2014. DOI: 10.13140/2.1.3048.9283. 38, 41, 50

[143] H. Wenzl, I. Baring-Gould, R. Kaiser, B. Y. Liaw, P. Lundsager, J. Manwell, A. Ruddell, and V. Svoboda, "Life prediction of batteries for selecting the technically most suitable and cost effective battery," in Selected Papers from the Ninth European Lead Battery Conference*; : Amsterdam, The Netherlands Volume 144*, 2005, pp. 373–384. 27

[144] W. L. Winston, *Operations Research. Applications and Algorithms*, 4th. Brooks/Cole, 2004, ISBN: 0534423620. [Online]. Available: http://www.amazon.com/exec/obidos/redirect?tag=citeulike07-20\&path=ASIN/0534380581. 17

[145] J. Yoo, B. Park, K. An, E. A. Al-Ammar, Y. Khan, K. Hur, and J. H. Kim, "Look-ahead energy management of a grid-connected residential pv system with energy storage under time-based rate programs," *Energies*, vol. 5, no. 4, p. 1116, 2012, ISSN: 1996-1073. DOI: 10.3390/en5041116. 38, 51

[146] M. Zeraati, M. E. H. Golshan, and J. M. Guerrero, "Distributed control of battery energy storage systems for voltage regulation in distribution networks with high pv penetration," *IEEE Transactions on Smart Grid*, vol. 9, no. 4, pp. 3582–3593, 2018, ISSN: 1949-3053. DOI: 10.1109/TSG.2016.2636217. 2

[147] S. Zhang, R. Martins, M. Gul, and P. Musilek, "Economy of residential photovoltaic generation and battery energy storage in alberta, canada," in *2017 IEEE Electrical Power and Energy Conference (EPEC)*, 2017, pp. 1–5. DOI: 10.1109/EPEC.2017.8286177. 76, 95

Appendix A: Literature Survey

Table A.1: Literature review for battery performance parameters used in this study. For all table fields the value used for simulations is given first. In some cases, other values are given in brackets—these are for information to the reader only, but not further used in the paper.

Parameter	Variable	Unit	PbA	LFP	NMC
Battery round trip efficiency	η_{batt}	%	85 [124], [126] * (80 [50])	98 [124], [126] * (95 [50])	95 [50] **
Battery self-discharge	SD	%/day	0.17 [126] (0.2 [60], [109] 0.1 [60])	0.02 [124], [126] * (0.33 [109] 0.1 [60], [109])	0.02 [86]
Calendric lifetime	$Life_{Cal}^{80\%}$	(years)	10 [126] (5 [60] 8 [104])	15 [60] (12–20+ [124])	13 [86], [109]
Cyclic lifetime	$Life_{Cyc}^{80\%}$	FEC	1500 [104] *** (200–1300 [60], [126])	10,000 [86] **** (6000 [20], [124] 1000–10,000+ [60], [100])	4500 [36] (700–1000 [122])

* Experiments conducted at the following parameters: 1/10 C, 25 °C, 50% SOC; ** Experiments conducted at the following parameters: 1 C, 25 °C, 50% SOC; *** Derived at 50% DoD; **** Tested at 60–100% DoD.

Appendix B: Battery Power Profiles

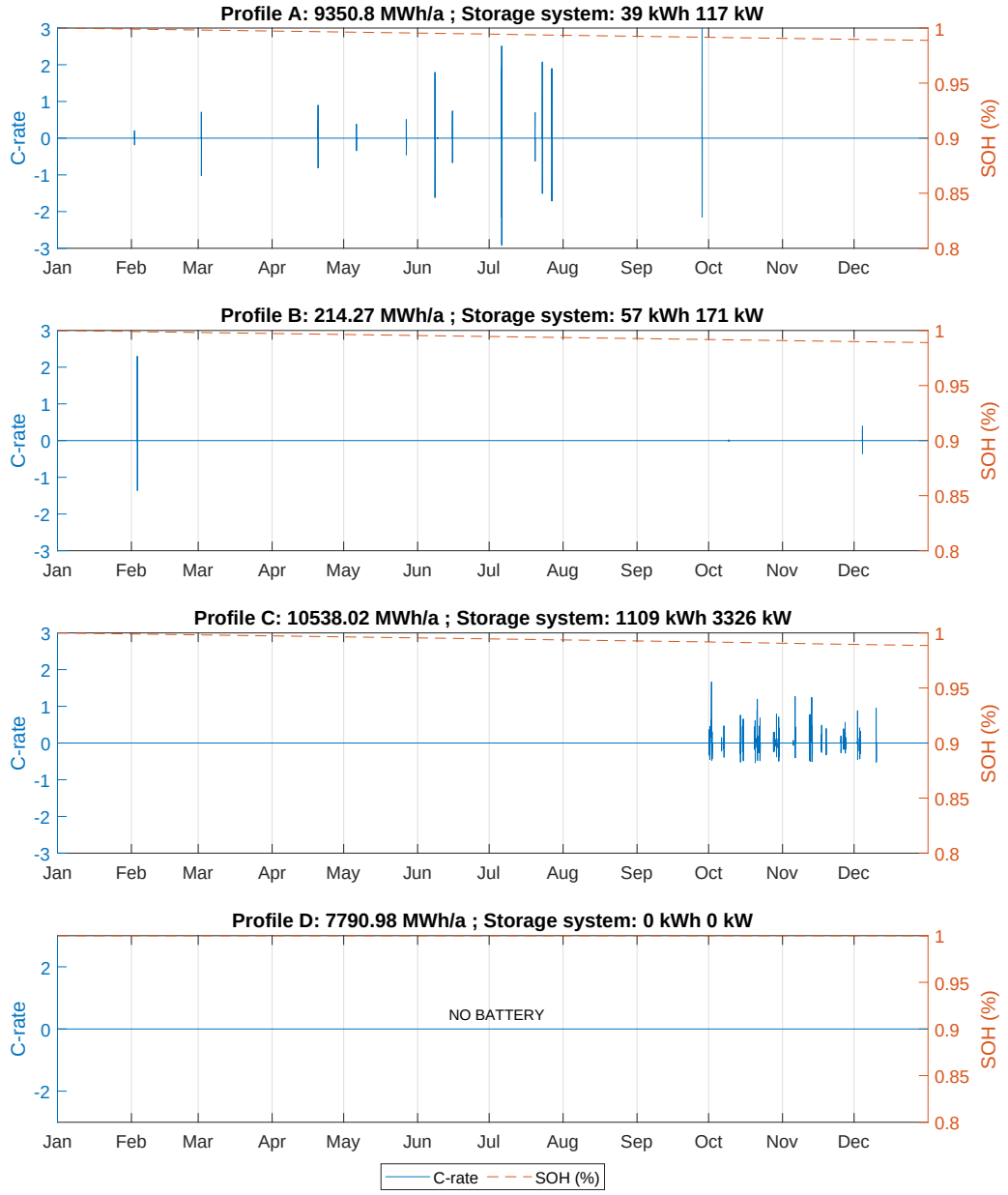

Figure B.1: Battery power profile with yearly billing scheme and resulting state of health decline.

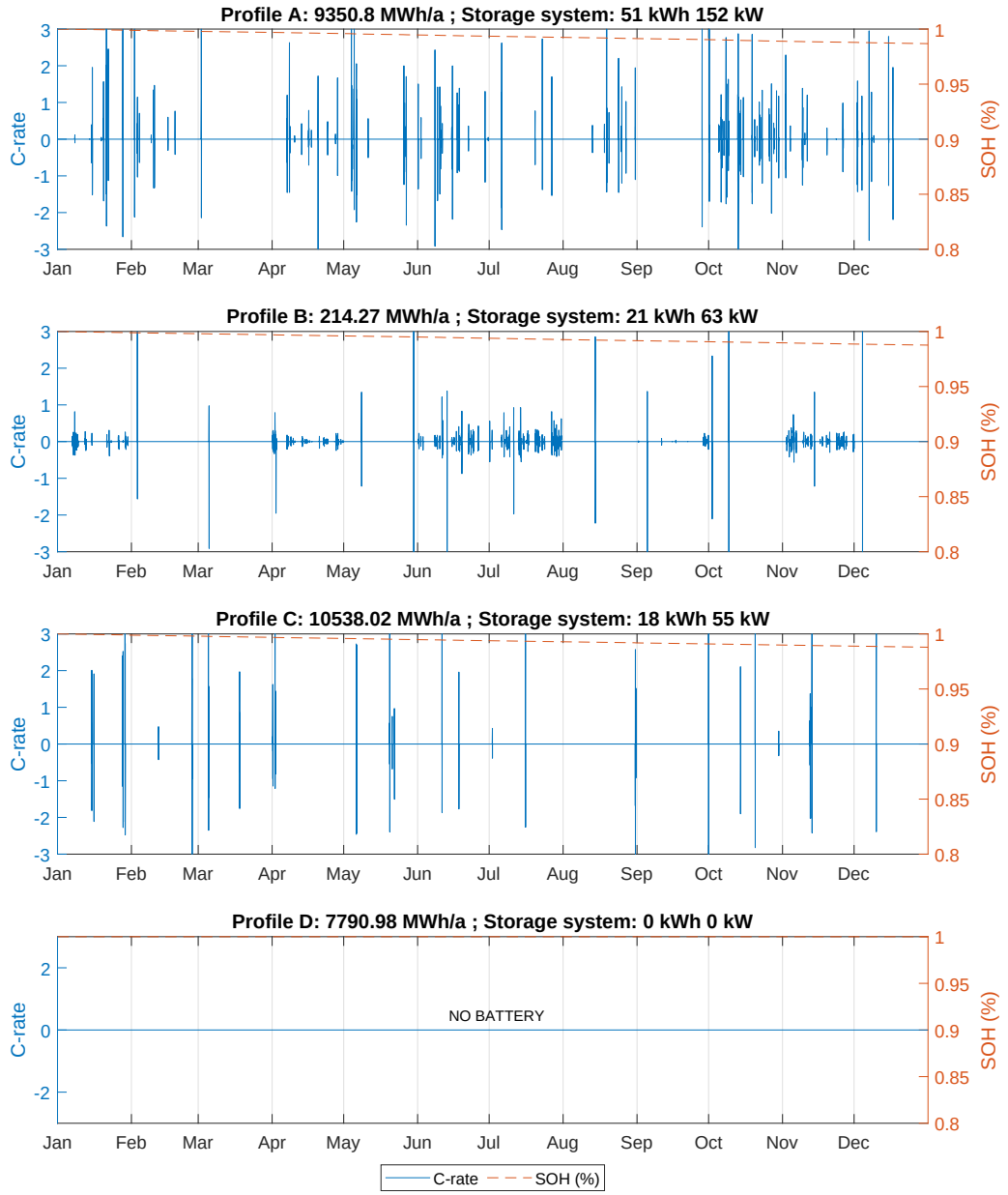

Figure B.2: Battery power profile with monthly billing scheme and resulting state of health decline.

Appendix C: Power flows in the examined PV/BESS

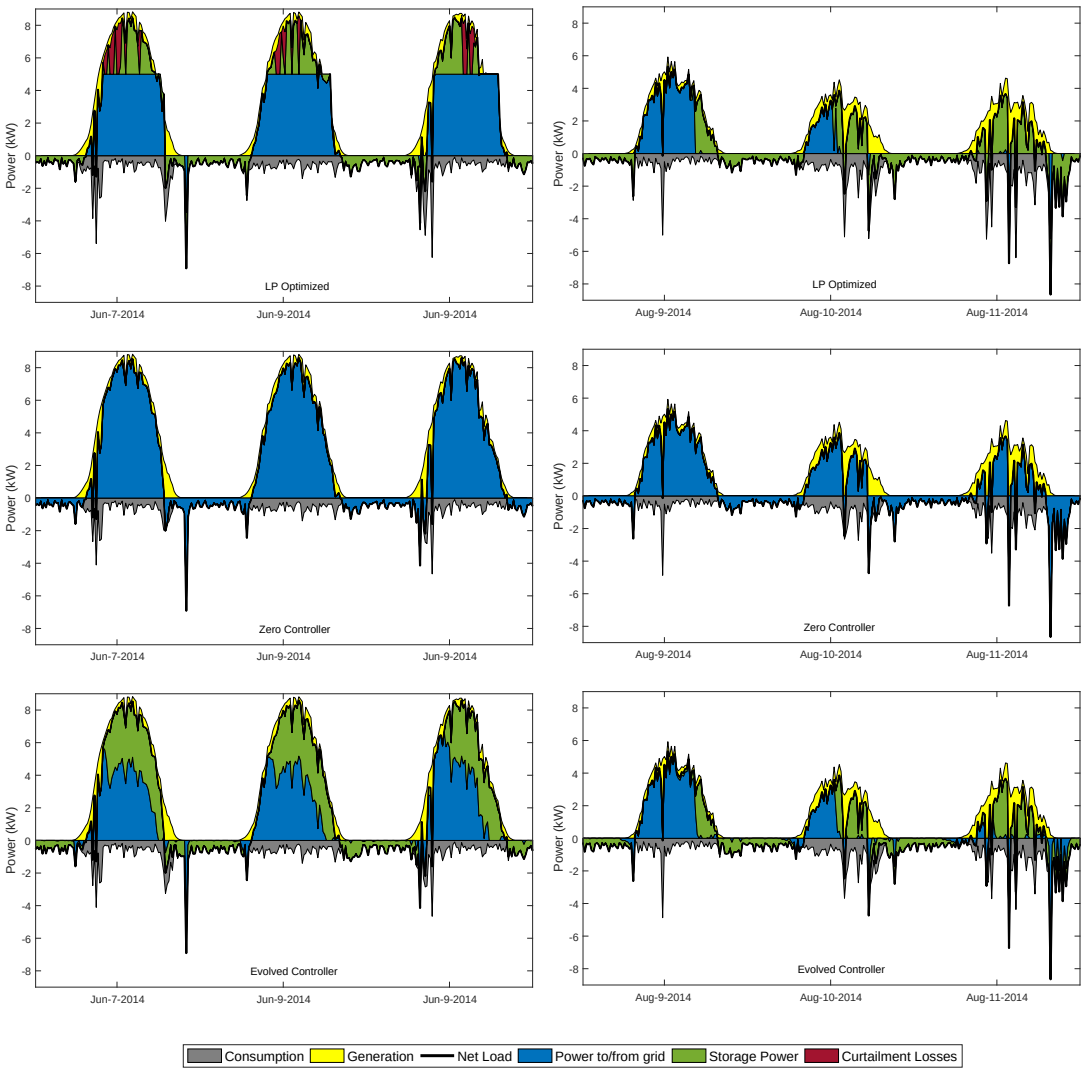

Figure C.1: Power flows in the examined PV/BESS for different time periods (left: June 2014 with high availability of solar energy; right: August 2014 with low and highly variable availability), and different controllers (top: system optimized using linear programming; center: baseline/zero controller; bottom: best evolved fuzzy controller).